Hochschule für Angewandte Wissenschaften Hamburg
*Hamburg University of Applied Sciences*

# Master's Thesis

Xiang Shan Liew

# Stiffness analysis of a nylon sandwich core structure produced by a Markforged Mark Two printer

*Fakultät Technik und Informatik*
*Department Fahrzeugtechnik und Flugzeugbau*

*Faculty of Engineering and Computer Science*
*Department of Automotive and Aeronautical Engineering*

**Xiang Shan Liew**

# Stiffness analysis of a nylon sandwich core structure produced by a Markforged Mark Two printer

Master's thesis submitted in partial fulfilment of master's degree examination

in the Degree Course of Aeronautical Engineering
at the Department of Automotive and Aeronautical Engineering
of the Faculty of Engineering and Computer Science
in the Hamburg University of Applied Sciences

First Examiner : Prof. Dr. Jens Baaran
Second Examiner : Prof. Dr. Christoph Großmann

Submission Date : 28.02.2022

# Abstract

**Name of Student: Xiang Shan Liew**

**Title of the paper**

Stiffness analysis of a nylon sandwich core structure produced by a Markforged Mark Two printer

**Keywords**

3D printing, sandwich structure, composite material, carbon fibre reinforced polymers, nylon, tensile test, four-point flexural test, finite element analysis, orthotropic material

**Abstract**

Sandwich panels are commonly utilised in lightweight construction due to their high stiffness-to-weight ratio. The Markforged Mark Two 3D printer launched by Markforged is able to fabricate sandwich panels with continuous fibre reinforced face sheets and cellular structured nylon core. This thesis focus on the laboratory investigation of the 3D printed sandwich panel components' stiffness properties. The aim of this thesis is to determine the stiffness properties of the nylon sandwich core structure experimentally. Besides, an update of the materials was released by Markforged. Therefore, the stiffness properties of the new nylon and carbon filaments will also be determined. Tensile tests and four-point flexural tests are conducted in this thesis. Additionally, analytical and numerical analyses are carried out to model the sandwich core behaviour and improve the previously built finite element models of sandwich panels.

**Name des Studierenden: Xiang Shan Liew**

**Thema der Masterthesis**

Steifigkeitsermittlung einer mit einem Markforged Mark Two Drucker hergestellten Nylon-Sandwichkernstruktur

**Stichworte**

3D Druck, Sandwichbauweise, Verbundwerkstoff, Kohlenstofffaserverstärkter Kunststoff, Nylon, Zugversuch, Vierpunktbiegeversuch, Finite-Elemente-Analyse, Orthotropie

**Kurzzusammenfassung**

Sandwichplatten werden aufgrund ihres hohen Steifigkeits-Gewichts-Verhältnisses häufig im Leichtbau eingesetzt. Der von Markforged eingeführte 3D-Drucker Markforged Mark Two ist in der Lage, Sandwichplatten mit endlosfaserverstärkten Deckschichten und einer Kernstruktur aus Nylon herzustellen. Diese Arbeit konzentriert sich auf die Laboruntersuchung der Steifigkeitseigenschaften von 3D-gedruckten Sandwichplatten. Das Ziel dieser Arbeit ist es, die Steifigkeitseigenschaften der Nylon-Sandwich-Kernstruktur experimentell zu bestimmen. Außerdem wurde von Markforged ein Update der Materialien veröffentlicht Daher werden auch die Steifigkeitseigenschaften der neuen Nylon- und Kohlenstoff-Filamente durch Versuche ermittelt. In dieser Arbeit werden Zugversuche und Vierpunkt-Biegeversuche durchgeführt. Darüber hinaus werden analytische und numerische Analysen durchgeführt, um das Verhalten des Sandwichkerns zu modellieren und die zuvor gebauten Finite-Elemente-Modelle der Sandwichplatten zu verbessern.

# List of Contents

# I List of Abbreviations

| | |
|---|---|
| 2D | Two dimensional |
| 3D | Three dimensional |
| ABS | Acrylonitrile butadiene styrene |
| CAD | Computer-aided design |
| CFF | Continuous Filament Fabrication |
| CFR | Carbon fibre reinforced |
| CFRP | Carbon fibre reinforced polymers |
| CLT | Classical Laminate Theory |
| FE | Finite element |
| FEA | Finite element analysis |
| FFF | Fused Filament Fabrication |
| FSDT | First Order Deformation Theory |
| HT | High tenacity |
| LBL | Lightweight Construction Laboratory |
| PA | Polyamide |
| PEEK | Polyether ether ketone |
| PLA | Polylactic acid |
| UD | Unidirectional |
| | |
| UDV | “Unidirektionaler Verbund” |
| AWV | “Ausgeglichener Winkelverbund” |
| FL | “Flugzeugbaulaminat” |

# II List of Symbols

## Latin Symbols

| | |
|---|---|
| $b$ | Width of laminate |
| $d$ | Distance between neutral plane of two face sheets |
| $f_m$ | Deflection at the middle of specimen |
| $(f_m - f_s)$ | Difference of deflections |
| $f_s$ | Deflection of specimen at the location of the loading pins |
| $h$ | Thickness of sandwich specimen |
| $k$ | Shear correction factor |
| $r$ | Crosshead speed |
| $s$ | Crosshead displacement |
| $t$ | thickness |
| $x$ | x-coordinate (longitudinal direction of the laminate) |
| $y$ | y-coordinate (transverse direction of the laminate) |
| $z$ | z-coordinate (stacking direction of the laminate) |
| $A$ | Area or cross section |
| $[A\ B\ D]$ | Rigidity matrix of laminate |
| $[A]$ | Extension rigidity matrix of laminate |
| $[A_S]$ | Transverse shear rigidity matrix of laminate |
| $[B]$ | Bending-extension(coupling) stiffness matrix of laminate |
| $[C]$ | Stiffness matrix |
| $[D]$ | Flexural rigidity matrix of laminate |
| $E$ | Elastic modulus |
| $EI$ | Flexural stiffness |
| $F$ | Force or load |

| | |
|---|---|
| $G$ | Shear modulus |
| $L \times W \times H$ | Dimension: length X width X height |
| $\{N\}$ | Vector of distributed forces (forces per unit length) |
| $\{M\}$ | Vector of distributed moments (moments per unit length) |
| $\{V\}$ | Vector of distributed transverse shear forces (forces per unit length) |
| $[Q]$ | Stiffness matrix of a lamina |
| $[T]$ | Transformation matrix |
| $V$ | Volume |

## Greek Symbols

| | |
|---|---|
| $\alpha$ | Angle of ply orientation |
| $\varepsilon$ | Strain |
| $\kappa$ | Curvature |
| $\gamma$ | Shear strain |
| $\sigma$ | Normal stress |
| $\tau$ | Shear stress |
| $\varrho$ | Shifting of the neutral plane in an asymmetric layup |
| $\phi$ | Fibre volume ratio |
| $\varphi$ | Proportion of printed CFRP in specimens |
| $\nu$ | Poisson’s ratio |

## Indices

| | |
|---|---|
| $()'$ | Parameter in local coordinate system |
| $()^{-1}$ | Inverse matrix |
| $()_1$ , $()_{11}$ | Parameter in fibre direction or in printing direction (local coordinate system) |
| $()_2$ , $()_{22}$ | Parameter transverse to fibre direction or in printing direction (local coordinate system) |
| $()_3$ , $()_{33}$ | Parameter in the stacking direction (local coordinate system) |
| $()_{eff}$ , $()_{exp}$ | Experimentally obtained values |
| $()_{fs}$ | Values of face sheets |
| $()_k$ | “k” layer of the laminate |
| $()_m$ | Values of matrix |
| $()_n$ | Values of nylon |
| $()_S$ | Parameter for transverse shear |
| $()_{sc}$ | Values of sandwich core |
| $()_{sym}$ | Symmetric layup |
| $()_{sym}$ | Symmetric layup |
| $()_x$ , $()_{xx}$ | Parameter in longitudinal direction (global coordinate system) |
| $()_y$ , $()_{yy}$ | Parameter transverse to longitudinal direction (global coordinate system) |
| $()_z$ , $()_{zz}$ | Parameter in the stacking direction (global coordinate system) |

# III List of Figures

# IV List of Tables

# 1 Introduction

## 1.1 Motivation

Sandwich panels consist of three parts: two thin, strong, and stiff face sheets located at the top and bottom of the sandwich panel and a comparatively thick and soft core in between the face sheets. Adhesive is used to join the face sheets to the core. The face sheets resist the external bending moment, while the core resists shear and prevents the face sheets from buckling and wrinkling. [1, pp. 3-4]. Sandwich panels are commonly utilised in lightweight construction due to their high stiffness-to-weight ratio. Furthermore, the components of a sandwich panel are made from various basic materials. This allows the designer to design an optimal structure by selecting the material for each component of the sandwich panel based on the job requirements. One of the well-known applications of sandwich panels is in the aeronautical industry, as mass and strength are the crucial parameters in the design of aircraft structures.

Markforged Mark Two is a 3D printer developed by Markforged that can print a fibre reinforced composite structure. The Continuous Filament Fabrication (CFF) process introduced by Markforged is a process to reinforce 3D printed thermoplastics components with continuous fibres such as carbon fibre, Kevlar, and glass fibre. On top of that, a sandwich panel with a cellular structured nylon core can be fabricated by the Markforged Mark Two 3D Printer. Such structure was investigated in the previous projects by *Suer 2018* [2] and *Wolf 2020* [3] in the Department of Automotive and Aeronautical Engineering (F+F) at the Hamburg University of Applied Sciences (HAW Hamburg). However, the stiffness properties of the core material between the face sheets were not studied in these research projects and remain unknown. Estimated values for material properties of the core material were used in the previous project.

## 1.2 Aim and Scope

The scope of this thesis includes preparation, testing, calculation, and analysis of the various type of specimens printed by Markforged Mark Two printer for tensile test and flexural test.

The aim of this thesis is to determine the stiffness properties of the cellular structured nylon sandwich core printed by Mark Two experimentally. Analytical and numerical analyses were also carried out to model the sandwich core behaviour and improve the previous models developed by *Suer 2018* [2] and *Wolf 2020* [3].

Besides, the nylon filament used in the previous projects was brought to end-of-life, and a new type of nylon filament was introduced by Markforged. The specimens in this thesis were fabricated with this new nylon filament; Therefore, experiments were also conducted to determine the basic stiffness properties of this new nylon.

## 1.3 Structure of Work

**Chapter 2** Includes a summary of previous studies, an overview of the materials used and the influences of printing settings on the stiffness of printed parts and a brief discussion about the selection of test processes and test standards

**Chapter 3** Gives an overview of the important hardware and software used in this thesis

**Chapter 4** Gives a brief discussion of mathematical fundamentals and theories used for estimation of stiffness properties of the specimens

**Chapter 5** Contains the details of specimens' fabrication, test setup and procedures, test results evaluation, as well as difficulties and challenges in the tensile test session with printed nylon specimens

**Chapter 6** Contains the details of specimens' fabrication, test setup and procedures, test results evaluation, as well as difficulties and challenges in the tensile test session with printed carbon fibre reinforced specimens

**Chapter 7** Contains the details of specimens' fabrication, test setup and procedures, finite element modelling and simulation, test results evaluation, as well as difficulties and challenges in the four-point flexural test session of the nylon sandwich core specimens

**Chapter 8** Shows the details and steps for validation test of the results obtained in *chapter 5*, *chapter 6* and *chapter 7*

**Chapter 9** Includes the conclusion of the findings in this thesis and suggestions for the future research

# 2 Literature Review

This chapter includes a summary of previous studies, an overview of the materials used in this thesis and the influences of printing settings on the stiffness of printed parts. This chapter also includes a brief discussion about the selection of test processes and test standards.

## 2.1 Previous Work

### 2.1.1 Suer (2018)

Two material tests were carried out by *Suer 2018* [2], a tensile test and a four-point-flexural test with the specimens produced with the Markforged Mark Two 3D printer. The aim of the tensile test was to determine the basic stiffness properties of the carbon filament by Markforged.

#### 2.1.1.1 Tensile Test

During the tensile test, three sets of specimens with the dimensions shown in *Figure 2-1* were produced [2, p. 34]:

- "Unidirektionaler Verbund" (UDV) $[0°_8]$: 5 pieces
- "Ausgeglichener Winkelverbund" (AWV) $[\pm 45°_4]$: 5 pieces
- "Flugzeugbaulaminat" (FL) $[0°/\pm 45°/90°]_s$: 5 pieces

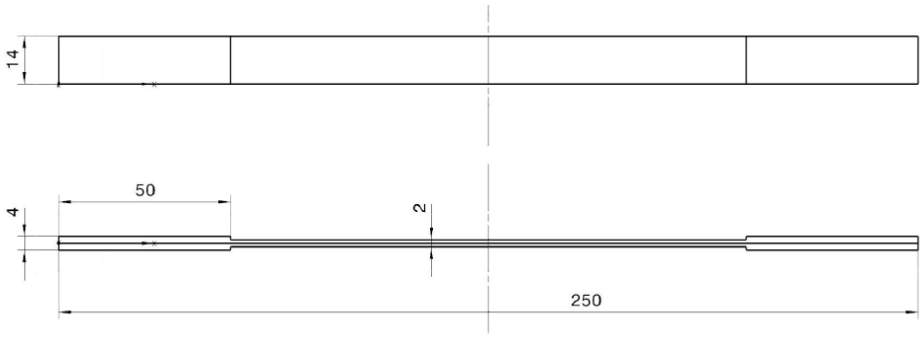


Figure 2-1: Dimensions of the tensile test specimens by *Suer 2018* [2, p. 33]

The specimens were subjected to a cyclic tensile load of five cycles, with test speed $r = 2\frac{mm}{min}$ and strain $\varepsilon_{max} = 1\%$ [2, p. 36]. The test results within the range of strain $0.05\% \leq \varepsilon \leq 0.25\%$ were then observed [2, p. 37].

Among all stiffness properties of the layers printed by carbon filament, only the $E_1$ was determined experimentally with the UDV specimens, and the rest was calculated based on the theory of micromechanics of composite materials, with an assumption of fibre

volume ratio, $\phi = 0.65$. The stiffness properties of carbon printed layers are shown in *Table 2-1*.

Table 2-1: Stiffness properties of carbon printed layers determined by Suer [2, p. 44]

| $E_1$ [MPa] | $E_2$ [MPa] | $G_{12}$ [MPa] | $\nu_{12}$ [-] | $\phi$ [-] |
|---|---|---|---|---|
| 60520 | 5150 | 2000 | 0.27 | 0.65 |
| Test | Calculated based on micromechanics theory | | | |

After that, the test results with AWV and FL specimens were taken to compare with the calculated stiffness properties with $\phi$ in the range of $0.50 - 0.65$, see *Table 2-2*. As observed, the experimental and theoretical stiffness properties values do not match each other, as the $\phi$ for FL and AWN do not match with each other.

Table 2-2: Comparison of the experimental stiffness properties and theoretical values with various fibre volume ratios [2, p. 48]

| $\phi$ [-] | 0.65 | 0.62 | 0.59 | 0.56 | 0.53 | 0.50 | Test |
|---|---|---|---|---|---|---|---|
| $E_{t,T,FL}$ [MPa] | 12215 | 12029 | 11875 | 11744 | 11632 | 11537 | 11328 |
| $E_{t,T,AWN}$ [MPa] | 4113 | 3760 | 3449 | 3186 | 2959 | 2752.4 | 3892 |

### 2.1.1.2 Four Point Flexural Test

After that, the flexural stiffness of a sandwich panel produced by Markforged Mark Two printer was obtained through the four-point flexural tests. Three specimens with $L \times W \times H = 192 \times 39 \times 8\text{mm}$ dimensions were printed [2, p. 53]. The face sheets of the sandwich panel specimens consist of nylon and carbon filament printed layers, and a triangular infill with 50% fill density was printed in the core. The cross section and details of the specimens are described in *Figure* 2-2.

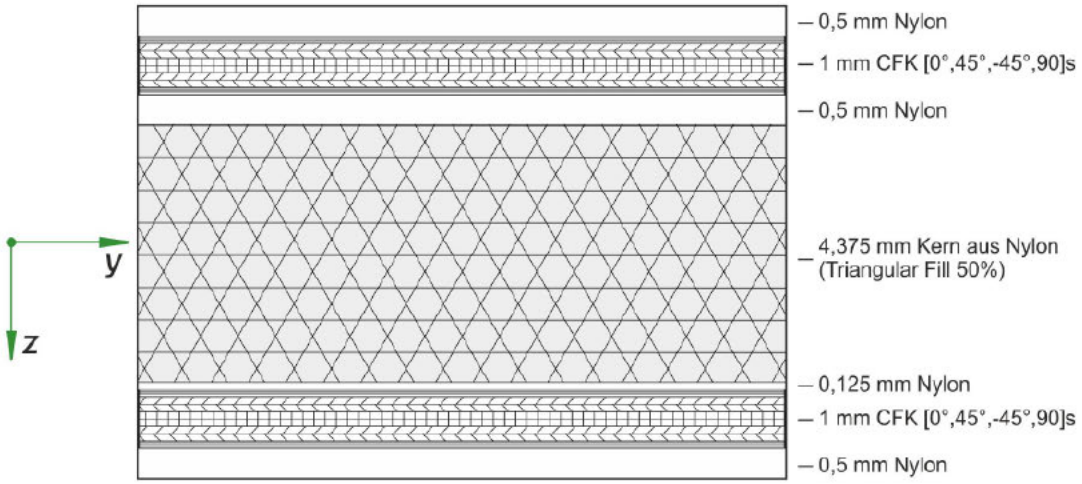


Figure 2-2: Details of the four-point flexural test specimen by *Suer 2018* [2, p. 54]

During the flexural test, the specimens were pressed in the transverse direction of the specimens with a load path $s = 8mm$ and the fixture displacement rate of $r \approx 5.5 \frac{mm}{min}$ [2, p. 55]. The test results obtained are shown in the table below.

Table 2-3: Results of the four-point-flexural test [2, p. 56]

| | $(EI)_{eff1}$ $[Nm^2]$ | $(EI)_{eff2}$ $[Nm^2]$ | $max(F)$ $[N]$ | $max(f_m)$ $[mm]$ | $max(f_m - f_s)$ $[mm]$ |
|---|---|---|---|---|---|
| **Specimen 1** | 25.53 | 19,57 | 1933 | 8,93 | 1,11 |
| **Specimen 2** | 23,29 | 17,35 | 2045 | 9,06 | 1,17 |
| **Specimen 3** | 23,35 | 18,12 | 2035 | 9,04 | 1,18 |
| **Average** | 24,06 | 18,35 | 2010 | 9,01 | 1,15 |

$(EI)_{eff1}$: flexural stiffness of when the specimen is loaded
$(EI)_{eff2}$: flexural stiffness of when the load is released
$max(F)$: maximum load exerted to the specimen
$max(f_m)$ : maximum displacement at the middle of the specimen

In addition, an analytical mathematic model and a finite element (FE) model that replicates the bending behaviour of the sandwich panel in a four-point flexural test were built. The results of these models were afterwards compared with the experimentally obtained values. However, the FE model built in this project did not produce satisfactory and plausible results. Hence, the results of the FE simulation will not be discussed. The task to improve the FE model was passed down to another student and later taken over by *Wolf 2020* [3].

## 2.1.2 Wolf (2020)

The research of *Wolf 2020* [3].mainly focused on developing FE models to validate the four-point-flexural test results of the sandwich panel specimen produced by Markforged Mark Two 3D printer. FE models for both sandwich core and entire sandwich panel were developed in this work.

### 2.1.2.1 FE Modelling of the Sandwich Core

Due to the limitation of student version NASTRAN, a FE sandwich core model with a 4×8 triangular cell structure was built in this research project [3, p. 25]. The edge length of each cell is $2{,}8146mm$, and the thickness of each cell wall is approximately $0.5mm$ [3, p. 30]. Shell elements were chosen for modelling the sandwich core cellular structure. The geometry and mesh of the sandwich core structure are displayed in *Figure 2-3a-b*. Various boundary conditions are defined on the core structure FE model to obtain the sandwich cores approximation values of the stiffness properties, see *Figure 2-4a-f*.

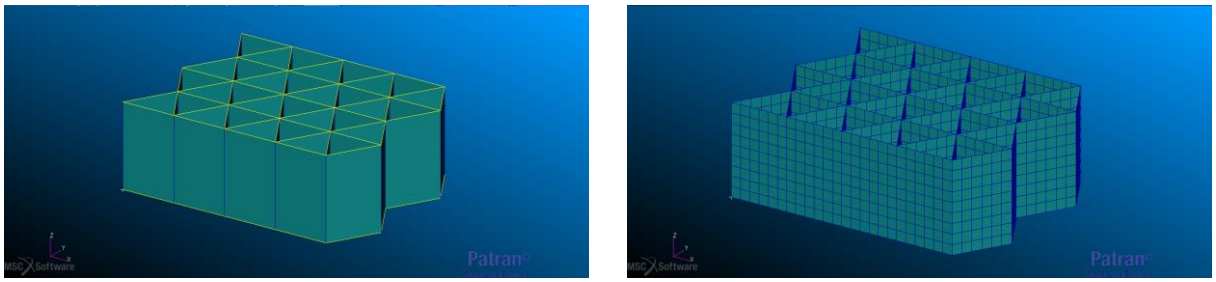

(a) (b)

Figure 2-3: (a) Geometry of sandwich core structure FE model (b) Mesh in the sandwich core structure FE model [3, p. 30]

(a) (b)

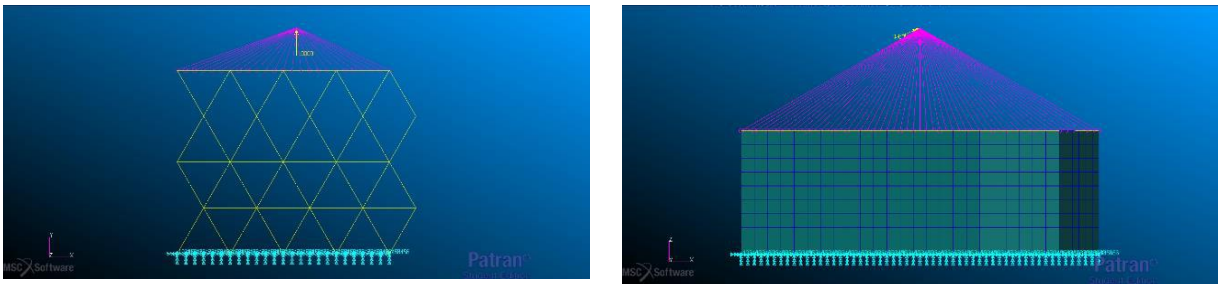

(c) (d)

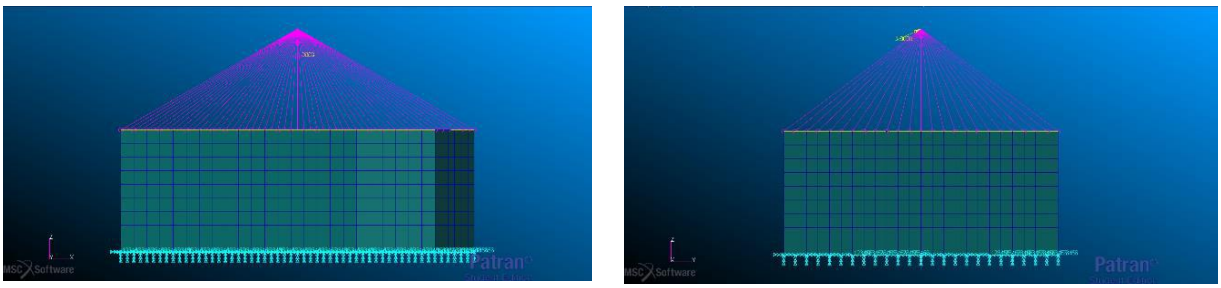

(e) (f)

Figure 2-4: Boundary conditions to determine the (a) $E_x$ (b) $G_{xy}$ (c) $E_y$ (d) $G_{xz}$ (e) $E_z$ (f) $G_{yz}$ of the sandwich core structure [3, p. 31]

The simulated results were then corrected and adjusted based on the infill density of the core structure and the symmetrical condition of orthotropic material. Due to the new nylon released by Markforged and the old nylon being brought to end-of-life, the stiffness properties of the sandwich core structures obtained from FE are not relevant to this thesis. Therefore, only the modelling methods by *Wolf 2020* [3] was studied.

### 2.1.2.2 FE Modelling of Sandwich Panel

Two types of FE sandwich panel models were created by *Wolf 2020 [3]*: simplified shell models with QUAD4 and QUAD8 elements, and volume-shell model with QUAD4 element for the face sheets and HEX8 elements for the core.

**Shell Models with QUAD4 and QUAD8 Elements**

QUAD4 and QUAD8 are element types used in a 2D structure. The difference between these elements is that QUAD4 has linear shape functions; conversely, shape functions in QUAD8 are quadratic. Two load cases: “Surface Load” and “Displacement”, were defined for both models. The boundary conditions of these load cases are illustrated in *Figure 2-5* and *Figure 2-6*.

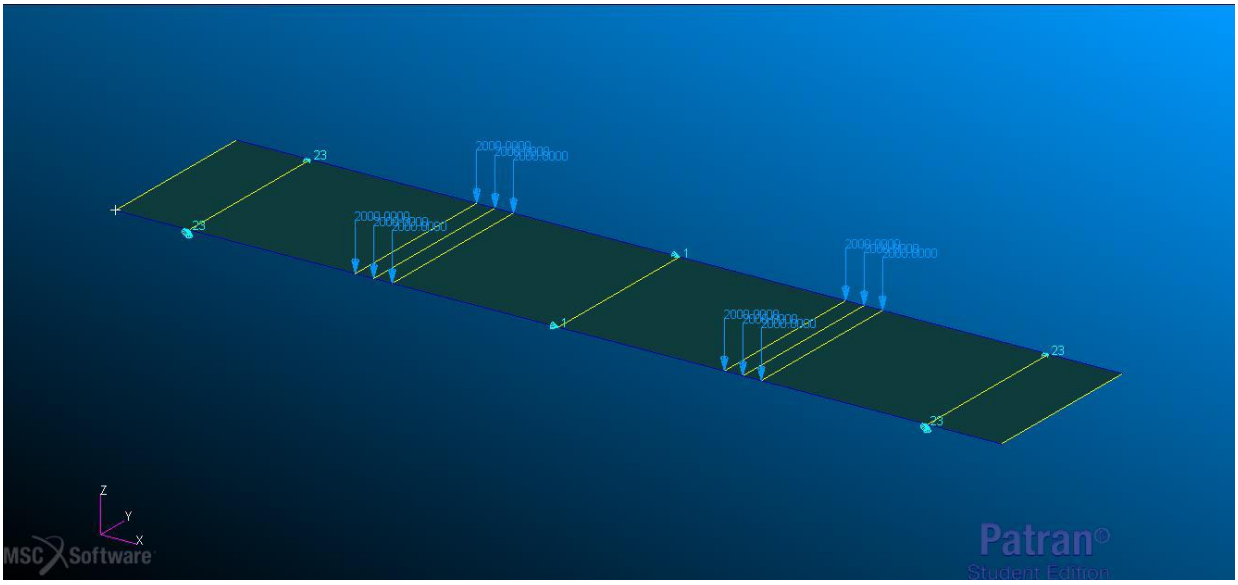


Figure 2-5: Boundary conditions of shell model under load case "Surface Load" [3, p. 27]

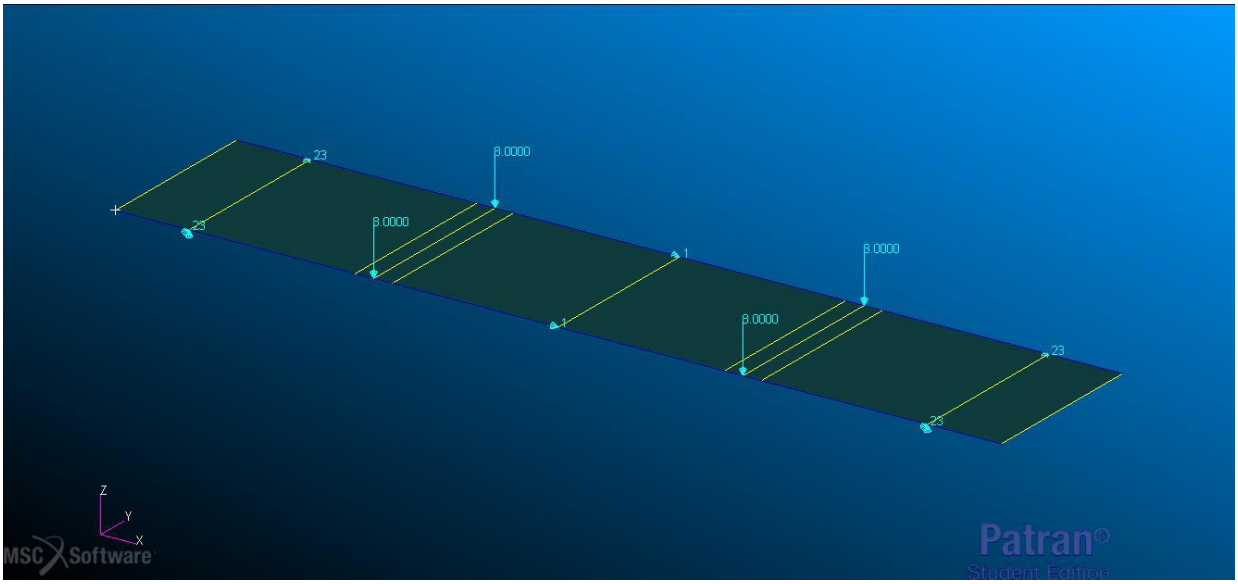


Figure 2-6: Boundary conditions of shell model under load case "Displacement" [3, p. 27]

**Shell/Solid Model QUAD4/HEX8**

The face sheets and core were modelled separately and defined with different material properties in this model. The face sheets were modelled with shell element QUAD4, while the solid elements were used in modelling the core. Three load cases were defined in this model: “Surface Load”, “Displacement A”, and “Displacement B”, *Figure 2-7* - *Figure 2-9*. In the load case “Displacement A”, it was defined that there is no change in thickness occurring in the model under the load application point; in “Displacement B”, the change in thickness in the model is allowed.

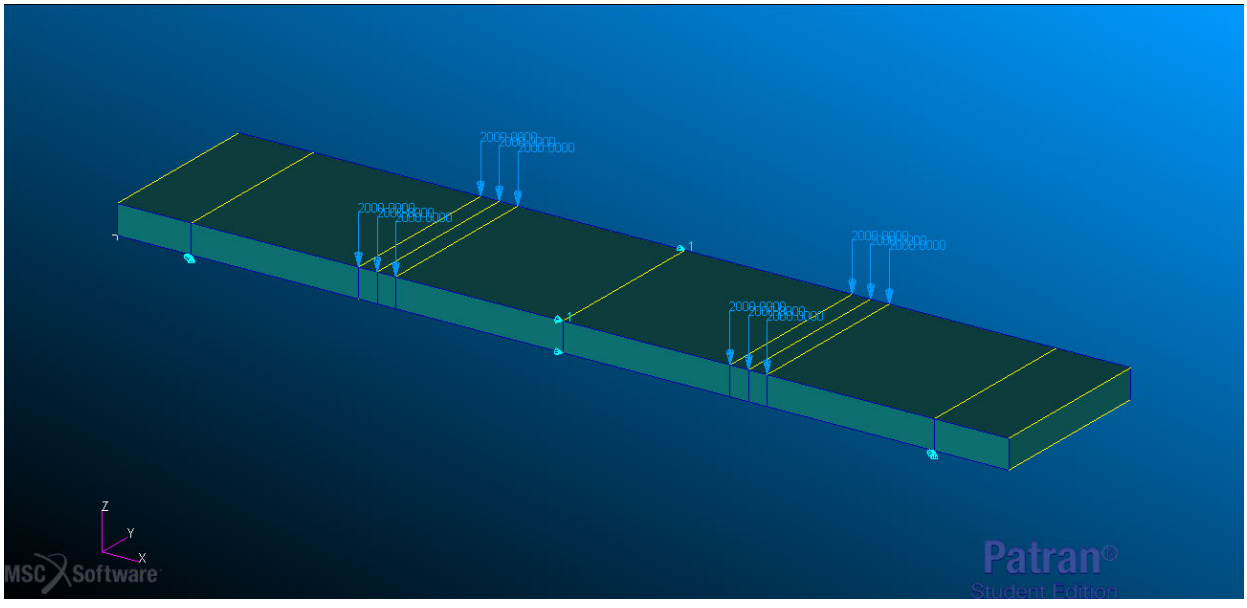


Figure 2-7: Boundary conditions of shell/solid model under load case "Surface Load" [3, p. 28]

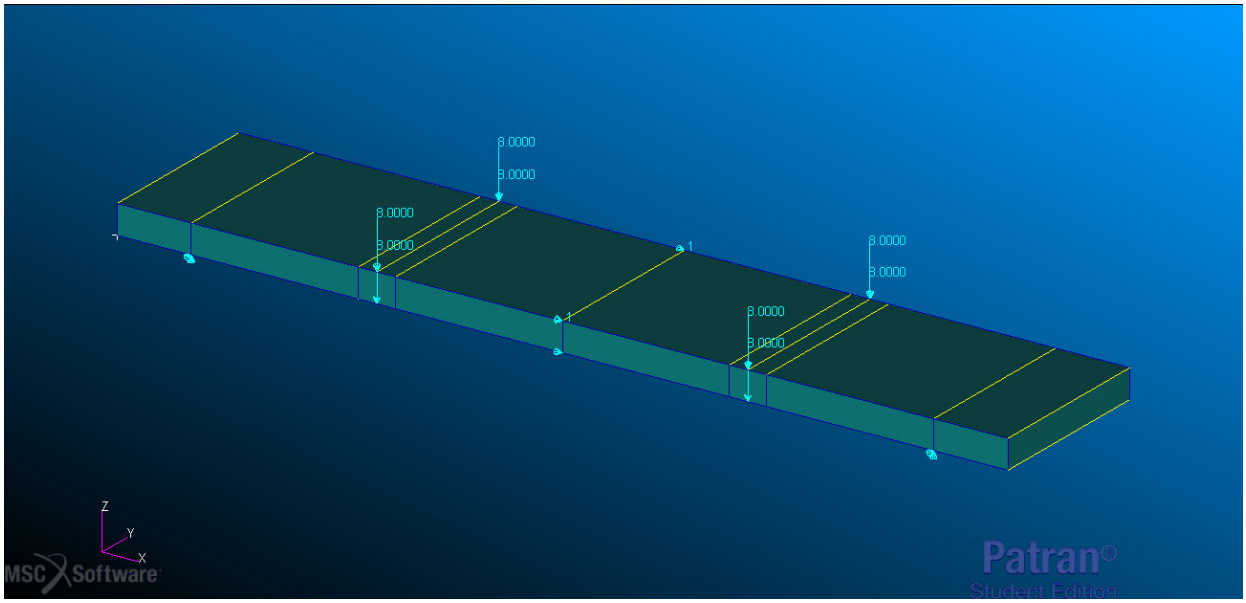


Figure 2-8: Boundary conditions of shell/solid model under load case "Displacement A" [3, p. 28]

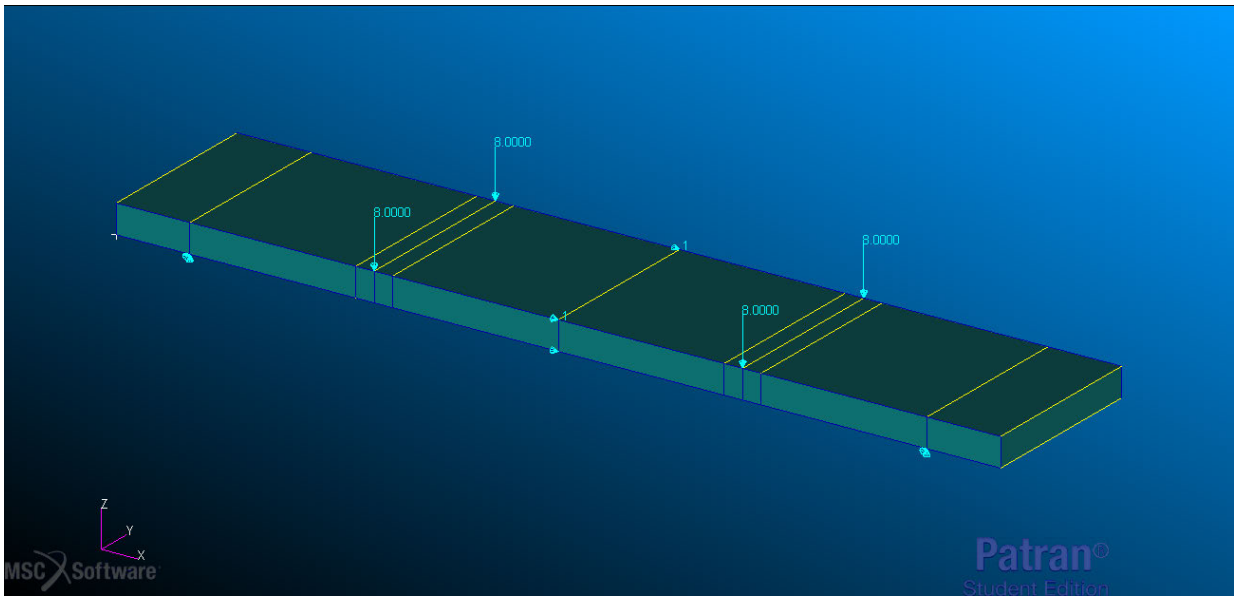


Figure 2-9: Boundary conditions of shell/solid model under load case "Displacement B" [3, p. 29]

The FE simulated results from NASTRAN were then compared with the experimental results by *Suer*, refer to *Table 2-4.*

Table 2-4: Comparison of experimental (Suer) and numerical (Wolf) results [3, p. 39]

| Description | | | Data | | | Deviation | Comments |
|---|---|---|---|---|---|---|---|
| **Details** | **Load Case** | **Element types** | **Displacement $f_m$ [mm]** | **Load F [N]** | **Rigidity $F/f_m$ [N/mm]** | **relative deviation in stiffness** | |
| **Experimental (*Suer*)** | | | | | | | |
| **4PB-Test** | | | 9.01 | 1005.00 | 223.09 | Reference | |
| **Numerical (*Wolf*)** | | | | | | | |
| **Shell** | Surface Load | QUAD4 | 7.90 | 1000.00 | 253.16 | 13% | Total load applied: 2 x 1000 N |
| | Displacement | QUAD4 | 10.60 | 1339.87 | 252.81 | 13% | Displacement of loading pins: 8mm |
| **Shell** | Surface Load | QUAD8 | 7.91 | 1000.00 | 252.84 | 13% | Total load applied: 2 x 1000 N |
| | Displacement | QUAD8 | 10.60 | 1339.58 | 252.75 | 13% | Displacement of loading pins: 8mm |
| **Solid/Shell** | Surface Load | QUAD4/HEX8 | 8.19 | 1000.00 | 244.20 | 9% | Total load applied: 2 x 1000 N |
| | Displacement A | QUAD4/HEX8 | 10.50 | 1289.97 | 245.71 | 10% | No change of thickness |
| | Displacement B | QUAD4/HEX8 | 10.50 | 1286.47 | 245.04 | 10% | With change of thickness |

## 2.2 Material

This subchapter includes information on materials used to produce the specimens and the values of material data chosen from literature for the theoretical calculation of the stiffness properties of the specimens.

### 2.2.1 Nylon Filament

Markforged released a new type of nylon, which was used to prepare the specimens in this thesis. However, there are no details provided by Markforged regarding the exact material of the nylon manufactured by them. It is assumed that the nylon filament is made of Polyamide (PA) 6, PA6.6 (also known as PA66) or a mixture of both. *Table 2-5* shows the material data of nylon obtained from various sources. The material data of both new and old (shaded) nylon are included in this table.

Table 2-5: Material data of nylon from various sources

| Source | Nylon Type | $E_m$ [MPa] | $\nu_m$ [−] | Comments |
|---|---|---|---|---|
| **Schürmann 2007 [4]** | PA6.6 | 2000 | 0.4 | – |
| **Dominingaus 2012 [5]** | PA6 | 1200 | – | – |
| | PA6.6 | 1500 | – | – |
| **MatWeb [6] [7]** | PA6 | 360 - 3750 | 0.35 – 0.45 | Averaged value of test results in database |
| | PA6.6 | 350 - 1900 | 0.38 – 0.45 | Averaged value of test results in database |
| **Markforged 2021 [8]** | – | 1700 | – | Tensile test under standard ASTM D638 |
| **Markforged 2018 [9]** | – | 940 | – | Tensile test under standard ASTM D638 |
| **Suer 2018 [10]** | – | 940 | 0.4 | $E_m$ taken from Markforged 2018, $\nu_m$ taken from Schürmann 2007 |
| **Sauer 2018 [10]** | – | 750 | 0.35 | Tensile test under standard ASTM D638-10 |
| **Pyl et al. 2018 [11]** | – | 700 | – | Tensile test under standard ASTM D3039/3039M |
| **Chabaud et al. 2019 [12]** | – | 290±10 | – | Tensile test under standard ASTM D3039 |
| **Finke & Kreuziger 2019 [13]** | – | 592.77 | – | Tensile test under standard DIN EN ISO 527-1 |
| | – | 1117.38 | – | Second round of tensile tests was carried out with specimen printed with a new nylon spool |

The material data provided by Markforged was obtained experimentally under the test standard ASTM D638. Nevertheless, the specimens' print settings, such as the specimens' print orientation, numbers of walls in the specimens, and layer height, are not provided. A tensile test was carried out by *Finke and Kreuziger 2019* [13], and the test

results do not match the value provided by *Markforged 2018* [9]. Besides, *Sauer 2018* [10] and *Pyl et al. 2018* [11] also obtained a lower value of $E_m$ during their research. This difference might be caused by the test standard used, print settings, degree of moisture absorption in the nylon, or all of those mentioned.

### 2.2.2 Carbon Fibre Reinforced Filament

Same as the nylon, only minimal material data information is provided and insufficient to conduct any calculation for the specimens stiffness prediction. The fibre volume ratio $\phi$, material data of fibres $E_f$ and material data of matrix $E_m$ are important parameters to characterise the stiffness properties of a carbon fibre reinforced (CFR) lamina. The carbon fibre by Markforged is an ultra-high-strength Continuous Fiber [14]; therefore, material data of high tenacity (HT) fibre are taken from *Schürmann 2007* [4].

Table 2-6: Material data of HT fibre [4, p. 41]

| $E_{f1}$ [MPa] | $E_{f2}$ [MPa] | $G_{f12}$ [MPa] | $\nu_{f12}$ [−] |
|---|---|---|---|
| 23000 | 28000 | 50000 | 0.23 |

Various researches were carried out to study the $\phi$ as well, following table summarises the founding of $\phi$ with different methods.

Table 2-7: Comparison of the fibre volume ratio in various research

| | Printer model | Test item | Measuring method or apparatus | $\phi$ [−] |
|---|---|---|---|---|
| **Sauer 2018 [10]** | Mark Two | Carbon printed layers | Laser scanning microscope with ImageJ software | 0.28 |
| **Pyl et al. 2018 [11]** | Mark Two | Carbon printed layers | Scanning electron microscope ImageJ software | 0.27 |
| **Chabaud et al. 2019 [12]** | Mark Two | Carbon filament | Thermogravimetric analysis | 0.35 |
| **Block et al. 2018 [15]** | Mark One | Carbon printed layers | Optical microscopy with ImageJ software | 0.20 |
| | | Carbon filament | Optical microscope with ImageJ software | 0.27 |
| **Goh et al. 2018 [16]** | Mark One | Carbon filament | Thermogravimetric analysis with analytical balance | 0.41 |

It is observed that the $\phi$ measured by the optical microscopy generally has a lower value than the value obtained from the thermogravimetric analysis. The difference may cause by either the image processing errors in the ImageJ software or the residual of nylon matrix remaining in the balance.

Several researches studied the tensile stiffness properties of the printed CFR specimens by Markforged printer. However, in most research, only the average elastic modulus of specimens $E$ are studied, and the elastic modulus of printed carbon fibre reinforced polymers (CFRP) layers in the specimens $E_c$ remain unknown. If the proportion of the printed CFRP layers in the specimens $\varphi$ is given, the $E_c$ can be calculated by the rule of mixture, *equation 2.1*. The elastic modulus of specimens is summarized in *Table 2-8*.

$$E = E_c\,\varphi + E_m\,(1-\varphi) \qquad 2.1$$

Table 2-8: Summary of the elastic modulus obtained from literature

| | Printer model | $E_x$ [MPa] | $\varphi$ [−] | $E_c$ [MPa] |
|---|---|---|---|---|
| **Markfoged 2021 [8]** | – | – | – | 60000 |
| **Markforged 2018 [9]** | – | – | – | 54000 |
| **Suer 2018 [2]** | Mark Two | 30700 | ~ 0.5 | **60520 |
| **Frankfurt 2018 [17]** | Mark Two | 23700 | 0.364 | * **63467 |
| **Sauer 2018 [10]** | Mark Two | 51400 | 0.78 | 65900 |
| **Pyl et al. 2018 [11]** | Mark Two | 20900 – 57090 | 0.294 – 0.8 | *65618.75 – 71187.5 |
| **Finke & Kreuziger 2019 [13]** | Mark Two | 29135 | ~ 0.5 | * **57677 |
| | | 29950 | ~ 0.5 | *58786 |
| **Chabaud et al. 2019 [12]** | Mark Two | – | –, matrix is removed | ~ 60000 |
| **Block et al. 2018 [15]** | Mark One | – | ~0.75 | 62500 |

* Calculated by Liew

** $E_m$ value provided by *Markforged 2018* [9] is taken.

According to *Table 2-8,* all $E_c$ values found in the researches are higher than the value given by *Markforged 2018* [9]. The $E_c$ by Markforged [8, 9] are obtained experimentally with unidirectionally reinforced specimens ($0°$ orientation) and printed without any wall. Although specimens in the research mentioned in *Table 2-8* have the fibre orientation in $0°$, the discrepancy in $E_c$ might be caused by material composition in specimens (with or without nylon), the specimen's dimension, and the test method as well as the test standard applied.

## 2.3 3D Printing Settings vs Stiffness Properties

The stiffness properties of the printed part can be affected by the printing settings, such as raster angle, fill patterns, infill density and layer thickness. Hence, selecting the right setting for specimen fabrication is very important.

### 2.3.1 Raster Angle

Raster angle is the printing direction of the raster with reference to the direction of force applied. Several studies have proven that the stiffness properties of 3D printed parts can be varied by the raster angles [18–21]. The research of *Zhang et al. 2019* [19] shows that specimens printed with 0° raster angle have the highest tensile strength and elastic modulus; meanwhile, specimens printed with 90° raster angle have the lowest [19, pp. 2124-2126]. This is similar to the orthotropic material properties in fibre reinforced composite materials. Hence, in this thesis, the raster angle of each layer in the printed part will be denoted the same as the fibre angles in the composite layup.

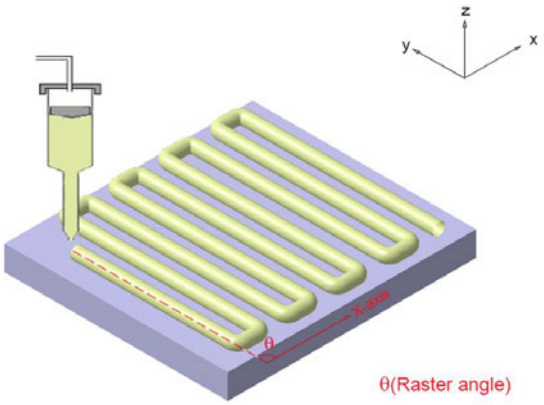


Figure 2-10: Raster angle of a 3D printed part [18, p. 5836]

### 2.3.2 Print Orientation

Print orientation is the position and inclination of part on the print bed with respect to the coordinate system of the print bed. *Durgun and Ertan 2014* [22] investigated the stiffness properties of printed parts with varying raster angles and print orientation. The parts were printed under three different orientations: horizontal, vertical, and perpendicular, see *Figure 2-11*.

It is discovered that parts printed under horizontal orientation generally have the lowest elastic modulus, followed by parts printed under vertical orientation, and those printed under perpendicular orientation have the highest elastic modulus. The tensile strength behaviour is, however, opposed to this trend. The parts printed under horizontal orientation generally have the highest tensile strength, and those printed under perpendicular orientation have the lowest strength. The research by *Cantrell et al. 2017* [21] also delivered similar results.

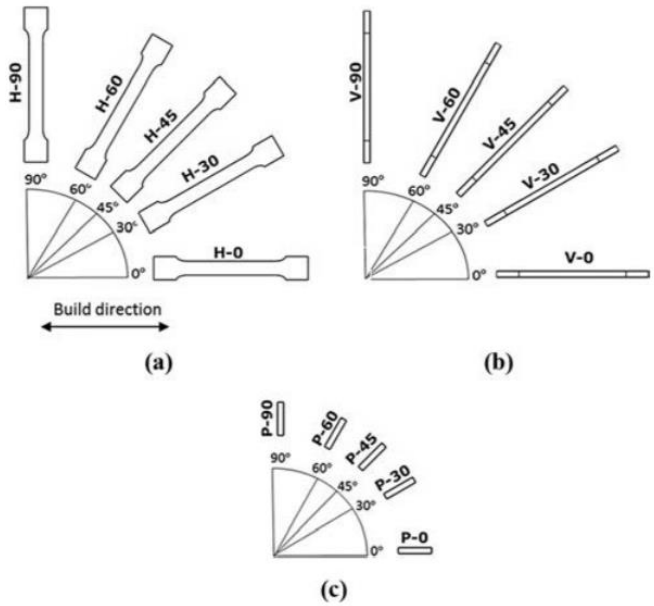


Figure 2-11: (a) horizontal, (b) vertical, (c) perpendicular orientation [22, p. 229]

### 2.3.3 Infill Types and Fill Density

The relationship between stiffness properties of printed parts, infill type and the fill density was analysed by *Wang et al. 2020* [23]. Specimens with two types of infill (triangular and hexagonal) with various fill densities were fabricated and tested. The specimens with triangular infill are stiffer, less ductile and have higher elastic modulus than those with hexagonal infill. However, hexagonal infill specimens have higher tensile strength. The tensile strength and elastic modulus of specimens increased along with the increase in infill density of the specimens, meanwhile decrease in ductility of the specimens was observed.

### 2.3.4 Wall Numbers

The thesis of *Chen 2020* [24] (tensile test with specimens printed with Onyx by Mark Two) reported that the elastic modulus of the specimens increased with the increasing number of walls.

### 2.3.5 Layer Height

The layer height is the thickness of material deposited on each layer of the printed part by the nozzle. The research of *Sood et al. 2012* [25, 26] with 3D printed ABS specimens, *Tymrak et al. 2014* [27] with ABS and PLA specimens, and *Wu et al. 2015* [18] with PEEK specimens had obtained different results. The elastic modulus and tensile strength of the specimens in each research behave differently along with the increase in layer height.

According to *Markforged* [28], the part strength is not significantly affected by the layer heights but the type of materials or printers.

## 2.4 Test Processes and Standards

There is no test standard available for material test of a 3D printed CPRP plate or sandwich panel. Therefore, test standards for CFRP plate or sandwich panel produced by the conventional method were chosen as guidelines to conduct the material test in this thesis. The following subchapters listed the test standard suitable for conducting the material tests in this thesis.

### 2.4.1 Testing Process of Face Sheet Material

#### 2.4.1.1 Tensile Test

The tensile stiffness properties of the face sheets can be determined by the tensile test. The face sheets are made from two materials: nylon and carbon fibre. To investigate the stiffness properties of the face sheets, the elastic modulus of both materials shall be tested separately. Following are the standards chosen to conduct the tensile test for nylon and CPR specimens.

Nylon specimens:

*DIN EN ISO 527–2: Plastics – Determination of tensile properties Part 2 – Test conditions for moulding and extrusion plastics* [29]

CFR specimens:

*DIN EN ISO 527–4: Plastics – Determination of tensile properties Part 4 – Test conditions for isotropic and orthotropic fibre-reinforced plastic composites* [30]

*DIN EN ISO 527–5: Plastics – Determination of tensile properties Part 5 – Test conditions for unidirectional fibre-reinforced plastic composites* [31]

#### 2.4.1.2 Flexural Test

The flexural stiffness properties of the face sheets are also essential to determine the stiffness properties of the sandwich panel, as the face sheets hinder the bending moment exerted on the sandwich panel. Two test methods can be carried out: three-point flexural and four-point flexural tests. The test standards available are listed below:

Nylon specimens:

*DIN EN ISO 178: Plastics – Determination of flexural properties* [32]

CFR specimens:

*DIN EN ISO 14125: Fibre-reinforced plastic composites – Determination of flexural properties* [33]

#### 2.4.1.3 Shear Test

The shear properties of the face sheets shall be investigated as well. The V-notched beam method can be applied to determine the in-plane as well as interlaminar shear properties of the CFR laminate, based on the laminate orientation and stacking direction of the laminate [1, p. 258]. The test standard for this method is

*ASTM D5379/D5379M: Standard Test Method for Shear Properties of Composite Materials by the V-notched Beam Method* [34]

### 2.4.2 Testing Process of Sandwich Core Material

The shear and compressive properties in the flatwise direction are the two most important material properties of the sandwich core structure, as the core resists the shear deformation caused by the transverse shear load. The tests to obtain the shear and compressive properties can be performed in accordance with the standards:

Shear test:

*DIN 53 294: Testing of sandwiches; shear test in flatwise plane* [35]
*ASTM C273/C273M: Standard Test Method for Shear Properties of Sandwich Core Materials* [36]

Compression test:

*ASTM C365/C365M: Standard Test Method for Flatwise Compressive Properties of Sandwich Cores* [37]

Besides the compression test, a tensile test in flatwise direction of the specimens can also be performed to the sandwich core. Both tests provide result of elastic modulus of the core in the normal direction of face sheets. The test standard for this purpose is:

*DIN 53 292: Testing of sandwiches; tension test in flatwise plane* [38]

For the sandwich core manufacturer, the tensile properties of the core in parallel to the face sheets are beneficial, as it is used for the quality control of the sandwich core during the fabrication process [39, p. 16]. The tensile properties of the sandwich core structure can be obtained from tensile test comply with:

*ASTM C363/C363M: Standard Test Method for Node Tensile Strength of Honeycomb Core Materials* [40]

### 2.4.3 Testing Process of Entire Sandwich Panel

The four-point flexural test can be carried out to investigate the stiffness properties of the sandwich panel. In the four-point flexural test, the specimen is subjected to a constant bending moment, and no deformation initiated by shear forces occurs in the area between two loading pins. Therefore, more accurate results for flexural stiffness of the sandwich panel can be measured. The standard for the four-point flexural test is:

*DIN 53 293: Testing of sandwiches; flexure test of flat sandwiches* [41]

### 2.4.4 Selection of Test Processes

The following table listed the test process that could be carried out and the remarks for each test process.

Table 2-9: Type of test process that could be carried out and the remarks for each test process

| Component | Type of test | Test Standard | Remarks |
|---|---|---|---|
| **Face sheet** | Tensile test (nylon) | *DIN EN ISO 527–2* | – |
| | Tensile test (CFRP) | *DIN EN ISO 527–4*<br>*DIN EN ISO 527–5* | – |
| | Flexural test (nylon) | *DIN EN ISO 178* | Fixture not available |
| | Flexural test (CFRP) | *DIN EN ISO 14125* | Shortage of fibre filament<br>Fixture not available |
| | Shear test | *ASTM D5379/D5379M* | Fixture not available |
| **Sandwich core** | Shear test | *DIN 53 294*<br>*ASTM C273/C273M* | Fixture not available |
| | Compression test | *ASTM C365/C365M* | Fixture not available |
| | Tensile test in flatwise plane | *DIN 53 292* | Fixture not available |
| | Tensile test | *ASTM C363/C363M* | Fixture not available<br>Core structure cannot be printed without the roof and floor layers (printer limitation) |
| **Sandwich panel** | Four-point flexural test | *DIN 53 293* | – |

Only tensile tests can be carried out to determine the stiffness properties of materials in the face sheet. A four-point-flexural test was chosen for the sandwich panel; therefore, it is essential to carry out the flexural tests for the face sheet materials. However, these tests could not be performed due to the limitations listed in *Table 2-9*. During the production of specimens, the layer height of both nylon and CFRP were set to very thin ($0.125mm$). Hence, it was assumed that the materials' elastic moduli and flexural moduli are similar. The shear test could not be conducted as well. Nevertheless, the in-plane shear modulus can be obtained from the tensile test with "$\pm 45°$" layer orientation in the specimens.

As for the sandwich core structure, none of the test processes listed above can be conducted due to the limitation of test fixtures and the predefined settings of the printer.

The core structure can only be printed with the roof and floor layers, which can be considered as the face sheets of a sandwich panel. Therefore, the four-point flexural test in accordance with DIN 53 293 was selected to test the sandwich core structure, and the stiffness properties of the core structure can be obtained by reverse calculation of the test results.

Four test processes were selected to determine the stiffness properties of the sandwich panel's components in this thesis.

1) Tensile test under *DIN EN ISO 527–2* for nylon
2) Tensile test under *DIN EN ISO 527–4* and *DIN EN ISO 527–5* for CFRP
3) Four-point flexural test under DIN 53 293 for sandwich core structure
4) Four-point flexural test under DIN 53 293 for entire sandwich panel

# 3 Hardware and Software

This chapter includes the hardware and software used in this thesis, such as the 3D printer and its user interface, test machine with fixtures and sensors according to the test processes and the finite element analysis (FEA) software.

## 3.1 3D Printer and User Interface

### 3.1.1 Markforged Mark Two

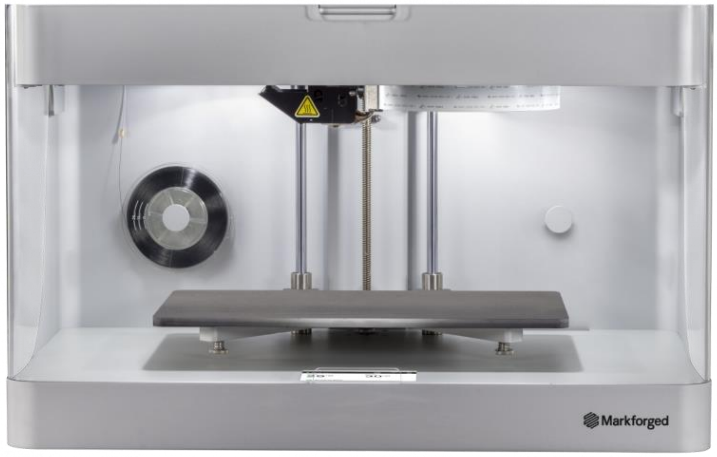


Figure 3-1: Markforged Mark Two 3D printer [42]

The Markforged Mark Two Printer is a 3D printer that can print parts in which the continuous fibres are embedded in a plastic matrix. It has a build volume of $L \times W \times H = 320 \times 132 \times 154\, mm$ and works in a double-nozzle mode: one nozzle to deposit thermoplastics filament during the printing process with the Fused Filament Fabrication (FFF) process, and the other to print the continuous fibre filament with Continuous Filament Fabrication (CFF) process [43].

Under the FFF process, the plastic filament is heated up near its melting point and then extruded out of the nozzle [44]. The plastic parts are printed layer by layer on the print bed. The CFF process is a process introduced and patented by Markforged. It is a process by which the printer embeds continuous composite fibre strands into conventional FFF thermoplastics parts with a second nozzle [44]. Based on the observation of the printing process, the round cross section fibre filament is “flattened” when it is deposited onto the print part. This process helps to improve the infill of fibres by reducing the voids in the mesostructure. Hence, the consistency of printed fibre layers and the print quality are improved. Due to the reinforcing fibres, the parts printed with CFF have higher strength and stiffness than those printed with the FFF process.

It is predefined by Markforged that the printed composite reinforced layers are surrounded by thermoplastics. This is believed to prevent the fibre from being exposed to the users and improve users' safety in case fibre breakage occurs during the printing process or

the printed parts are loaded. The downside of this predefined setting is that the printed part's overall fibre volume ratio is reduced as well as its maximum achievable mechanical strength.

### 3.1.2 Eiger

The Eiger software by Markforged is an online cloud-based slicing software compatible with the Mark Two printer. It has a simple and user-friendly interface. For the printing preparation, users can export a .stl file from computer-aided design (CAD) software, upload it into Eiger, and define the settings in the interface. The 3D model designed in CAD software is then sliced into layers in Eiger and configured based on the users' needs.

However, there are some limitations in this software, i.e., the users are not able to adjust the nozzle temperature, the extrusion rate, the printing orientation of plastic filament, the printing speed, etc. This may simplify the settings for the printing process to a certain extent. However, on the other hand, it also causes difficulties in specimen preparation and experiment planning in this thesis.

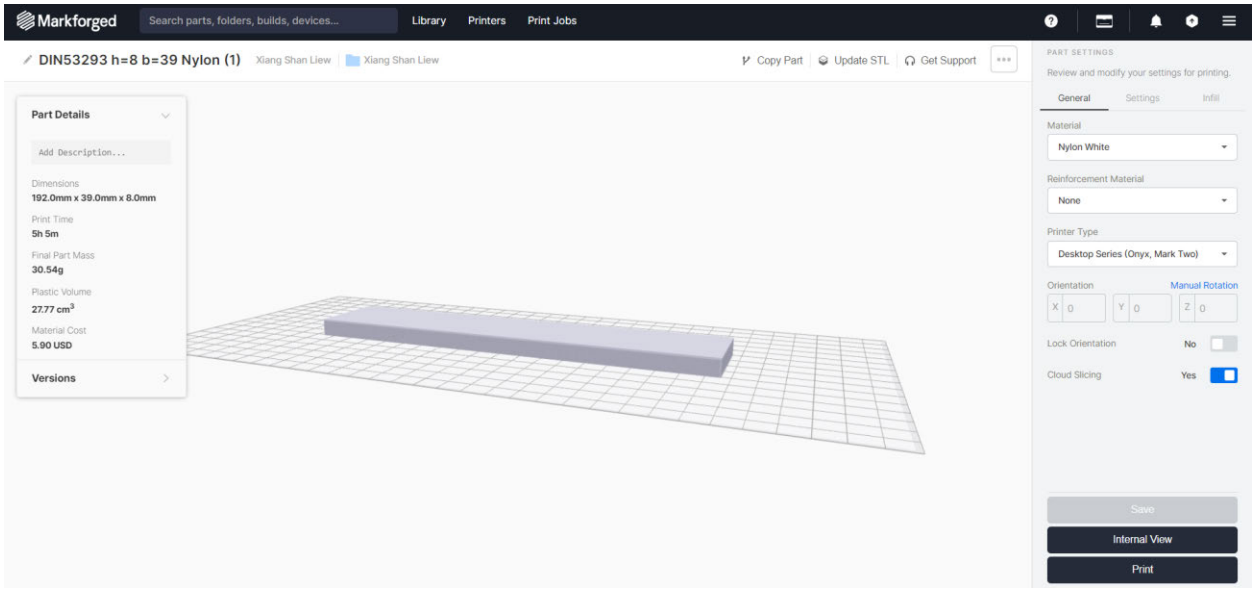


Figure 3-2: The user interface of Eiger software

The part detail such as the dimension of parts, print time, final part mass, plastic volume, fibre volume and material cost is shown on the left-hand side of the Eiger user interface. Users can define the print settings of parts at the right-hand side of the user interface under the “Part Settings” section. There are four tabs available: “General”, “Settings”, “Infill”, and “Reinforcement”.

In the “General” tab, *Figure 3-3a*, the type of thermoplastics and reinforced fibre can be selected by users. The printer type also can be chosen by users. The position and orientation of the parts can be defined by the user in this tab as well.

In the “Settings” tab, *Figure 3-3b*, Eiger offers options such as “Layer Height”, “Use Support”, “Raise Part”, “Expand Thin Features”, and “Use Brim”. When there is no reinforcement material selected in the “General” tab, the “Layer Height” can be varied by

users; otherwise, the layer height is set by default to $0.125mm$. “Brim” can be selected to prevent the warping phenomena on narrow printed parts. “Support” can be chosen to add an extra plastic column to the bottom of the desired print part in order to hold up regions of the part to maintain stability during the printing process. If the “supports” are too small to be removed, “Raise Part” can be selected.

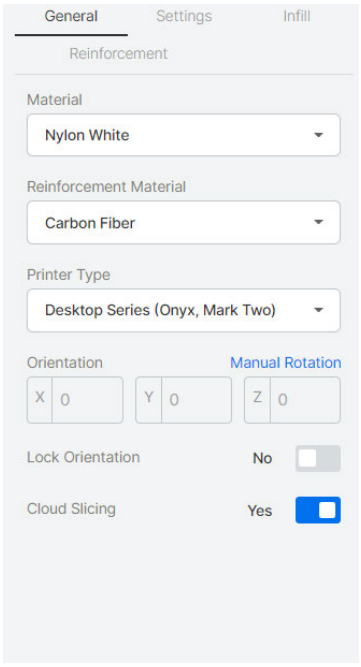


(a)

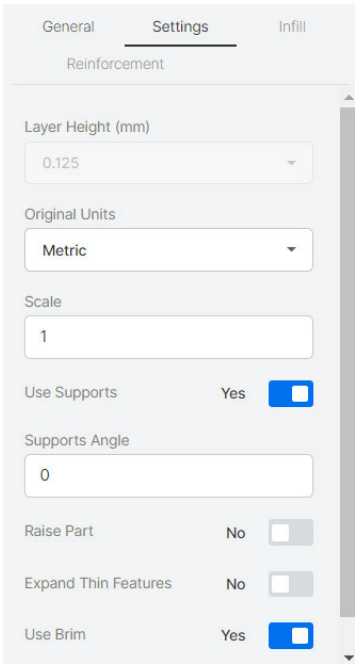


(b)

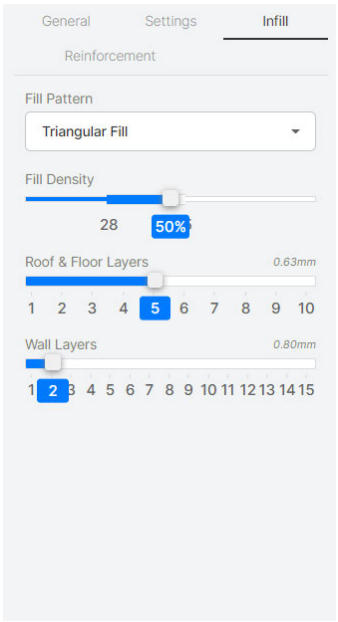


(c)

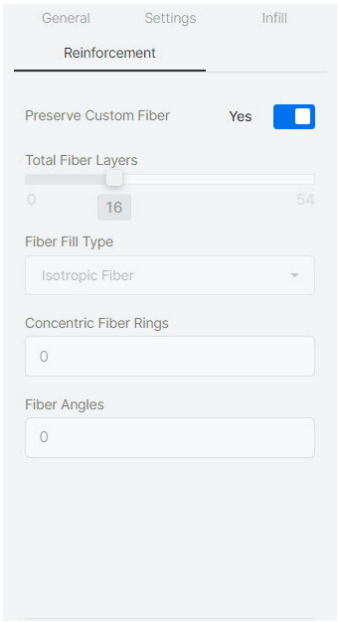


(d)

Figure 3-3: Tabs under Part Settings section in Eiger user interface: (a) “General” tab (b) “Settings” tab (c) “Infill” tab, (d) “Reinforcement” tab

In the “Infill” tab, *Figure 3-3c*, users can select the type of infill structure for the print parts. Besides, “Fill Density”, “Number of Roof & Floor Layers”, as well as “Number of Wall Layers” can also be defined by users in this tab. In this thesis, the infill structure was considered as the sandwich core's cellular structure. According to Eiger, a minimum of five layers of roof and floor layers and two wall layers shall be selected to achieve a good surface finish and watertight surface.

The “Fiber Fill Type” option is available in the “Reinforcement” tab, *Figure 3-3d*. Besides, the total number of fibre layers can also be selected. Precaution shall be taken, as a minimum of five layers of nylon will be printed at each top and bottom of the carbon layers. The fibre orientation of each print layer with fibres can be defined by users in Eiger if “Isotropic Fibre” (*Figure 3-4b*) is selected under the “Fiber Fill Type” section.

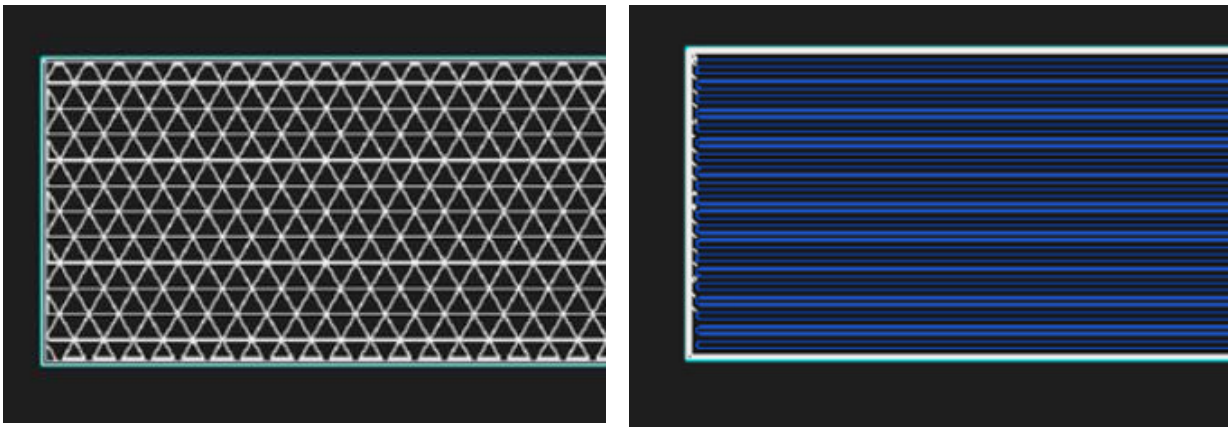

(a) “Triangular Infill” (b) “Isotropic Fiber”

Figure 3-4: Internal structure of a print part: a) “Triangular Infill” with nylon, b) “Isotropic Fiber” with carbon fibre

## 3.2 Test Machine, Fixture and Sensors

### 3.2.1 Test Machine EZ20

The EasyTest EZ20 test machine by Lloyd Instruments Ltd. - AMETEK GmbH is used to conduct both tensile and four-point-flexural tests in this thesis. The EZ20 can perform a wide range of tests up to $20kN$. It has a dual column design with up to $870mm$ crosshead travel distance and a crosshead speed range of $0.001$ to $508\,mm/min$ with $< 0.2\%$ speed deviation at steady state [45]. The test results acquired by the machine are recorded by material test and control software (NEXYGEN Ondio) which is also developed by Lloyd -AMETEK. In this software, users can define test settings and processes according to their preferences. The experimentally obtained data can then be exported from NEXYGEN Ondio to perform further analysis of the test results.

### 3.2.2 Fixture and Sensors for Tensile Test

During the tensile test for both nylon and carbon filament printed specimens, two clamps are used to hold the specimens upright in the test area of EZ20. An extensometer with 50mm gauge length was used to measure the strain in the specimens. For the load measurement, load cells of $1kN$, $5kN$, and $20kN$ were available in the Lightweight Construction Laboratory (LBL). The load cells selection process and tensile test setup are discussed in *Subchapter 5.2.1*.

### 3.2.3 Fixture and sensors for flexural test

The fixture for the four-point-flexural test consists of two parts. The upper part of the fixture with two loading pins applies compression load in the transverse direction of test specimens, and the specimen is supported by the bottom part with two support pins, as shown in *Figure 7-3*. The flexural deflections of the specimens are recorded by two position sensors, which are located at the upper and lower fixture each. The position sensor at the top fixture records the difference between the deflection of the specimen and the loading pin travel distance $(f_m - f_s)$, while the sensor at the bottom records the deflection $f_m$, see *Subchapter 7.2.1.* Unlike the tensile test, only the load cell $20kN$ is compatible with the four-point-flexural test.

## 3.3 FEA Software

Besides the tensile and four-point-flexural tests, virtual material tests with FEA software were also be conducted. MSC PATRAN version 2017.02 and MSC NASTRAN version 2017.0 by MSC Software are used in this thesis. MSC PATRAN is the most widely used pre- and postprocessing software and is compatible with majority of the solvers used in the industry. It serves as a user graphic interface for building models for a wide range of finite element solutions, as well as displays detailed simulation results in image form [46]. On the other hand, MSC NASTRAN is a numerical equation solver for the simulation of linear and non-linear static, dynamic, buckling and thermal analysis [47].

# 4 Mathematical Fundamental and Theory

This subchapter summarises the important mathematical theory used for theoretical estimation of the stiffness properties of the specimens as well as test results calculation in this thesis, including micromechanics of composite materials, macromechanics of composite materials, determination of stiffness properties of a sandwich core material, and the determination of flexural and shear stiffness of a sandwich panel.

## 4.1 Micromechanics of Composite Material

In micromechanics of composite material, material properties of a unidirectional (UD) lamina ( $E_1, E_{2,} G_{12}, \nu_{12}, \nu_{23}$) can be determined from the properties of fibres ($E_{f1}, E_{f2,} G_{f12}, \nu_{f12}, \nu_{f23}$) and matrix ($E_m, G_m, \nu_m$) used, as well as the fibre volume ratio $\phi$ in the lamina. Following are the equations to determine the material properties of UD lamina:

The Elastic modulus of the lamina in the fibre direction according to the rule of mixtures [4, p. 190]

$$E_1 = E_{f1}\,\phi + E_m\,(1-\phi) \tag{4.1}$$

with the fibre volume ratio, $\phi$

$$\phi = \frac{V_f}{V_m} = \frac{A_f}{A_m} = \frac{t_f}{t_m} \tag{4.2}$$

which $V, A, t$ represent the volume, crosssection and thickness of fibre or matrix in the UD lamina, respectively.

In order to obtain accurate estimation values of the lamina material properties, Elastic modulus of the lamina in the transverse direction by *Puck* $E_2$ [4, p. 190] and in-plane shear modulus corrected by *Förster* $G_{12}$ [4, p. 197] are applied:

$$E_2 = \frac{E_m}{1-{\nu_m}^2} - \frac{1+0.85\,\phi^2}{(1-\phi)^{1.25} + \frac{E_m}{(1-{\nu_m}^2)\,E_{f2}}\,\phi} \tag{4.3}$$

$$G_{12} = G_m \cdot \frac{1+0.4\,\phi^{0.5}}{(1-\phi)^{1.45} + \frac{G_m}{G_{f12}}\,\phi} \tag{4.4}$$

With

$$G_m = \frac{E_m}{2(1+\nu_m)} \tag{4.5}$$

The major Poisson's ratio of the lamina $\nu_{12}$ can be obtained from the rule of mixtures [4, p. 199]

$$\nu_{12} = \nu_{f12}\,\phi + \nu_m\,(1-\phi) \tag{4.6}$$

And the relation between major $\nu_{12}$ and minor Poisson's ratio $\nu_{21}$ can be expressed as [48, p. 65]

$$\frac{\nu_{12}}{E_1} = \frac{\nu_{21}}{E_2} \tag{4.7}$$

For the case of thick plate or lamina, the Poisson's ratio according to *Foye* $\nu_{23}$ [4, p. 201] and out-of-plane shear modulus $G_m$ [4, p. 202] of the lamina are also be considered.

$$\nu_{23} = \phi\,\nu_{f23} + (1-\phi)\,\nu_m \left[\frac{\left(1+\nu_m - \nu_{12}\,\frac{E_m}{E_1}\right)}{\left(1-{\nu_m}^2 + \nu_m\,\nu_{12}\,\frac{E_m}{E_1}\right)}\right] \tag{4.8}$$

$$G_{23} = \frac{E_2}{2(1+\nu_{23})} \tag{4.9}$$

## 4.2 Macromechanics of Composite Material

The stiffness properties of a composite laminate are determined by the macromechanichs theory of composite material, including the Classical Laminate Theory (CLT) for the case of thin plate and shell structures and First Order Deformation Theory (FSDT) for thick plates.

### 4.2.1 Classical Laminate Theory (CLT)

In Classical Laminate Theory (CLT), the laminate is assumed to be very thin, and the transverse (out-of-plane) shear deformation effects are negligible. Due to the low plasticity of a composite laminate, its material properties can be described by the ideal elastic material law (Hook's Law). The stress-strain $(\sigma - \varepsilon)$ behaviour of the laminate is then described with the stiffness matrix $[C]$ as:

$$[\sigma] = [C]\,[\varepsilon] \tag{4.10}$$

For an UD lamina that has transverse isotropic material properties, the reduced stiffness matrix $[Q']$ is obtained from the parameters discussed in the previous subchapter and formulated as [48, pp. 71-72]:

$$[Q'] = \begin{bmatrix} Q'_{11} & Q'_{12} & 0 \\ Q'_{12} & Q'_{22} & 0 \\ 0 & 0 & Q'_{66} \end{bmatrix} \quad 4.11$$

Which

$$Q'_{11} = \frac{E_1}{1 - v_{12}v_{12}} \; ; \; Q'_{22} = \frac{E_2}{1 - v_{12}v_{12}} \; ;$$
$$Q'_{12} = \frac{v_{12}E_2}{1 - v_{12}v_{12}} = \frac{v_{21}E_1}{1 - v_{12}v_{12}} \; ; \quad 4.12$$
$$Q'_{66} = G_{12}$$

A composite laminate is formed by stacking several laminae with different fibre orientations, see *Figure 4-1b*. Thus, the description of stiffness properties of a laminate is resulted from the sum of the stiffness matrix of each member lamina. Due to the variation of fibre orientation in the laminae, the stiffness matrix of each lamina is required to be transformed from the coordinate system of each lamina (local) into the coordinate system of the laminate (global), see *Figure 4-2.*

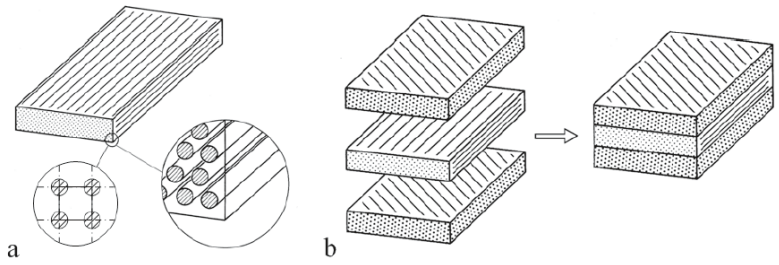


Figure 4-1: (a) Unidirectional Lamina (b) Formation of composite laminate from several unidirectional laminae [4, p. 15]

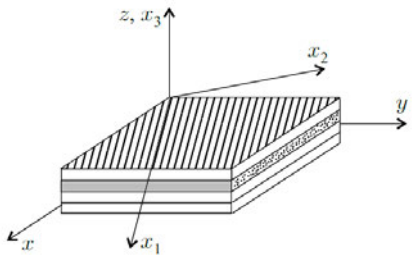


Figure 4-2: The global ($x$, $y$, $z$) and local ($x_1$, $x_2$, $x_3$) coordinate systems [49, p. 4]

The transformation of the reduced stiffness matrix of a lamina is expressed as [4, p. 212]:

$$[Q] = [T]^{(\sigma)}_{1,2\rightarrow x,y} \; [Q'] \; [T]^{(\varepsilon)}_{x,y\rightarrow 1,2} \quad 4.13$$

With the transformation matrix $[T]$ and fibre orientation $\alpha$ [48, pp. 74-77]:

$$[T]_{1,2\to x,y}^{(\sigma)} = \begin{bmatrix} \cos^2\alpha & sin^2\alpha & -2\sin\alpha\cos\alpha \\ sin^2\alpha & \cos^2\alpha & 2\sin\alpha\cos\alpha \\ \sin\alpha\cos\alpha & -\sin\alpha\cos\alpha & \cos^2\alpha - sin^2\alpha \end{bmatrix};$$

$$[T]_{x,y\to 1,2}^{(\varepsilon)} = \begin{bmatrix} \cos^2\alpha & sin^2\alpha & \sin\alpha\cos\alpha \\ sin^2\alpha & \cos^2\alpha & -\sin\alpha\cos\alpha \\ -2\sin\alpha\cos\alpha & 2\sin\alpha\cos\alpha & \cos^2\alpha - sin^2\alpha \end{bmatrix} \qquad 4.14$$

Next, the stiffness matrix of the laminate (ABD-Matrix) can then be obtained from the combination of the transformed stiffness matrix of the laminae, refer to *equation 4.15*. *Figure 4-3* shows the schema of a composite laminate, which the laminate has a thickness $h$, and $z_i$ represents the distance away from the reference plane, $z = 0$.

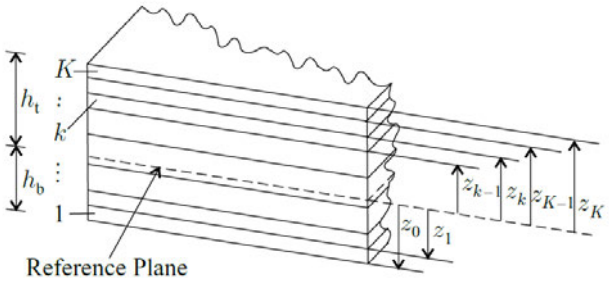


Figure 4-3: Geometry of laminate with $K$ layers [49, p. 69]

$$[ABD] = \begin{bmatrix} [A] & [B] \\ [B] & [D] \end{bmatrix} \qquad 4.15$$

Which $[A]$ is the extension rigidity matrix, $[B]$ is the bending-extension(coupling) stiffness matrix, and $[D]$ represents the flexural rigidity matrix [49, p. 71]:

$$\begin{aligned} [A] &= \sum_{k=1}^{K} [Q]_k \, (z_k - z_{k-1}) \\ [B] &= \frac{1}{2}\sum_{k=1}^{K} [Q]_k \, ({z_k}^2 - {z_{k-1}}^2) \\ [D] &= \frac{1}{3}\sum_{k=1}^{K} [Q]_k \, ({z_k}^3 - {z_{k-1}}^3) \end{aligned} \qquad 4.16$$

Moreover, the law of elasticity of a composite laminate can be expressed as [4, p. 330]:

$$\begin{bmatrix} \{N\} \\ \{M\} \end{bmatrix} = \begin{bmatrix} [A] & [B] \\ [B] & [D] \end{bmatrix} \begin{bmatrix} \{\varepsilon^0\} \\ \{\kappa\} \end{bmatrix} \qquad 4.17$$

Which $\{N\}$ and $\{M\}$ are the normal force and moment distribution vectors exerted on the laminate.

In the case of symmetric laminate, the reference plane always lies on the laminate's middle plane. However, the reference plane is shifted away from the midplane for asymmetric laminate, *Figure 4-4*.

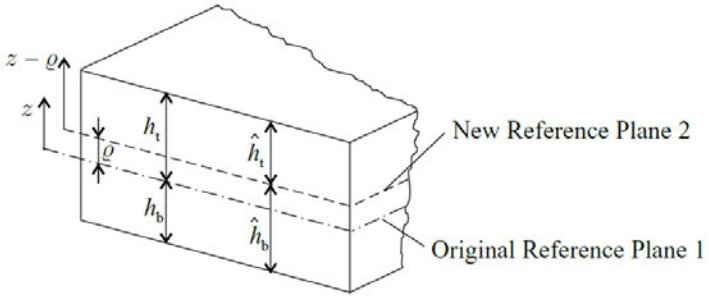


Figure 4-4: Shifting of the reference plane with the distance $\varrho$ [49, p. 80]

The stiffness matrices $[A^{\varrho}]$, $[B^{\varrho}]$, and $[D^{\varrho}]$ that are based on the shifted reference plane are expressed as follows [49, p. 80]:

$$[A^{\varrho}] = [A]$$

$$[B^{\varrho}] = [B] - \varrho[A] \qquad 4.18$$

$$[D^{\varrho}] = [D] - 2\,\varrho[B] + \varrho^2[A]$$

### 4.2.2 First Order Deformation Theory (FSDT)

In the previous subchapter, the transverse shear effects are neglected. However, in a thick wall structure, such as a sandwich panel, the transverse shears are very significant. Therefore, an extension of the CLT was developed.

The reduced transverse shear stiffness matrix of a lamina, $[Q_S']$ is written as [50, p. 3]

$$[Q_S'] = \begin{bmatrix} Q_{44} & 0 \\ 0 & Q_{55} \end{bmatrix} \qquad 4.19$$

$$Q_{44} = G_{23}\,;\; Q_{55} = G_{31} \qquad 4.20$$

And the transformation of the transverse shear reduced stiffness matrix is [50, pp. 4-5]

$$[Q_S] = [T_S]^{(\tau)}_{1,2\to x,y}\;[Q_S']\,[T_S]^{(\gamma)}_{x,y\to 1,2} \qquad 4.21$$

With

$$[T_S]^{(\tau)}_{1,2\to x,y} = \begin{bmatrix} \cos\alpha & \sin\alpha \\ -\sin\alpha & \cos\alpha \end{bmatrix};$$
$$[T_S]^{(\gamma)}_{x,y\to 1,2} = \begin{bmatrix} \cos\alpha & \sin\alpha \\ -\sin\alpha & \cos\alpha \end{bmatrix} \quad 4.22$$

Therefore the shear stiffness matrix of the laminate, $[A_s]$ is obtained [50, p. 8]

$$[A_S] = \sum_{k=1}^{K} [Q_S]_k \, (z_k - z_{k-1}) \quad 4.23$$

The material law for transverse shear is then expressed as

$$\{V\} = k \, [A_S] \, \{\gamma^0\} \quad 4.24$$

$\{V\}$ is the transverse shear forces exerted to the laminate, and $k$ is the shear correction factor. $k = \frac{5}{6}$ for a flat rectangular plate was used in this thesis.

The complete law of material in FSDT is then expressed as

$$\begin{bmatrix} \{N\} \\ \{M\} \\ \{V\} \end{bmatrix} = \begin{bmatrix} [A] & [B] & [0] \\ [B] & [D] & [0] \\ [0] & [0] & k \, [A_S] \end{bmatrix} \begin{bmatrix} \{\varepsilon^0\} \\ \{\kappa\} \\ \{\gamma^0\} \end{bmatrix} \quad 4.25$$

## 4.3 Engineering constants of Composite Laminate

The engineering constants, i.e., the Youngs's modulus, shear modulus, and Poisson's ratio of the entire composite laminate, can be determined from the stiffness matrix of laminate in CLT. The estimation of the engineering constant of the laminate can be obtained from the inversed extension stiffness matrix, $[A]^{-1}$ by dividing the elements in $[A]^{-1}$ by the total thickness of the laminate.

For the load case of tensile force, elastic modulus in the longitudinal direction of the specimens, $E_x$ can be measured. The equation for $E_x$ is as follows [4, p. 226]

$$E_x = \frac{1}{(A^{-1})_{11} \, t_{total}} \quad 4.26$$

As for the bending load case, specimens with rectangular cross sections were used in the four-point flexural test. The flexural stiffness of the composite structure is then calculated as

$$EI = D_{11}\, b \qquad 4.27$$

Similarly, the shear stiffness, $S$ of the composite structure can also be expressed as

$$S = k\, A_{S,55}\, b \qquad 4.28$$

Which $b$ is the width of the laminated composite structure.

Due to the limitation of the sensors available in LBL, only the engineering constants mentioned above can be acquired from the test. Thus, the equations for the rest of the constants are not discussed.

## 4.4 Material Properties of Sandwich Core

The stress-strain behaviour of the sandwich core can also be described with Hook's Law of elasticity, see *equation 4.10*. By assuming that the sandwich core has orthotropic material properties, the important material parameters of the sandwich core are described with the symmetric condition as follows:

Young's moduli: $E_1$ ; $E_2$ ; $E_3$

Poisson's Ratios [51, p. 27]: $\frac{\nu_{ij}}{E_i} = \frac{\nu_{ji}}{E_j}$ with $i, j = x, y, z$

Shear moduli: $G_{xy}$ ; $G_{xz}$ ; $G_{yz}$

Similar to Hook's law for the tensile load in a specimen, which elastic modulus is determined by the tensile stress, $\sigma$ and tensile strain, $\varepsilon$, the shear modulus can be obtained from shear stress, $\tau$ and shear strain, $\gamma$. Under the condition that the elastic limit is not exceeded and the shear strain is given as a very small angle, the shear stress is directly proportional to the shear strain. Thus, [52]

$$G = \frac{\tau}{\tan\gamma} \approx \frac{\tau}{\gamma} \qquad 4.29$$

*Figure 4-5* shows the schema of the sandwich core under shear deformation with shear force, $F$ and the shear strain, $\gamma$. The dimension of the sandwich core is given by $l_0 \times b_0 \times h_0$.

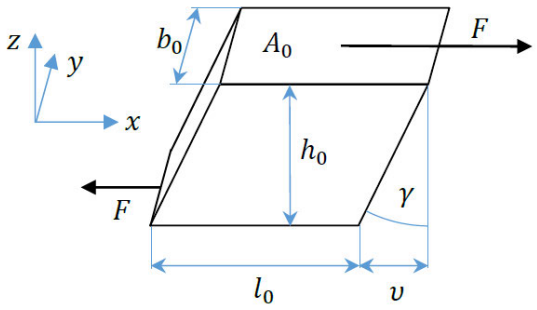


Figure 4-5: The sandwich core under shear deformation [3, p. 15]

The equation of $\tau$ and $\gamma$ can be written as [35, p. 3]

$$\tau = \frac{F}{A_o} = \frac{F}{l_o\, b_o} \tag{4.30}$$

$$\gamma = \frac{\upsilon}{h} \tag{4.31}$$

Hence, by substitution of equation *4.30* and *4.31* into *4.29*, the formula for $G$ of the core is resulted as [35, p. 3]:

$$G = \frac{h}{l_o\, b_o}\,\frac{F}{\upsilon} \tag{4.32}$$

## 4.5 Flexural Stiffness and Shear Stiffness of a Sandwich Panel

### 4.5.1 Flexural Stiffness of Symmetrical Sandwich

The symmetrical sandwich consists of face sheets with the same material properties and equal thickness. The flexural stiffness of the symmetrical sandwich panel $EI_{sym}$ can be formulated from the flexural rigidity $D_{sym}$ [1, p. 53]:

$$D_{sym} = \frac{E_{fs}\, t_{fs}^3}{6} + \frac{E_{fs}\, t_{fs}\, d^2}{2} + \frac{E_{sc}\, t_{sc}^3}{12} \tag{4.33}$$

and

$$EI_{sym} = D_{sym}\, b \tag{4.34}$$

With

$E_{fs}$ : flexural modulus of face sheet
$E_{sc}$ : flexural modulus of the core
$t_{fs}$ : thickness of face sheet
$t_{sc}$ : thickness of the sandwich core
$d$ : distance between the centroids of face sheets
$b$ : width of sandwich panel

The equation of $EI_{sym}$ can be reduced when the conditions listed below are fulfilled [41, p. 4]:

$$\frac{d}{t_{fs}} \geq 5.8 \;;\; \frac{E_{fs}\, t_{fs}}{E_{sc}\, t_{sc}} \left(\frac{d}{t_{sc}}\right)^2 \geq 16.7 \qquad 4.35$$

Hence, the reduce $EI_{sym}$ is

$$EI_{sym,reduced} = \frac{E_{fs}\, t_{fs}\, d^2\, b}{2} \qquad 4.36$$

### 4.5.2 Shear Stiffness of Sandwich

With the condition in *equation 4.35*, the shear stiffness of the sandwich panel can be estimated with [1, p. 56]

$$S = \frac{G_{sc}\, d^2}{t_{sc}} \qquad 4.37$$

# 5 Tensile Test of Nylon Specimens

The stiffness properties of the 3D printed nylon specimens were determined using the tensile test. The details of test procedures and evaluation methods for the test results are described in this chapter. Besides, the ideas of test planning, specimen production, and development of the test methods are also included in this chapter. Problem and difficulties encountered during this test session will be discussed at the end of this chapter.

## 5.1 Design and Production of Test Specimens

As mentioned in *subchapter 2.3.1*, the raster angle is similar to the fibre orientation in a UD lamina; hence, several specimens consisting of varying raster angles were designed and produced by the Markforged Mark Two 3D printer to determine the direction dependent stiffness properties of the printed nylon layers in the specimen. Three sets of specimens were decided for this purpose:

- “ $0°$ ” specimens with only 0° raster angle
- “ $0°/90°$ ” specimens with alternating 0° and 90° raster angle in each layer (0°/90° layups)
- “ $\pm 45°$ ” specimens with +45°/-45° layups

Each set consists of six pieces of specimens.

As the specimens in this test session only consist of nylon(thermoplastic) and no fibre reinforced filament was used for specimens’ production, the specimen dimension of *DIN EN ISO 527-2 Type B* was chosen for this tensile test. This type of specimen should have a total length of $150mm$ and gauge length of approximate to $50mm$. The specimens' thickness was set to $4mm$. However, due to the predefined settings by Markforged, the “ $0°$ ” specimens could not be printed. A solution was found in the master thesis of *Chen 2020* [24], in which the “ $0°$ ” specimens were printed with four walls and have a thickness of $3.2mm$ [24, p. 18].

Due to the predefined settings by Markforged, the nylon filament can only be printed with alternating $\pm 45°$ raster angle in each layer of the part. The $0°$ raster angle can only be achieved by printing with the wall layers. *Figure 5-1a-c* illustrates the internal view of the “ $0°$ ” specimen with different numbers of wall layers in Eiger. The middle part of the specimens would be printed with alternating $\pm 45°$ raster angle if the wall layers were set to two; a gap occurs in the middle of the specimens when three wall layers are defined for the printing process.

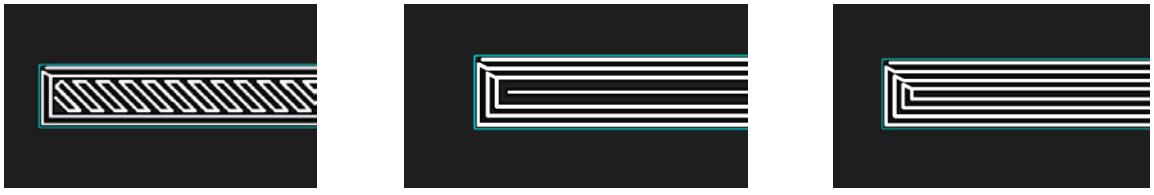

(a) (b) (c)

Figure 5-1: Internal view of the “ $0°$ ” specimen with (a) two (b) three (c) four wall layers in Eiger.

The dimensions of the specimens are summarized in *Figure 5-2* and *Table 5-1.*

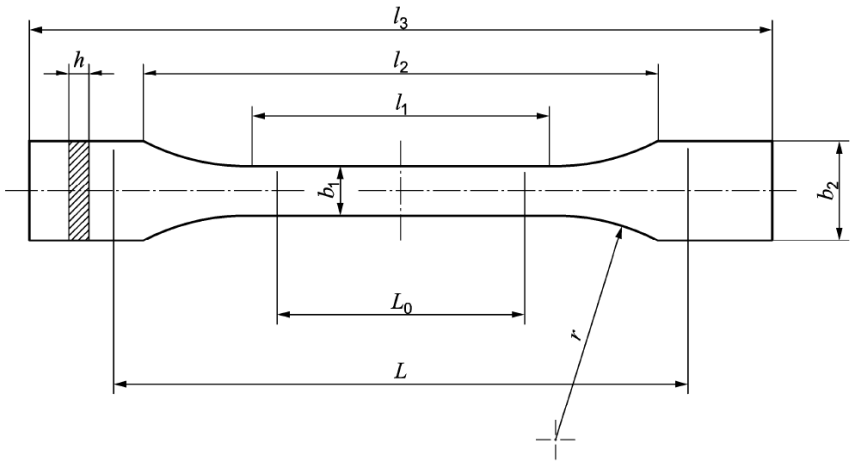


Figure 5-2: Specimens of *DIN ISO EN 527-2 Type 1B* [29, p. 8]

Table 5-1: Dimensions of specimens with printed nylon layers

| Symbol | Explanation | Dimension [mm] |
|---|---|---|
| $\boldsymbol{l_3}$ | Overall length | 150 |
| $\boldsymbol{l_2}$ | Distance between broad parallel sides | 108 |
| $\boldsymbol{l_1}$ | Length of narrow parallel-sided part | 60 |
| $\boldsymbol{b_2}$ | Width at the end | 20 |
| $\boldsymbol{b_1}$ | Width of narrow part | 10 |
| $\boldsymbol{h}$ | Thickness | 4 for “ $0°/90°$ ” and “ $\pm 45°$ ”<br>3.2 for “ $0°$ ” |
| $\boldsymbol{L_0}$ | Gauge length | 50 |
| $\boldsymbol{L}$ | Initial distance between clamps | 115 |
| $\boldsymbol{r}$ | Radius | 60 |

The 3D models in .stl format were imported into the Eiger. By changing the orientation of the specimens on the visual print bed in Eiger, different raster angles or layer orientations in the specimens can be achieved. The orientation of the specimens on the visual print bed is displayed in *Figure 5-3.* In the print settings in Eiger, the layer height of all specimens were set to $0.125mm$. Two wall layers were selected for “ $0°/90°$ ” and “ $\pm 45°$ ” specimens, but four wall layers were defined to the “ $0°$ ” specimens. All specimens were printed with solid infill. “Brim” was used to prevent warping on the specimens.

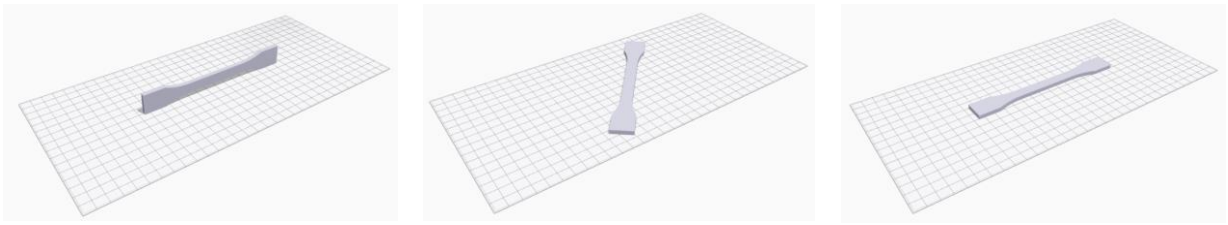

(a) (b) (c)

Figure 5-3: Orientation of specimens on Eiger visual print bed (a) “$0°$” specimens (b) “ $0°/90°$ ” specimens (c) “ $\pm 45°$ ” specimens

Precautions were taken during the production of specimens:

1. Only one specimen was printed each time to prevent:
    - repeated printing error in the specimens when the specimens are printed in a big batch
    - waste of material if the printing process is forced to stop halfway due to fatal error during the printing process
2. The specimens were let to sit on the print bed for at least 30 minutes to avoid damage of the specimens before properly cooled down and hardened.
3. “Brim” and “support” were removed carefully (and with a cutter knife if necessary) to avoid damage to the specimens by brute force.
4. One corner of the specimens was marked to assure that the specimens were fixed under the same orientation onto the test machine during test execution
5. The printed specimens are stored in an airtight container with silica gel to prevent moisture absorption. The specimens must not be stored for more than three days.

All precautions mentioned above were also applied to the other specimens in the following chapters.

## 5.2 Test Setup, Procedures and Results

### 5.2.1 Test setup

The setup of tensile test is shown in *Figure 5-4a-b*.

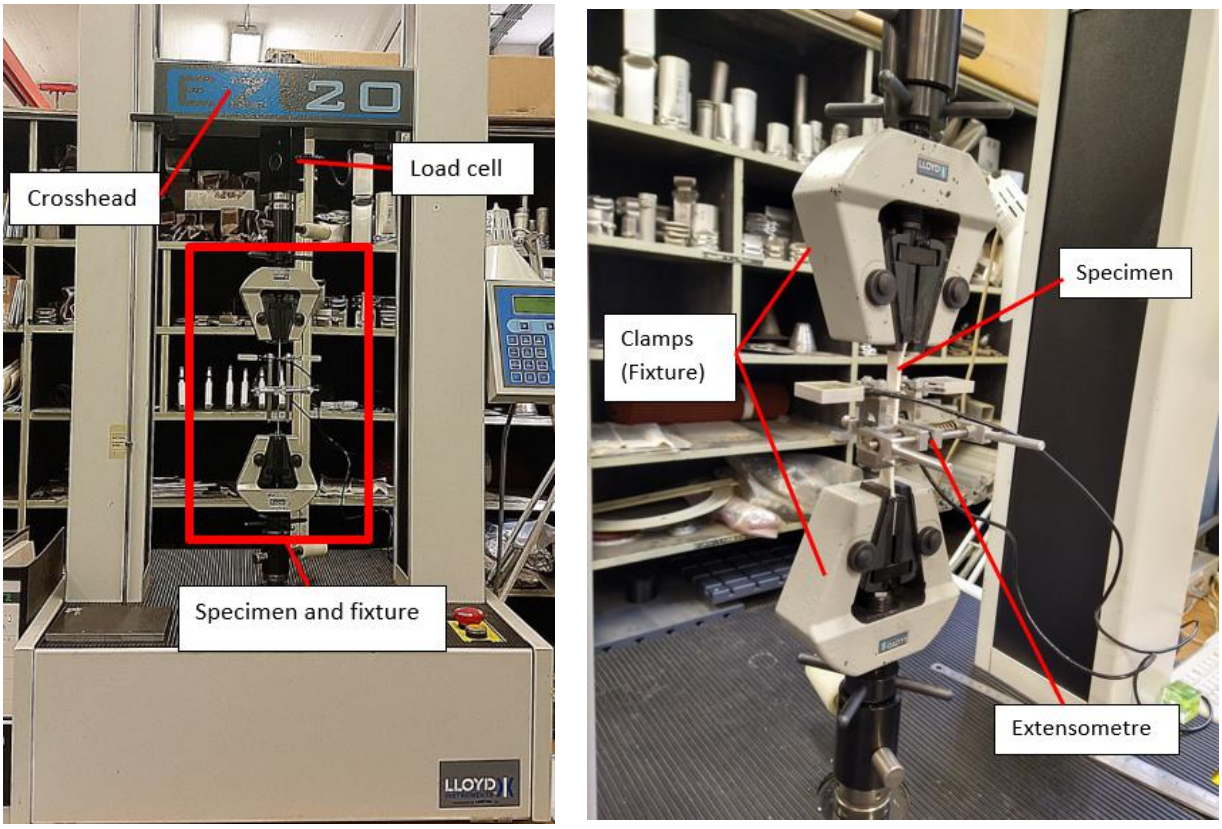


(a) (b)

Figure 5-4: (a) EZ20 test machine and tensile test setup (b) Close-up view of the test setup

As mentioned in *Subchapter 3.2.2*, three load cells are available in the LBL. Hence a simple calculation was performed to select the adequate sensor for the test. The calculation is shown as below:

$$F = E \cdot \varepsilon \cdot A$$
$$= 1700MPa \times 0.01 \times (10mm \times 4mm)$$
$$= 680N$$

Besides, a preliminary test was also carried out with the $20kN$ load cell. The maximum load acquired was around $500N$. Thus, the $1kN$ load cell was selected based on the calculation and preliminary test for the tensile test.

### 5.2.2 Test Procedures

Firstly, the dimensions of the specimens were measured and recorded before the tensile tests were conducted, refer to *Appendix A*. Then, the specimens and sensors were set up as shown in *Subchapter 5.2.1*. Same as the research of *Suer 2018* [2], a cyclic tensile load with five cycles is defined and applied to the specimens during the test. The crosshead speed $r$ was set to $1\frac{mm}{min}$ to achieve a corresponding strain rate of $1\%\ min^{-1}$ [29, p. 8]. The specimens were ensured to be fixed at the middle of clamps and aligned upright (parallel to the load path) to prevent imbalance force or torque in the specimens during the test, which will cause inaccuracy in test results. This precaution was also applied to the tensile test in *Chapter 6*.

### 5.2.3 Test Results

The tensile force exerted to specimens $F$ and elongation of the specimens $\Delta L_0$ were obtained from the test. The strain $\varepsilon$ of the specimen was calculated from $\Delta L_0$. Due to the zero error in the extensometer, measurements of $\Delta L_0$ were corrected manually. *Figure 5-5* shows examples of strain development in specimens over time. Moreover, the examples of force behaviour in specimens over time are illustrated in *Figure 5-6*.

It is observed that the strains recorded in some specimens were not returned to zero when the fixtures returned to their initial position; Besides, negative forces (compression) were also observed in the results when the fixtures were in their original position. This indicates that plasticity already occurred in the specimens during the first load cycle. Furthermore, buckling phenomena was noticed in the "$\pm 45°$" specimens, as the bottom part of the graph is "crooked". Therefore, only the results in the first load cycle were used for further analysis.

After that, the stress-strain curve in the range $0.05\% - 0.25\%$ in every specimen were plotted, refer to *Figure 5-7*. Generalised elastic modulus of the specimens along the load direction was obtained from the gradient of the linear regression line of the stress-strain plots and was used to calculate each layer's direction dependent (orthotropic) stiffness property. *Table 5-2* summarises the generalised elastic modulus of each specimen set.

Table 5-2: Generalised elastic modulus of each set of the nylon tensile test specimens and their averaged values

| Specimen No. | Generalised elastic modulus $E$ $[MPa]$ | | |
|---|---|---|---|
| | "$0°$" specimens | "$0°/90°$" specimens | "$\pm 45°$" specimens |
| 1 | 1654.200 | 1502.600 | 1465.600 |
| 2 | 1698.800 | 1376.100 | 1459.400 |
| 3 | 1688.600 | 1581.600 | 1406.600 |
| 4 | 1665.400 | 1461.800 | 1374.700 |
| 5 | 1680.500 | 1562.200 | 1460.200 |
| 6 | 1576.200 | 1581.400 | 1478.900 |
| **Average** | **1660.617** | **1510.950** | **1440.900** |

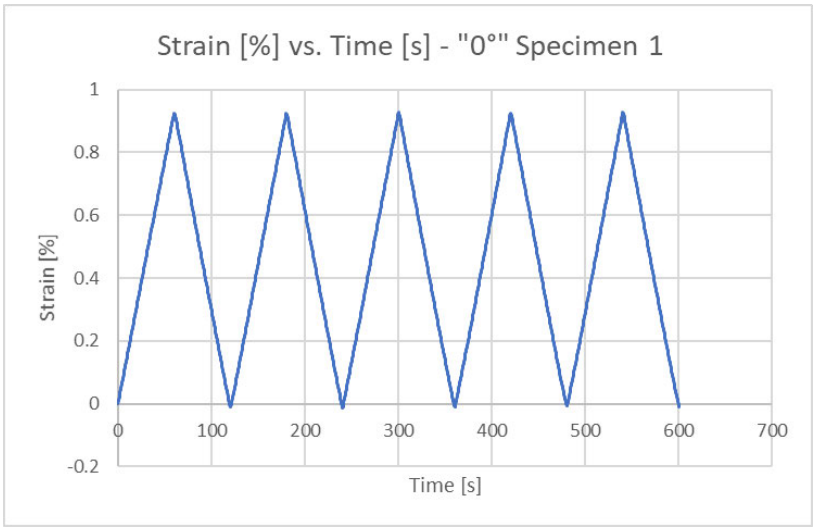


(a)

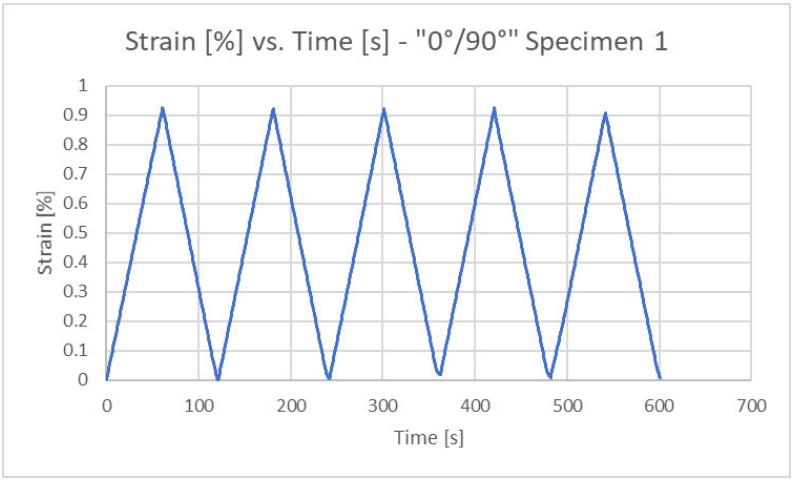


(b)

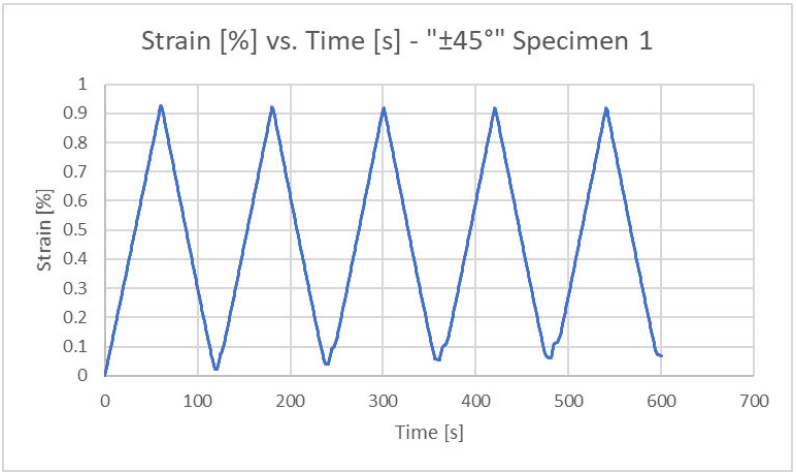


(C)

Figure 5-5: Examples of the graph of strain against time for nylon specimens (a) “ $0°$ ” specimen (b) “ $0°/90°$ ” specimen (c) “ $\pm 45°$ ” specimen

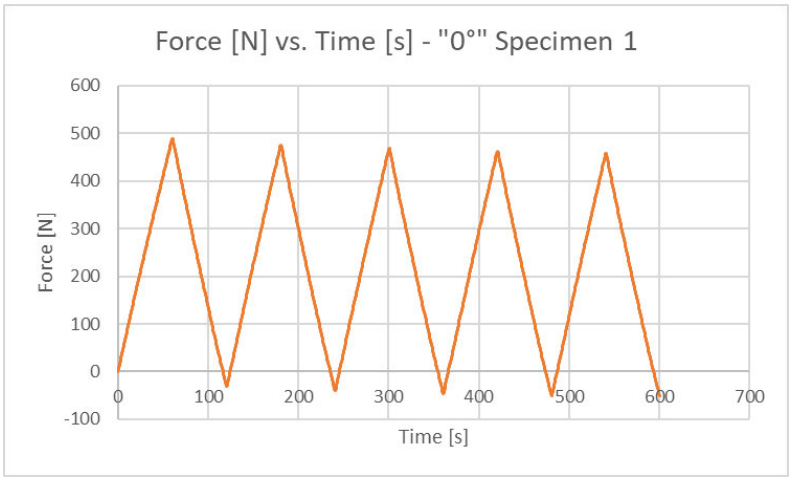


(a)

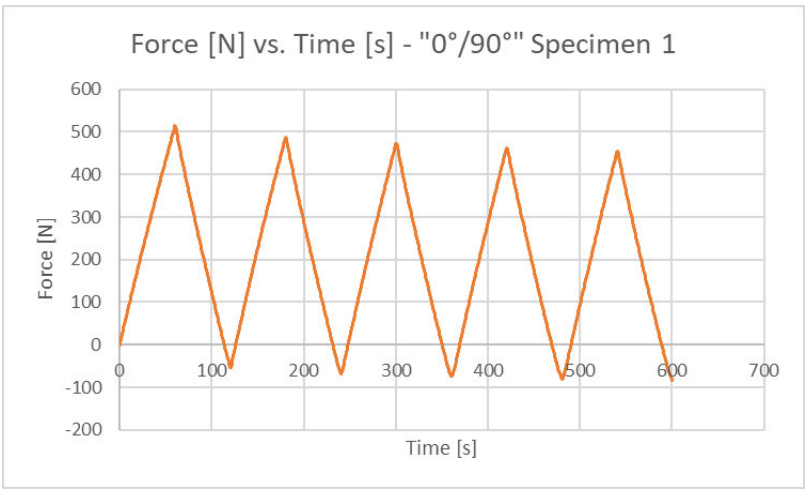


(b)

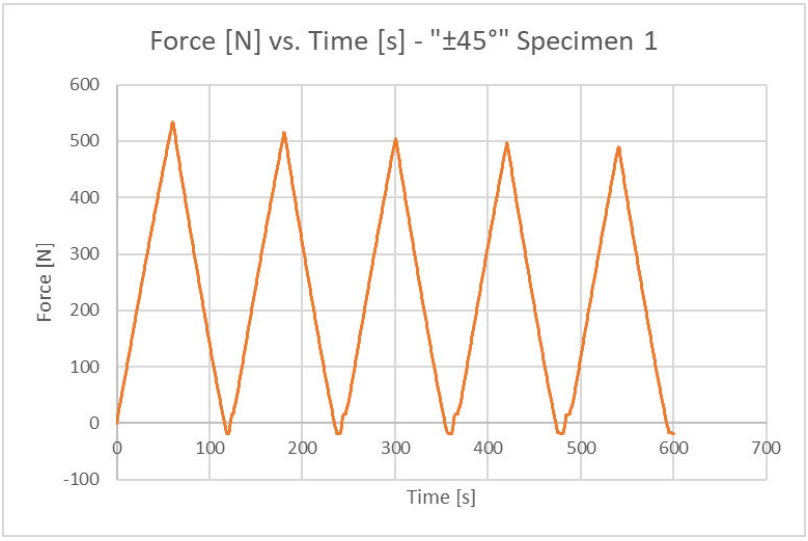


(c)

Figure 5-6: Examples of the graph of force against time for nylon specimens (a) “ 0° ” specimen (b) “ 0°/90° ” specimen (c) “ ±45° ” specimen

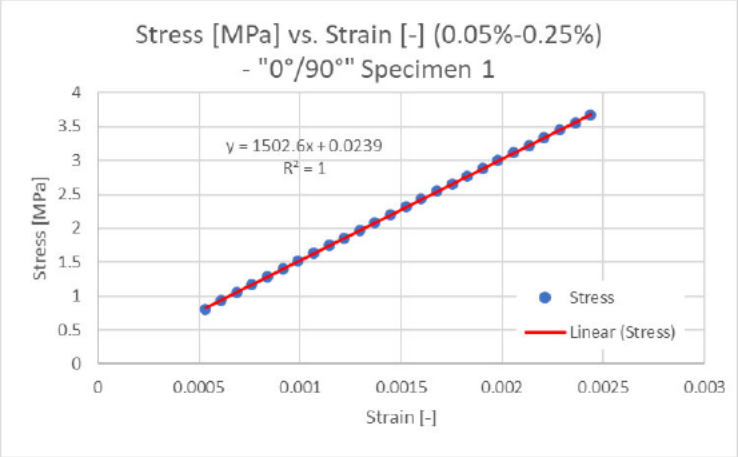


Figure 5-7: Example of the stress-strain curve within the strain range $0.05\% - 0.25\%$

Then, orthotropic stiffness properties of the printed nylon layers were determined from the generalised elastic modulus of each set of specimens with the aid of *equations 4.15* and *4.26*. An assumption value of $\nu_{n,12} = 0.4$ was used in the calculation. The orthotropic stiffness properties of the printed nylon layers are listed in the table below:

Table 5-3: Orthotropic stiffness properties of the printed nylon layers

| $\boldsymbol{\nu_{n,12}}$ $[-]$ | $\boldsymbol{E_{n,1}}$ $[\boldsymbol{MPa}]$ | $\boldsymbol{E_{n,2}}$ $[\boldsymbol{MPa}]$ | $\boldsymbol{G_{n,12}}$ $[\boldsymbol{MPa}]$ |
|---|---|---|---|
| 0.4 | 1660.617 | 1356.679 | 518.536 |

## 5.3 Evaluation and Discussion

Markforged has provided the elastic modulus of nylon in the material datasheet. However, the specimen fabrication settings (see *subchapter 2.3*) were unknown. The experimentally obtained elastic modulus of the specimens in this thesis are lower than the value given by Markforged. The $E$ of " $0°/90°$ " and " $\pm 45°$ " specimens are $> 10\%$ lower than the value given by Markforged. The difference in values can be caused by differences in the printing setting of specimens or different test standards applied. Based on the comparison, it is assumed that the nylon specimen tested by Markforged have similar settings as the "$0°$" specimen.

Table 5-4: Comparison of experimentally obtained generalised elastic modulus of the specimens with the elastic modulus of nylon given by Markforged

| **Source** | | $\boldsymbol{E}$ $[\boldsymbol{Mpa}]$ | $\boldsymbol{Diff}$ [%] |
|---|---|---|---|
| **Markforged 2021 [8]** | | 1700 | - |
| **Tensile Test** | **" 0° "** | 1660.617 | -2.32 |
| | **" 0°/90° "** | 1510.95 | -11.12 |
| | **"±45°"** | 1440.9 | -15.24 |

Due to some difficulties in calculations (see subchapter 5.4), an assumption value of $\nu_{n,12} = 0.4$ was taken. An analysis regarding the change in values of the other stiffness properties with regards to the variation of $\nu_{n,12}$ in a range $0.35 - 0.45$ was carried out.

Table 5-5: Variation of the nylon stiffness property values along with the $\nu_{12}$

| $\boldsymbol{\nu_{n,12}}$ $[-]$ | $\boldsymbol{E_{n,1}}$ $[\boldsymbol{MPa}]$ | $\boldsymbol{E_{n,2}}$ $[\boldsymbol{MPa}]$ | $\boldsymbol{G_{n,12}}$ $[\boldsymbol{MPa}]$ | $\boldsymbol{\nu_{n,21}}$ $[-]$ |
|---|---|---|---|---|
| **0.35** | 1660.617 | 1357.904 | 534.989 | 0.29 |
| **0.36** | 1660.617 | 1357.680 | 531.613 | 0.29 |
| **0.37** | 1660.617 | 1357.446 | 528.281 | 0.30 |
| **0.38** | 1660.617 | 1357.201 | 524.991 | 0.31 |
| **0.39** | 1660.617 | 1356.946 | 521.743 | 0.32 |
| **0.4** | **1660.617** | **1356.679** | **518.536** | **0.33** |
| **0.41** | 1660.617 | 1356.401 | 515.370 | 0.33 |
| **0.42** | 1660.617 | 1356.110 | 512.243 | 0.34 |
| **0.43** | 1660.617 | 1355.806 | 509.156 | 0.35 |
| **0.44** | 1660.617 | 1355.489 | 506.107 | 0.36 |
| **0.45** | 1660.617 | 1355.158 | 503.096 | 0.37 |

The variation of $\nu_{n,12}$ has not much effect on the $E_{n,1}$ and $E_{n,2}$. However, the change in $G_{n,12}$ is significant. The specimens in the following chapters were printed with $\pm 45°$ layup due to the predefined settings by Markforged. If the $\nu_{n,12}$ was wrongly assumed, the accuracy of the test results in the following chapters will be affected tremendously.

Besides, a comparison of differences in the elastic modulus of the specimens under the first and fifth load cycle was carried out, and the results are shown in *Appendix F*. It has been reported that the elastic modulus of " $\pm 45°$ " specimens tend to increase more than the other two sets of specimens. Thus, plasticity is more likely to happen in " $\pm 45°$ " specimens than the others.

## 5.4 Difficulties and Challenges

Initially, a fourth set of specimens with 90° layup was planned for the tensile test. The orientation of these specimens on the print bed is shown in *Figure 5-8*. However, due to its thin and narrow profile, several printing errors occurred during the printing process of specimens. One of the issues was that the part seemed to be overheated; a new layer of nylon was deposited before the previous layer was cooled down due to the thin and narrow profile. Besides, warping and dislocation errors also occurred during printing. Moreover, the hallway printed specimens sometimes separated from the print bed during printing by itself. Due to these problems, this set of specimens was scrapped out from the specimen list in tensile tests.

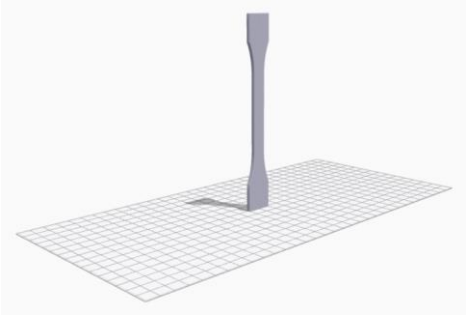

Figure 5-8: Orientation of " $90°$ "specimens on Eiger visual print bed

Besides, the calculation of the orthotropic stiffness properties of the printed nylon layers was previously planned with *equation 4.17*. Using the simplification of $\varepsilon_y^0, \gamma_{xy}, \kappa_x, \kappa_y, \kappa_{xy} = 0$, the $E_1, E_2, G_{12}, \nu_{12}$ can be determined. Through this equation, no assumption values are needed for the calculation. However, the equations are highly non-linear and could not be solved by MATLAB. This caused difficulties in determining the orthotropic stiffness properties.

Because of those two problems mentioned above, one parameter was missing to solve the orthotropic stiffness properties. Therefore, the $\nu_{12}$ value was taken from *Shürmann 2007* [4] and the equation to determine engineering constant (*4.26*) was applied to carry out the calculations. However, the extension-bending-coupling effect is neglected in *equation 4.26.* The " $0°/90°$ " and " $\pm 45°$ " specimens have an asymmetric layup; Therefore, the orthotropic stiffness properties of printed nylon layers, which were calculated with this equation, were expected to have slight inaccuracy.

During the printing of specimens, warping occurs in the " $0°$ " specimens, *Figure 5-9*. This is because the specimens are very thin. Attempts were made to fix the issue with all possible combinations of "brim", "support", and "raise parts", but the problem remains unsolved. Besides, there are some burnt marks seen on the printed specimens. A new nozzle replaced the clogged old one. The warping effect was reduced after nozzle replacement and no more burnt marks on the specimens. This issue was believed to be raised by dirty nozzle. Hence, the specimens with reduced warping were used to perform tensile tests. The inaccuracy of test results might be caused by warping in specimens.

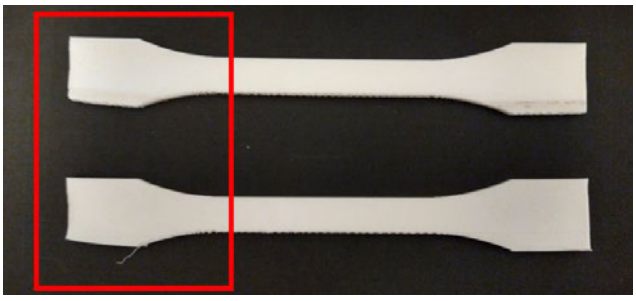

Figure 5-9: Warping in the " $0°$ " specimens

# 6 Tensile Test of Continuous Carbon Fibre Reinforced Specimens

It was discovered that there was an update on the stiffness properties of the carbon fibre filament in the material datasheet provided by Markforged. After the stiffness properties of the 3D printed nylon layers were determined, the stiffness properties of the printed CFRP layers were studied. The details of the tensile test for CFRP layers, including preparation of test specimens, test setup and procedures, test result processing and evaluation, as well as problem and difficulties encountered during the test, are discussed in this chapter.

## 6.1 Design and Production of Test Specimens

The orientation of the continuous fibre is aligned with the printing direction of the filament. When “Isotropic Fiber” is selected in Eiger during printing, the carbon filament is printed in only one direction. Hence, a printed CFRP layer can be considered as a UD carbon fibre composite lamina. Three sets of specimens were decided in this test session:

- “ $0°$ ” specimens with $[0°_8]$ layup
- “ $0°/90°$ ” specimens with $[0°\ 90°\ ]_{2s}$ layup
- “ $\pm 45°$ ” specimens with $[\pm 45°_2]_s$ layups

Symmetrical lamina layups were decided to prevent the extension-bending-coupling phenomena occurs in specimens during the test. *DIN EN ISO 527-5 Type A* specimen dimensions were selected for “ $0°$ ” specimens. Ideally, the “ $0°/90°$ ” and “ $\pm 45°$ ” specimens were supposed to be defined with the standard dimension *DIN EN ISO 527-4 Type 2* or *Type 3*. However, due to the shortage of carbon fibre filament for specimen production, the dimension *DIN EN ISO 527-5 Type A* was also selected for both “ $0°/90°$ ” and “ $\pm 45°$ ” specimens. Also, only four specimens instead of five were produced for each specimen set and tested in this test session due to carbon filament shortage. The specimens have a total length of $250mm$ and a width of $14mm$. There are two tabs at each end of the specimens; each has $1mm$ thickness. The dimension of the specimens are as follows:

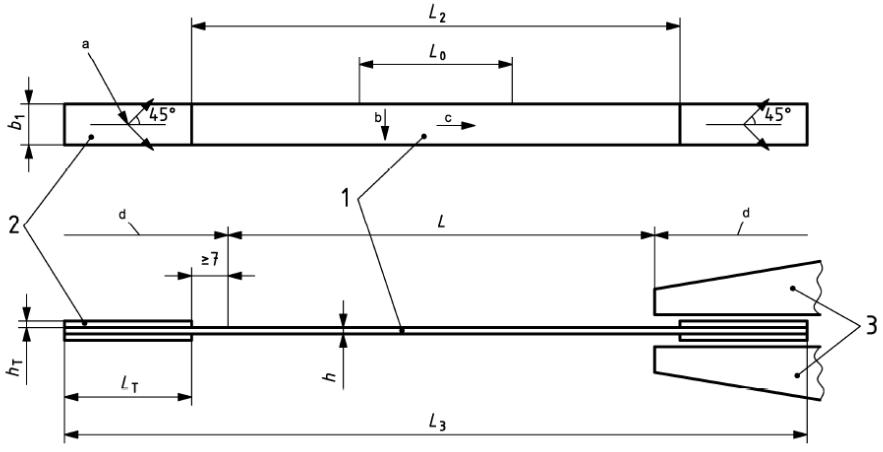


Figure 6-1: Specimens of *DIN ISO EN 527-5 Type A* [31, p. 8]

Table 6-1: Dimensions of printed CFR specimens

| Symbol | Explanation | Dimension $[mm]$ |
|---|---|---|
| $l_3$ | Overall length | 250 |
| $l_2$ | Distance between tabs | 150 |
| $b_1$ | Width | 14 |
| $h$ | Thickness | 2.25 |
| $L_0$ | Gauge length | 50 |
| $L$ | Initial distance between clamps | 136 |
| $L_0$ | Gauge length | 50 |
| $L_T$ | Length of end tabs | 115 |
| $h_T$ | Thickness of end tabs | 1 |

Generally, the dimensions of the printed carbon fibre reinforced (CFR) specimens complied with *DIN ISO EN 527-5 Type A*, except for the thickness due to the limitation of the printer and the width due to the carbon volume in the specimens. In Eiger, eight CFRP layers with isotropic fibre fill and without concentric fibre ring were defined. Two wall layers along with five layers of roof and floor made of nylon were also printed due to the predefined settings by Markforged. With eight CFRP layers, five roof layers and five floor layers, the specimens have a total thickness of $2.25mm$ (each layer has a layer height of $0.125mm$). There is no difference in the carbon filament volume used in specimens with a width of $14mm$ and $15mm$. Hence, to minimize the usage of nylon filament and reduce the print time of each specimen, the width of the specimens was set to $14mm$. The specimens were printed with “brim” to avoid warping in the specimens, and the “raise part” was used because of the narrow “support” at the bottom of the specimens. The orientation of each layer in the specimens are illustrated in *Figure 6-2.*

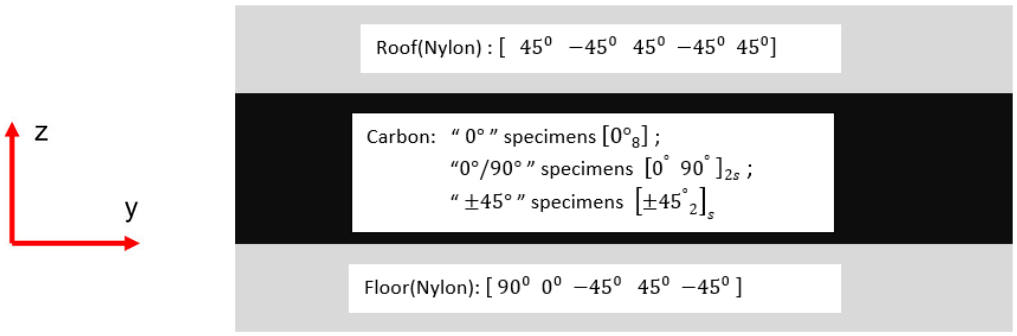


Figure 6-2: Layer orientation in the specimens

The orientation of the specimens on the print bed is illustrated in *Figure 6-3*.

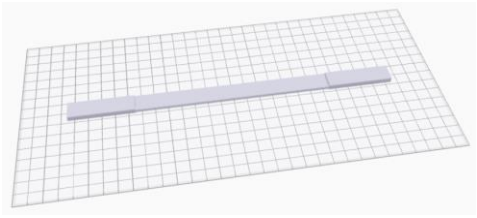

Figure 6-3: Orientation of the CFR specimens on the virtual print bed in Eiger

## 6.2 Test Setup, Procedures and Results

### 6.2.1 Test Setup

The tensile test for CFR specimens has the same setup as for nylon specimens. The close-up view of the test setup is with CFR specimens is shown in *Figure 6-4.*

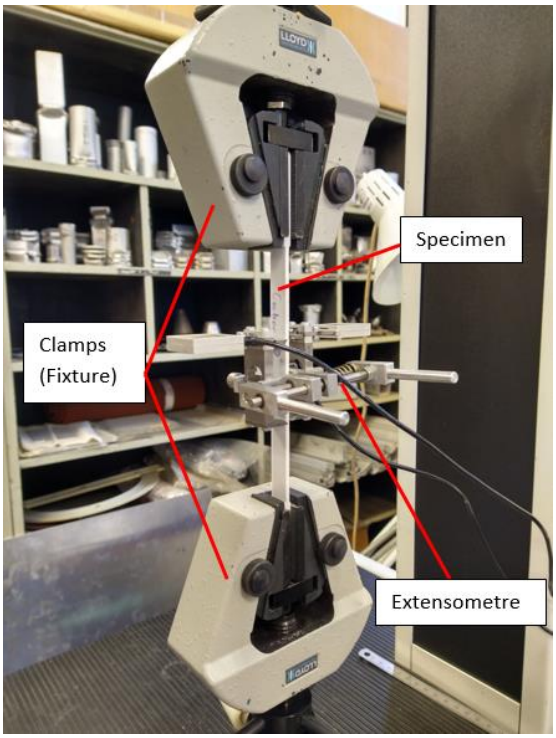


Figure 6-4: Close-up view of the test setup

As for the load cell selection, firstly, the stiffness properties of nylon obtained in *Subchapter 5.2.3* and the carbon stiffness properties obtained by *Suer 2018* [2] were applied to *equations 4.16* and *4.26,* and the generalised elastic modulus of the specimens is obtained. After that, the force was predicted similarly to the method mentioned in *Subchapter 5.2.1.* The values of $8730N$, $4905N$ and $1302N$ were obtained for "$0°$", "$0°/90°$" and "$\pm 45°$" specimens, respectively. A preliminary test was also performed, and approx. $8000N$, $4500N$ and $950N$ were obtained for "$0^{\circ}$", "$0°/90°$" and "$\pm 45°$" specimens. Therefore $20kN$ load cell was selected for the tensile test with "$0°$" specimen, $5kN$ for "$0°/90°$" specimens and $1kN$ for "$\pm 45°$" specimens.

### 6.2.2 Test procedure

A similar test procedure as described in *Subchapter 5.2.2* is applied in this session. The dimensions of the printed specimens are recorded in *Appendix B*. A five cycles cyclic tensile load with crosshead speed $r = 3\frac{mm}{min}$ and maximum crosshead displacement of $s = 3mm$ was exerted onto the specimens. The results acquired from the test were recorded and processed for further analysis.

### 6.2.3 Test Results

The results acquired from the tensile tests were corrected in the same way as described in *subchapter 5.2.3. Figure 6-5* and *Figure 6-6* show examples of the strain development over time and the force acting on the specimens over time during the tensile test. Strange patterns were observed at the bottom of both graph types, which is when the clamps return to their initial position at those points. This shows that the specimens already underwent plastic deformation when the first cycle of the tensile load was applied. Due to the plastic deformation, specimens were not able to return to their original length, and when the clamps returned to the initial position, the specimens were compressed. Buckling phenomena was found in some of the results.

Due to the plastic deformation and buckling phenomena, only the results of the first loops were taken to plot the stress-strain curve with a range of strain $0.05\% - 0.25\%$ to determine the generalised elastic modulus of each specimen. The results are summarised in *Table 6-2.* The deviations of experimentally obtained elastic modulus in each specimen set were studied. The " $0^{\circ}$ " specimens have the deviation of approx. $9\%$, " $0°/90°$ " specimens have approx. $2\%$ and " $\pm 45°$ " specimens have $7\%$.

Table 6-2: Generalised elastic modulus of each set of CFR tensile test specimens and their averaged values

| *Specimen No.* | Generalised elastic modulus $E$ $[MPa]$ | | |
|---|---|---|---|
| | " $0°$ "specimens | " $0°/90°$ " specimens | "$\pm 45°$"specimens |
| *1* | 21580.000 | 12447.000 | 3467.600 |
| *2* | 21753.000 | 12650.000 | 3540.100 |
| *3* | 23600.000 | 12359.000 | 3298.000 |
| *4* | 22244.000 | 12539.000 | 3462.300 |
| *Average* | **22294.250** | **12498.750** | **3442.000** |

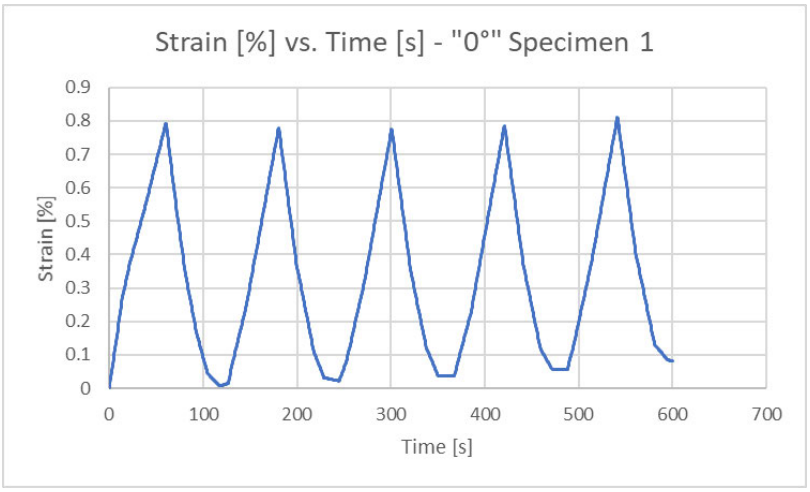


(a)

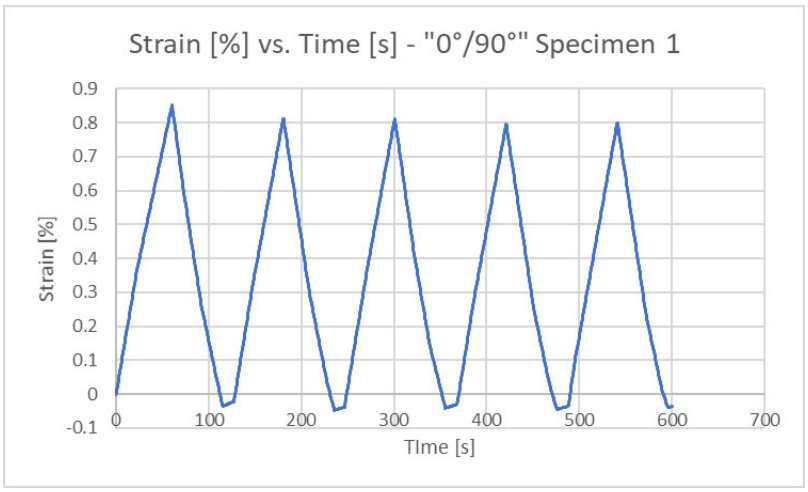


(b)

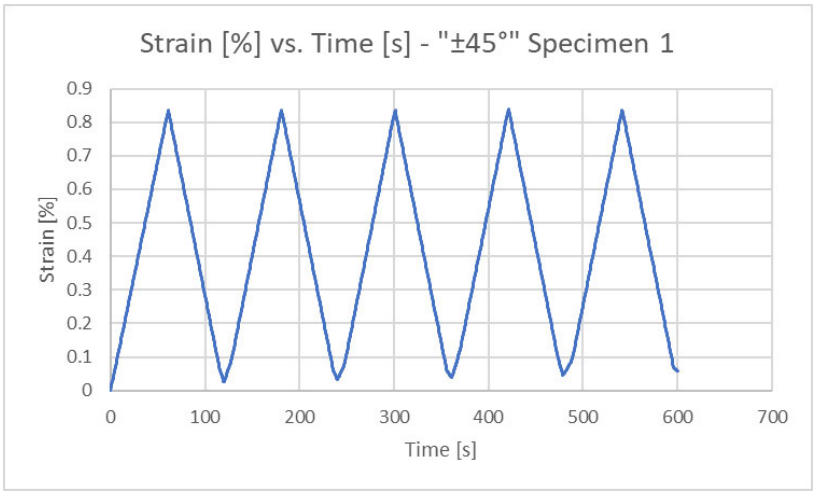


(c)

Figure 6-5: Examples of the graph of strain against time for CFR specimen (a) “ $0°$ ” specimen (b) “ $0°/90°$ ” specimen (c) “ $\pm 45°$ ” specimen

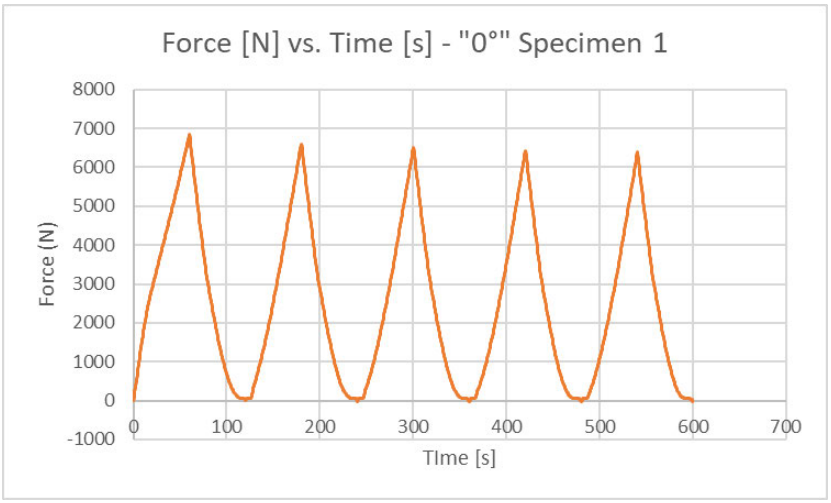


(a)

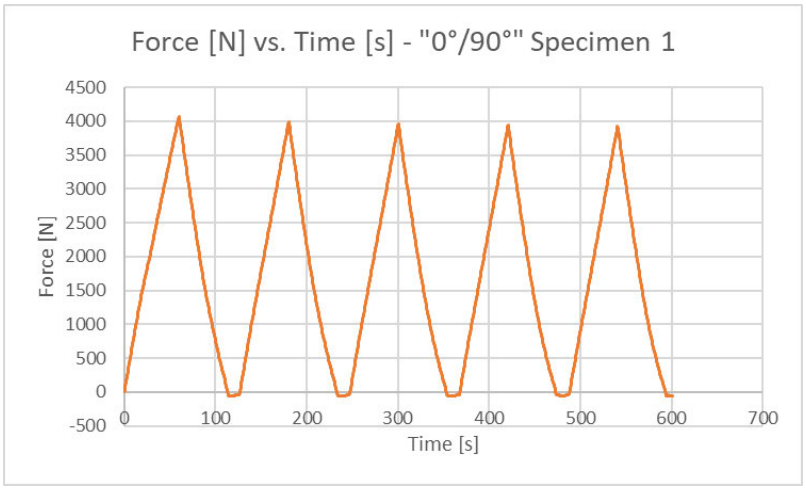


(b)

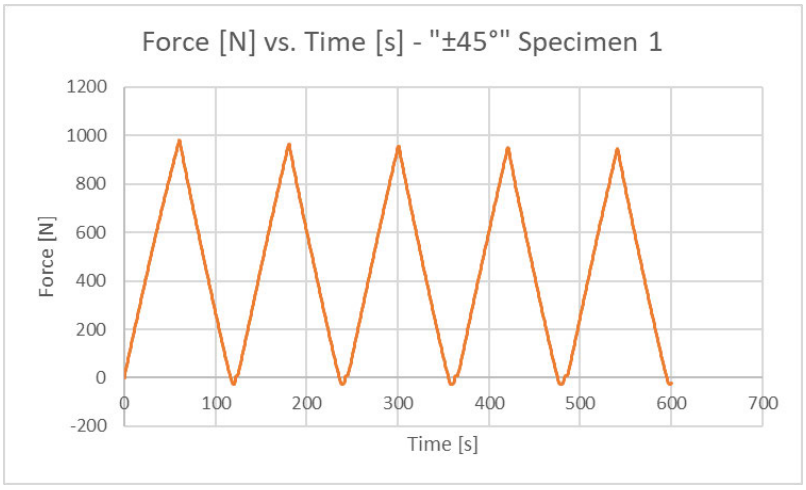


(c)

Figure 6-6: Examples of the graph of force against time for CFR specimen (a) “ 0° ” specimen (b) “ 0°/90° ” specimen (c) “ ±45° ” specimen

After the generalised elastic modulus of specimens was obtained, the elastic modulus of CFRP proportion in the specimens was calculated with *equation 2.1* and with condition $E_m = E_n$. The $\varphi$ in each specimen's set were obtained from Eiger. A model with dimension $250 \times 14 \times 2.25\ mm$ were drawn in Catia and imported into Eiger. Then, the volume of materials needed to print the specimens was then displayed in Eiger. The details of $\varphi$ and $E_c$ for each specimen set is shown in *Table 6-3*.

Table 6-3: Elastic modulus of CFRP proportion in the specimens

| SPECIMEN | VOL. OF CARBON $[cm^3]$ | VOL. OF NYLON $[cm^3]$ | $\varphi$ [%] | $E_c$ $[Mpa]$ |
|---|---|---|---|---|
| **" 0° "** | 2.74 | 4.55 | 37.59 | **56899.320** |
| **" 0°/90° "** | 2.66 | 4.58 | 36.74 | **31513.665** |
| **"±45°"** | 2.61 | 4.74 | 35.51 | **7050.297** |

After that, orthotropic stiffness properties of the printed CFRP layers were calculated with *equations 4.15* and *4.26.* An assumption value of $\nu_{c,12} \approx 0.36$ which was obtained based on micromechanics theory was used in the calculation. Based on the test results, $\phi \approx 0.24$ was estimated with micromechanics theory. The experimentally obtained orthotropic stiffness properties of the printed nylon layers are listed in the table below:

Table 6-4: Orthotropic stiffness properties of the printed CFRP layers

| $E_{c,1}$ $[MPa]$ | $E_{c,2}$ $[MPa]$ | $G_{c,12}$ $[MPa]$ | $\nu_{c,12}$ $[-]$ |
|---|---|---|---|
| 56899.320 | 5585.024 | 1968.613 | 0.36 * |

* calculated based on micromechanics theory

## 6.3 Evaluation and Discussion

Then, the test results were compared with the values estimated with micromechanics theory in *subchapter 4.1.* It was discovered that there are significant differences in $E_{c,2}$ and $G_{c,12}$ from both methods. The difference of values is likewise caused by the carbon filament loops printed at the edges of the specimens, *Figure 6-7*. When the nozzle reaches the edge of the printed part, it makes a u-turn, resulting in the carbon filament loops at the edge. These loops provide extra tensile and shear stiffness to the specimens. This also explains why the assumption by *Suer 2018* [2] regarding $E_{c,2}$ and $G_{c,12}$ with $\phi = 0.65$ were close to the test results.

Table 6-5: Comparison of tensile test results with micromechanics theory calculations

| Method | $\phi$ $[-]$ | $E_{c,1}$ $[MPa]$ | $E_{c,2}$ $[MPa]$ | $G_{c,12}$ $[MPa]$ | $\nu_{c,12}$ $[-]$ |
|---|---|---|---|---|---|
| **Tensile test** | 0.24 | 56899.320 | 5585.024 | 1968.613 | 0.36 |
| **Micromechanics** | 0.24 | 55914.400 | 2920.267 | 1076.355 | 0.36 |

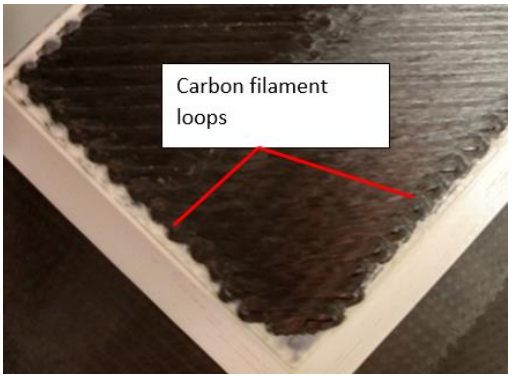


Figure 6-7: carbon filament loops printed at the edge of specimens

Compared with the other literature listed in *subchapter 2.2.2*, the experimentally obtained elastic modulus of printed CFRP layers is relatively low. Besides, the experimental obtained $E_{c,1}$ is approximate $5.2\%$ lower than the value of elastic modulus provided by *Markforged 2021* [8]. This issue might be caused by the low CFRP proportion in the specimen. Another reason for this problem is that the carbon filament spool was already wet before printing the specimens, or the specimens were damaged before the test started. There was no information on how long the carbon filament spool had been opened and how long it was installed onto the printer. To prevent this issue, the carbon filament spool should be stored in an airtight container with desiccant when it is not used and labelled with the date on which the package was open.

It was later discovered that the crosshead speed was mistakenly set too high and resulted in a higher strain rate than the one prescribed in standard *DIN EN ISO 527-5* in specimens. The plasticity and buckling issue mentioned in the previous subchapter might be caused by this mistake. However, when the strain rate is higher, a higher elastic modulus of CFRP will be obtained from the tensile test [53, pp. 210-211]. This statement contradicts the previous paragraph's observation, which the result obtained during the tensile test is lower than the other literature. This supports the point that wet carbon filament was used to fabricate the specimens.

Same as the previous chapter, the elastic modulus of the specimens under the first and fifth load cycle was also studied, results are shown in *Appendix G*. A reduction in elastic modulus was discovered in some of the specimens. This phenomenon can be explained by fibre breakage during the tensile test. The “ $0^{\circ}$ ” specimens have the most reduction with a maximum reduction value of $17.58\%$, followed by “ $0°/90°$ ” with maximum reduction value of $10.28\%$ and “ $\pm 45°$ ” specimens have the least reduction with reduction value of $0.40\%$.

## 6.4 Difficulties and Challenges

During the fabrication of specimens, a few problems occurred. Warping occurred while the specimens were printed despite the usage of “brim” to increase the contact area between printed parts and print bed. “Support” with different angles were also tried out: “support” with $45°$ initiated twisting in the specimens, “support” with $90°$ are tough to be removed, and “support” angle $0°$ brought no improvement to the warping situation. Besides, the removal process of “support” and “raise part” was challenging. A cutter knife was used to avoid damage to the specimens while removing those parts by pulling them.

Nevertheless, the cutter knife was not helpful. The removal of “support” and “raise part” might also cause some damage to the specimens.

A rough surface at the bottom of the specimens was observed after removing the “support” and “raise part”. This issue only occurs at the bottom of the specimens, and the top layer of specimens has good surface quality, see *Figure 6-8*. Attempts with different print settings were implemented to fix this issue. However, the issue was not fixed. Therefore, it is assumed that this issue is caused by the predefined setting by Markforged and cannot be corrected. As a result, the tensile tests were conducted with these faulty specimens. This error might lead to the wrong estimation of elastic modulus of CFRP proportion in the specimens based on rules of mixture.

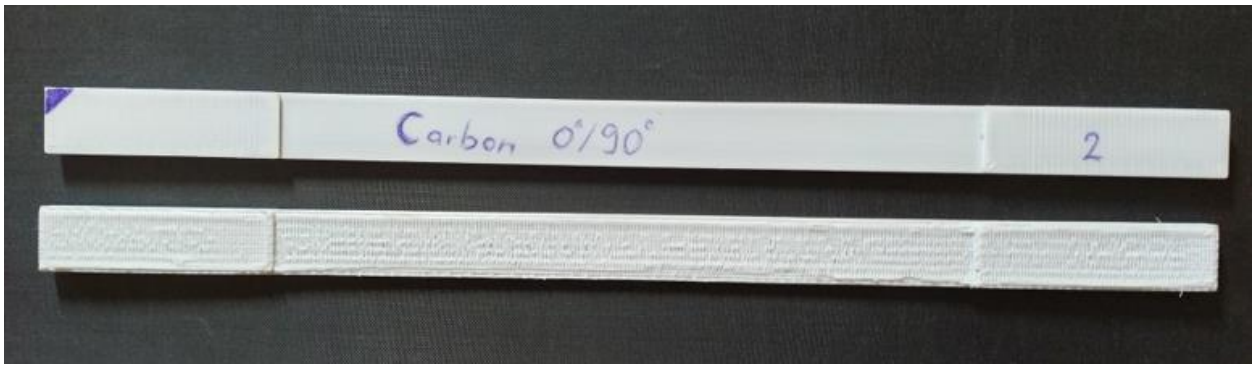


Figure 6-8: Comparison of top and bottom surface quality of the specimens

Initially, a fourth specimen set with $[0° \pm 45° \ 90°]_s$ CFRP layup was planned for the tensile tests in this session. However, this specimen set was removed from the specimen list and not tested due to the shortage of carbon filament, which led to insufficient data to calculate the orthotropic properties of the printed CFRP layers. Thus, a theoretical value $\nu_{c,12} \approx 0.36$ based on micromechanics theory was applied in the calculation.

It was also observed from the material datasheet from Markforged that there were changes in the stiffness properties of the carbon filament. There was no information regarding which batch of the carbon filament spool was used. An assumption was made that the carbon filament spool of batch 2018 was used.

# 7 Four-Point Flexural Test of Nylon Sandwich Core

Several types of infill structures can be printed by Markforged Mark Two 3D printer, and the infill was assumed as the cellular structured core of a sandwich panel. A four-point flexural test was conducted in this session to study the (flexural) stiffness property of the printed nylon infill/sandwich core. The details of the test, as well as FE modelling and simulation of the infill/sandwich core, are discussed in this chapter.

## 7.1 Design and Production of Test Specimens

Due to the limitation in Eiger, the infill structure can only be printed with a minimum of five layers of roof and floor. Thus, the printed specimens have a structure similar to a sandwich panel. The roof and floor were then assumed to be the face sheets; meanwhile, the infill was assumed as the core. Therefore, a four-point flexural test under standard *DIN 53 293* [41] was selected to determine the stiffness properties of the core.

A few factors were considered while designing and dimensioning the specimens:

- Build volume of Mark Two printer $L \times W \times H = 320 \times 132 \times 154\ mm$ , *Subchapter 3.1.1*
- Dimension of specimens prescribed in DIN 53 293 $L \times W \times H = 24h \times 2.5h \times h\ mm$ [41, p. 2]
- The loading and support pins shall have a diameter of range 0.5 – 1.5 times the thickness of the specimen $h$ [41, p. 2]. The narrowest pins available in the laboratory has a diameter of $10mm$.
- The specimens must contain at least nine cellular structural units width wise [41, p. 2]
- Five layers of roof and floor printed each above and below the infill structure(core)
- The conditions expressed in *equation 4.35* must not be (fully) fulfilled to calculate the core's stiffness properties

The $h$ was not specified. Thus, based on the factors above, the specimen dimension of $L \times W \times H = 192 \times 39 \times 8\ mm$ was decided. Bigger specimens would deliver better test results; however, this would increase the printing time and material consumption.

As mentioned in *Subchapter 2.3.3,* the stiffness properties of the specimens can be influenced by the infill shape and fill densities. It was decided to use the same infill type and fill density as *Suer 2018* [2], which is triangular infill with $50\%$ fill density.

Three specimens and a practice piece were printed in this session. The cross section and details of the specimens are shown in *Figure 7-1.* All these pieces were printed using “brim” to prevent warping. Figure 7-2 shows the specimen orientation on the print bed.

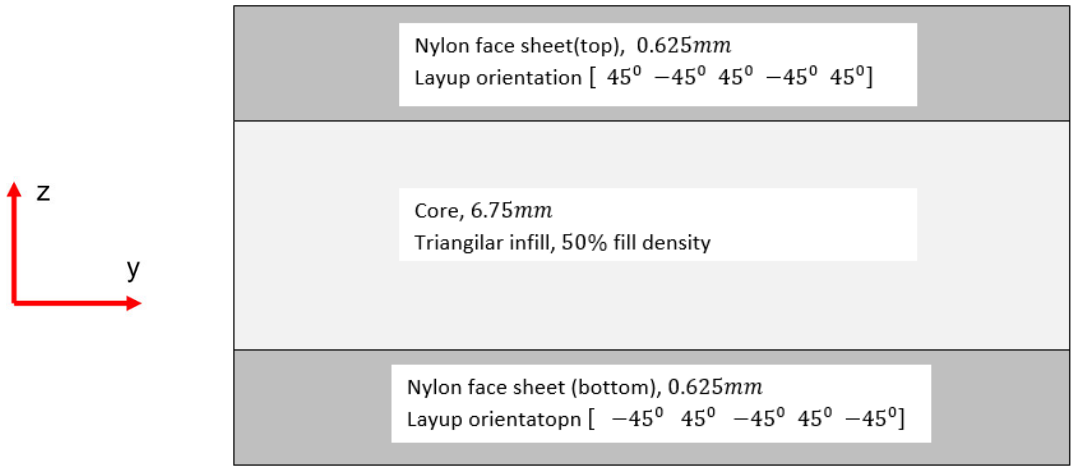


Figure 7-1: Cross section of the nylon sandwich core specimens

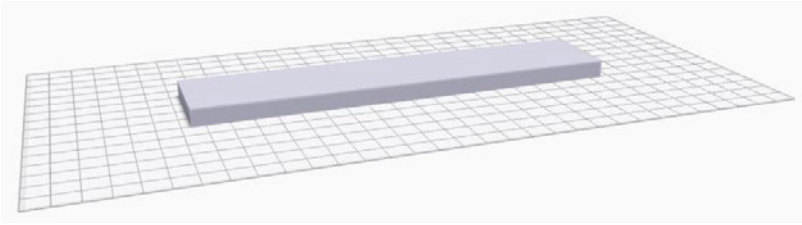

Figure 7-2: Orientation of the nylon sandwich core specimen on the virtual print bed in Eiger

## 7.2 Test Setup, Procedures and Results

### 7.2.1 Test Setup

The setup of the four-point flexural test is displayed in *Figure 7-3a & b.* The distances between the loading pins and also the support pins were adjusted according to *DIN53 292* [41] based on the thickness of the specimens, see *Figure 7-4.*

The specimens were placed in between the upper and lower fixtures. To avoid imbalance load exerted onto the specimens during the test, the specimens were ensured to be aligned parallelly to the fixtures and were placed in the middle of the load path.

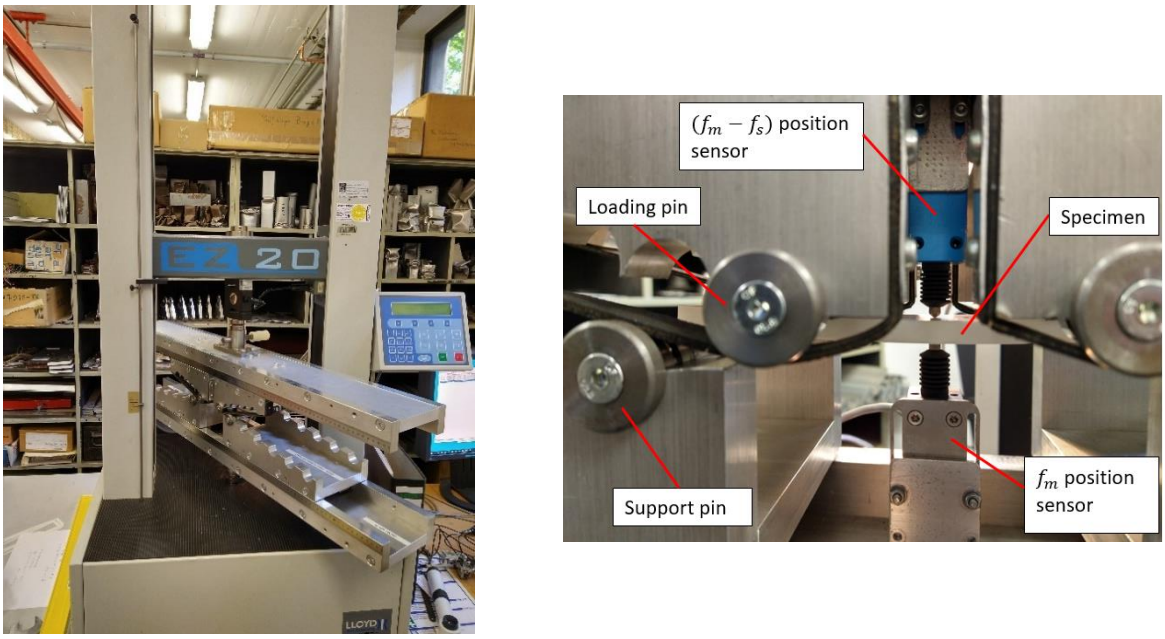


(a) (b)

Figure 7-3: (a) top and bottom fixture of the four-point flexural test (b) close up view of the test setup, which includes loading and support pins, sensors and specimen

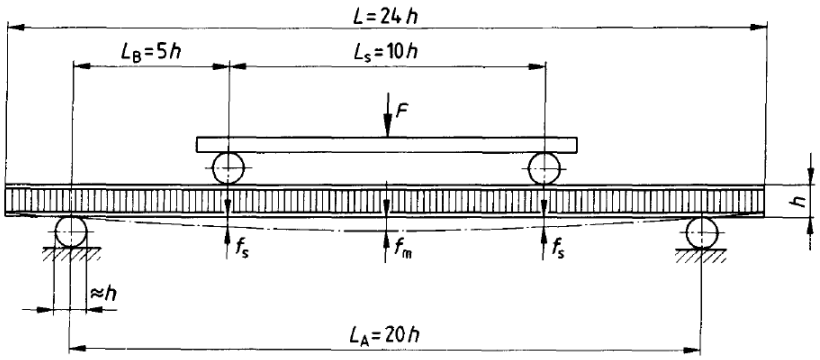


Figure 7-4: Schematic of the four-point flexural test [41, p. 1]

## 7.2.2 Test Procedures

Same as the previous test sessions, the dimension of the printed specimens were measured and recorded, see *Appendix C*. Preliminary tests were conducted to determine an adequate crosshead displacement and crosshead speed so that the limit of linear-elastic deformation behaviour of the specimens was not exceeded. As a result, a crosshead speed of $r = \frac{2mm}{min}$ and crosshead displacement $s = 5mm$ were selected for the test. The specimens are then subjected to a preload $1N$ force to ensure the pins are already in contact with the specimens before the tests begin. Because the nylon face sheets are very soft, metal sheets were attached to the specimens to prevent face indention in specimens, see *Figure 7-5*. Each specimen was tested five times.


Figure 7-5: Metal sheets attached on the specimen

### 7.2.3 Test Results

The results of load $F$, deflection at the middle of specimen $f_m$, and the difference of deflections $(f_m - f_s)$ were acquired from the tests. The deflection of specimen at the location of the loading pins $f_s$ were calculated manually based on the acquired quantities. There is zero error in the $f_m$ and $(f_m - f_s)$ positions sensors, hence, $f_m$ and $(f_m - f_s)$ were manually corrected. The $F$ and $(f_m - f_s)$ during the compression of the specimens were recorded, *Figure 7-6*. Only the results with linear relation (within the red box) were used for further results processing. The root cause of the nonlinearity in the graph is that the specimen was in contact with the loading pins but not properly pressed. Hence, these data were neglected. This process also applied to the graphs of $F - f_m$ and $F - f_s$ relations, *Figure 7-8* and *Figure 7-9*.

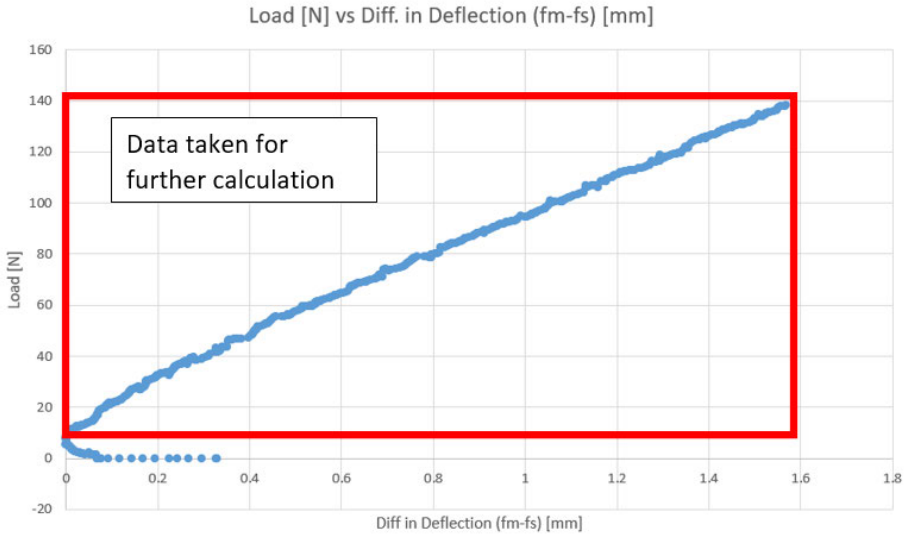


Figure 7-6: Example of the relation of $F$ and $(f_m - f_s)$. [Nylon core specimen 1 - Test 1 (raw data)]

Then, three graphs were plotted for each test round, and the examples are shown in *Figure 7-7 - Figure 7-9.* The gradient of linear regression line in each graph was taken to calculate experimental flexural stiffness $(EI)_{exp}$ and shear stiffness $S_{exp}$ of the nylon sandwich specimens.

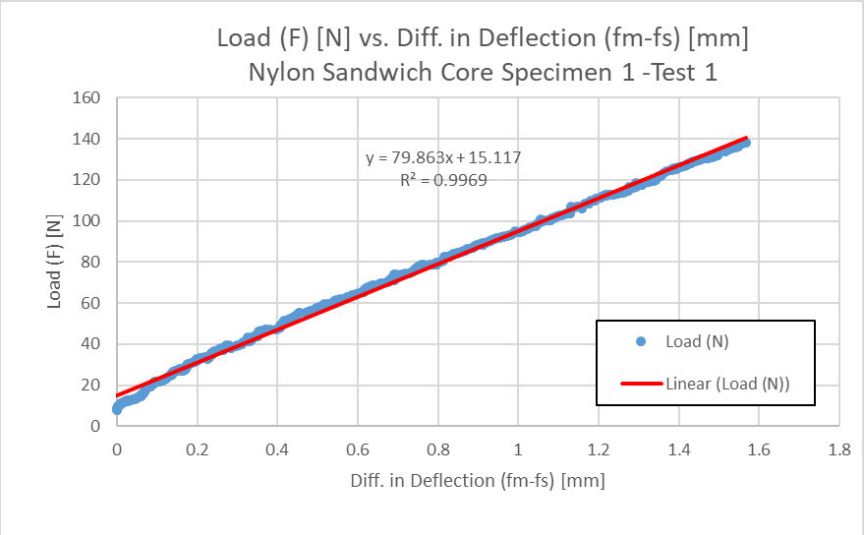


Figure 7-7: Graph of $F$ against $(f_m - f_s)$ (processed). [Nylon core specimen 1 - Test 1]

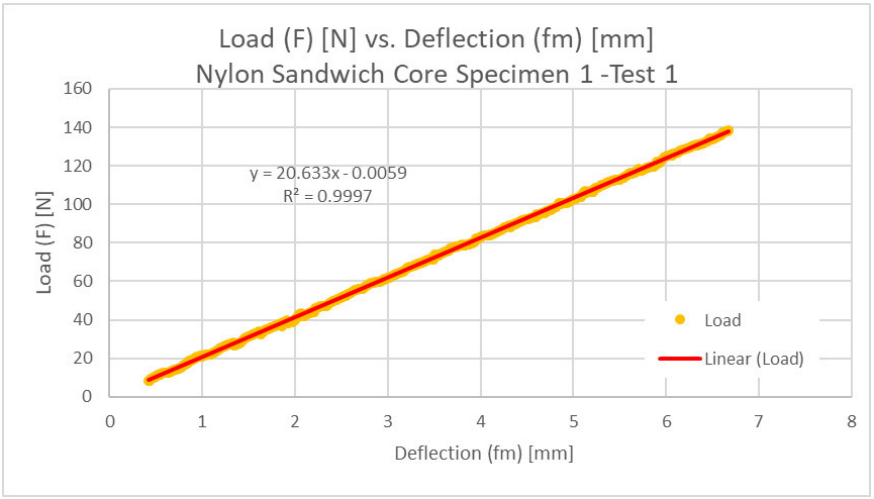


Figure 7-8: Graph of $F$ against $f_m$ (processed). [Nylon core specimen 1 - Test 1]

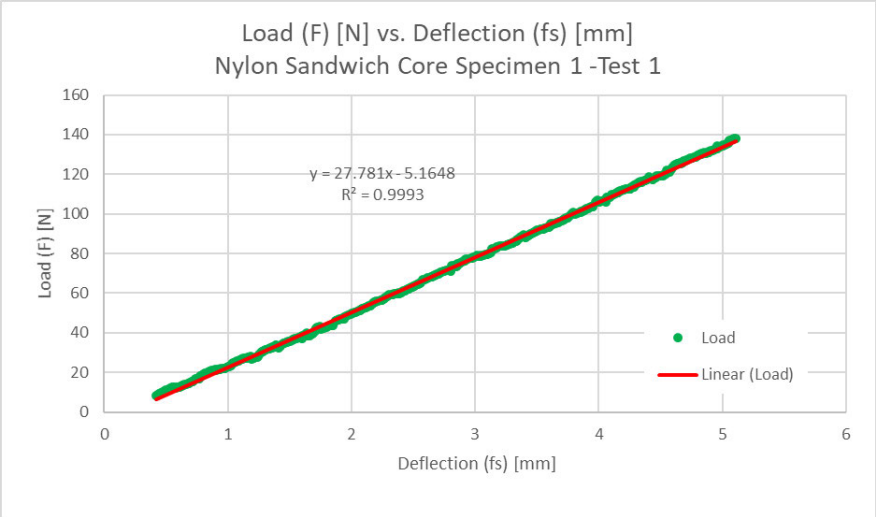


Figure 7-9: Graph of $F$ against $f_s$ (processed). [Nylon core specimen 1 - Test 1]

Experimental flexural stiffness $(EI)_{exp}$ [41, p. 3]:

$$(EI)_{exp} = \frac{F\ L_A^3}{256(f_m - f_s)} \qquad 7.1$$

Experimental shear stiffness $S_{exp}$ [54]:

$$S_{exp} = \frac{3\ F\ L_A}{89\ f_s - 64\ f_m} \qquad 7.2$$

The results are shown in *Table 7-1*. A deviation of $32.92\%$ in $(EI)_{exp}$ and $193.05\%$ in $S_{exp}$ were observed. Specimen 1 has the highest $(EI)_{exp}$ while specimen 2 has the lowest. On the other hand, specimen 3 has the highest $S_{exp}$ whereas specimen 1 has the lowest.

Table 7-1: Experimental obtained results of four-point flexural tests for sandwich specimens with nylon face sheets

| *Specimen* | *Test no.* | $max\ F$ $[N]$ | $max\ f_m$ $[mm]$ | $\frac{max\ F}{max f_m}\left[\frac{N}{mm}\right]$ | $\frac{F}{(f_m - f_s)}\left[\frac{N}{mm}\right]$ | $(EI)_{exp}$ $[Nmm^2]$ | $(EI)_{exp}$ $[Nm^2]$ | $\frac{F}{f_m}\left[\frac{N}{mm}\right]$ | $\frac{F}{f_s}\left[\frac{N}{mm}\right]$ | $S_{exp}$ $[N]$ |
|---|---|---|---|---|---|---|---|---|---|---|
| | 1 | 138.280 | 6.684 | 20.689 | 79.863 | 1277808.000 | 1.278 | 20.633 | 27.781 | 4715.072 |
| | 2 | 115.770 | 5.931 | 19.520 | 77.020 | 1232320.000 | 1.232 | 19.245 | 25.627 | 3257.316 |
| *1* | 3 | 123.530 | 6.392 | 19.325 | 73.418 | 1174688.000 | 1.175 | 19.192 | 25.942 | 4999.620 |
| | 4 | 133.810 | 6.432 | 20.804 | 79.598 | 1273568.000 | 1.274 | 20.714 | 27.967 | 5182.229 |
| | 5 | 145.310 | 6.728 | 21.597 | 79.985 | 1279760.000 | 1.280 | 21.121 | 28.671 | 6484.526 |
| | 1 | 115.210 | 6.726 | 17.130 | 64.555 | 1032880.000 | 1.033 | 17.137 | 23.296 | 5595.121 |
| | 2 | 105.500 | 6.352 | 16.610 | 62.041 | 992656.000 | 0.993 | 16.307 | 22.084 | 4555.285 |
| *2* | 3 | 110.880 | 6.722 | 16.495 | 60.283 | 964528.000 | 0.965 | 16.128 | 21.985 | 6002.947 |
| | 4 | 105.410 | 6.426 | 16.405 | 60.173 | 962768.000 | 0.963 | 16.248 | 22.235 | 7529.162 |
| | 5 | 114.790 | 6.594 | 17.407 | 62.965 | 1007440.000 | 1.007 | 17.084 | 23.427 | 9084.022 |
| | 1 | 125.660 | 6.625 | 18.969 | 70.235 | 1123760.000 | 1.124 | 18.675 | 25.403 | 6276.011 |
| | 2 | 121.850 | 6.465 | 18.848 | 69.719 | 1115504.000 | 1.116 | 18.385 | 24.929 | 5390.807 |
| *3* | 3 | 124.380 | 6.729 | 18.483 | 69.190 | 1107040.000 | 1.107 | 18.387 | 24.994 | 5989.927 |
| | 4 | 117.570 | 5.940 | 19.792 | 72.835 | 1165360.000 | 1.165 | 19.339 | 26.306 | 6496.694 |
| | 5 | 128.380 | 6.436 | 19.947 | 71.848 | 1149568.000 | 1.150 | 19.437 | 26.623 | 9545.605 |
| ***Average*** | | **121.755** | **6.479** | **18.801** | **70.249** | **1123976.533** | **1.124** | **18.535** | **25.151** | **6073.623** |

## 7.3 Finite Element Analysis of Sandwich Core

FEA was also conducted to estimate the stiffness properties of the nylon sandwich core. FE models were built to estimate the load exerted onto the specimens during the test and also to evaluate the four-point flexural test results.

### 7.3.1 FE Modelling of the Core Structure

As shown in *subchapter 2.1.2.1*, the stiffness properties of the sandwich core can be predicted by FE modelling core structure. The test results in chapter 5 have proven that printed nylon layers' stiffness properties are direction dependent. Thus, the shell elements used to model the sandwich core structure should be assigned with orthotropic material properties. However, an insolvable problem occurred during the modelling of the sandwich core structure with shell elements assigned with orthotropic material properties. As a solution, the FE models of sandwich core structure built by *Wolf 2020* [3], in which the isotropic material properties were assigned to the shell elements, were used in this test session, and the simulation results were manually modified.

In the models of *Wolf 2020* [3] to determine the $G_{xy}$, $G_{zx}$, and $G_{yz}$ of the sandwich core structure (*Figure 2-4*), mistakes in definition of the direction of the forces were discovered and corrected. The corrected models are shown in *Figure 7-10a-c.* No change is made in the FE models of $E_x$, $E_y$, and $E_z$. Besides, material data of the new nylon filament were assigned to the shell elements. Following are the material data assigned to the shell elements:

- $E = 1660.617\ MPa$
- $\nu = 0.4$
- $G = 518.536\ Mpa$

After the simulation results were obtained, the results of $E_z$ was corrected based on $E_2$ obtained in *chapter 5* and fill density of the core structure$(50\%)$. The $v_{xy}$, $v_{yz}$ , and $v_{zx}$ were corrected according to symmetric condition, refer *subchapter 4.4*. The stiffness properties obtained from the FE modelling of the sandwich core are:

Table 7-2: Stiffness properties of sandwich core obtained from FE simulation

| Stiffness Properties | *Values* |
|---|---|
| $\boldsymbol{E_x[MPa]}$ | 483.900 |
| $\boldsymbol{E_y\ [MPa]}$ | 421.569 |
| $\boldsymbol{E_z\ [MPa]}$ | 830.000 |
| $\boldsymbol{G_{xy}\ [MPa]}$ | 66.083 |
| $\boldsymbol{G_{xz}\ [MPa]}$ | 187.257 |
| $\boldsymbol{G_{yz}\ [MPa]}$ | 169.039 |
| $\boldsymbol{\nu_{xy}\ [-]}$ | 0.28 |
| $\boldsymbol{\nu_{yz}\ [-]}$ | 0.16 |
| $\boldsymbol{\nu_{xz}\ [-]}$ | 0.18 |

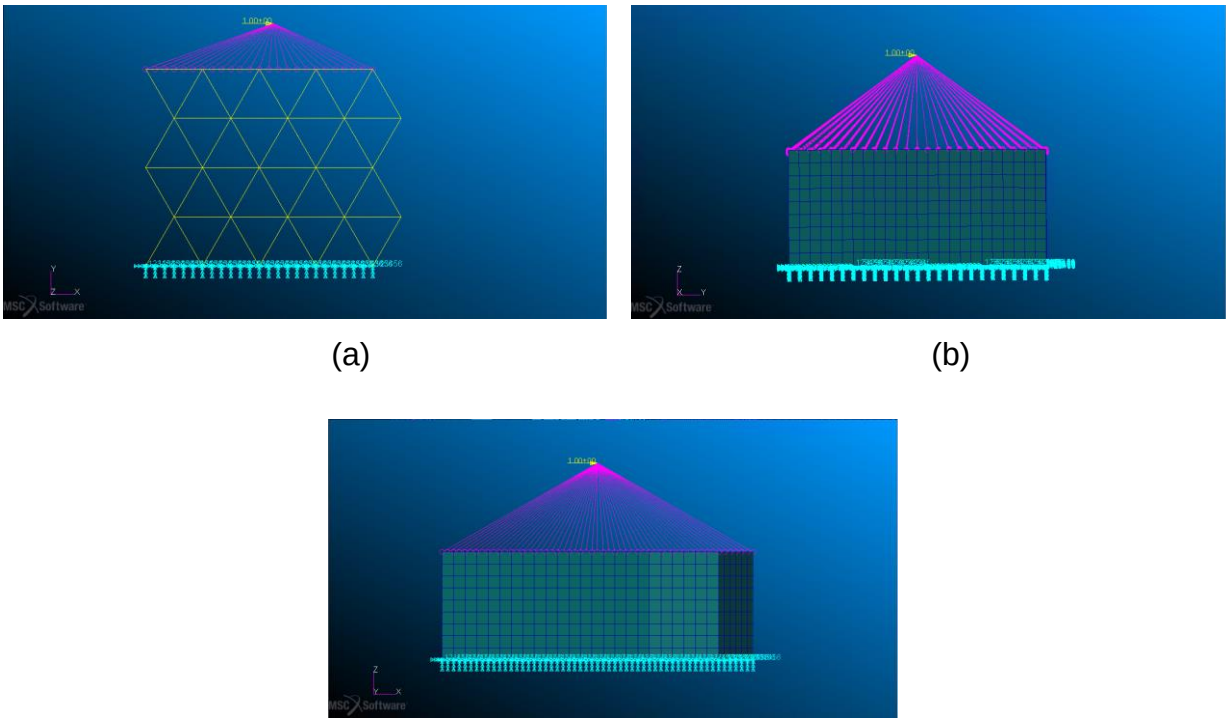

(a) (b)

(c)

Figure 7-10: Corrected FE model to determine (a) $G_{xy}$ (b) $G_{yz}$ (c) $G_{zx}$ of the sandwich core

### 7.3.2 FE Modelling of Entire Specimen

After the stiffness properties of core structure were obtained from FE simulation, modelling of the entire specimens (sandwich panel with nylon face sheets) was carried out to estimate the values of loads and displacements that will be obtained experimentally, and also to evaluate the test results.

Before modelling the sandwich panel with nylon face sheets, the FE model of the sandwich panel by *Wolf 2020* [3] was studied and modified in the modelling method. Improvements were made to assign the orientation angles and orthotropic material properties to nylon layers in the FE model. Only the Shell/Solid model with QUAD4/HEX8 elements was studied because it delivers the best results among all the models by *Wolf 2020* [3]. *Appendix H* shows the comparison of modelling methods before and after improvements.

As for the modelling of the sandwich panel with nylon face sheets, the improved modelling method was applied, and the material properties assigned to the models are stated in *Table 7-3*. After the orthotropic material properties of both nylon and CFRP were defined in PATRAN, the materials were then assembled with the “Composite Layup” function in PATRAN, and the material properties of the laminated shell was generated. Two models were created: one with 2D properties assigned to the face sheets; another with 3D properties assigned to face sheets. Three load cases were defined to each FE model:

- "Load" : Total load of $120N$ exerts to the sandwich panel model
- "Displacement A": Load path of $5mm$ at the point of load application on the sandwich panel
- "Displacement B": Load path of $5mm$ at the point of load application on the sandwich panel. No change in thickness occurs in the sandwich panel.

Table 7-3: Material data assigned to the FE model of sandwich panel with nylon face sheets

| Material Data | Core | Face Sheets (Nylon) | |
|---|---|---|---|
| | | 2D | 3D |
| $E_{11}$ $[MPa]$ | 483.900 | 1660.617 | 1660.617 |
| $E_{22}$ $[MPa]$ | 421.569 | 1356.679 | 1356.679 |
| $E_{33}$ $[MPa]$ | 830.000 | – | 1356.679 |
| $G_{12}$ $[MPa]$ | 66.083 | 518.536 | 518.536 * |
| $G_{23}$ $[MPa]$ | 169.039 | – | 518.536 * |
| $G_{31}$ $[MPa]$ | 187.257 | – | 518.536 * |
| $\nu_{12}$ $[-]$ | 0.28 | 0.40 | 0.40 |
| $\nu_{23}$ $[-]$ | 0.16 | – | – |
| $\nu_{31}$ $[-]$ | 0.18 | – | – |

* Assumption: $G_{12} = G_{31} = G_{23}$

Boundary conditions of the load cases are illustrated *in Figure 7-11 - Figure 7-13.*

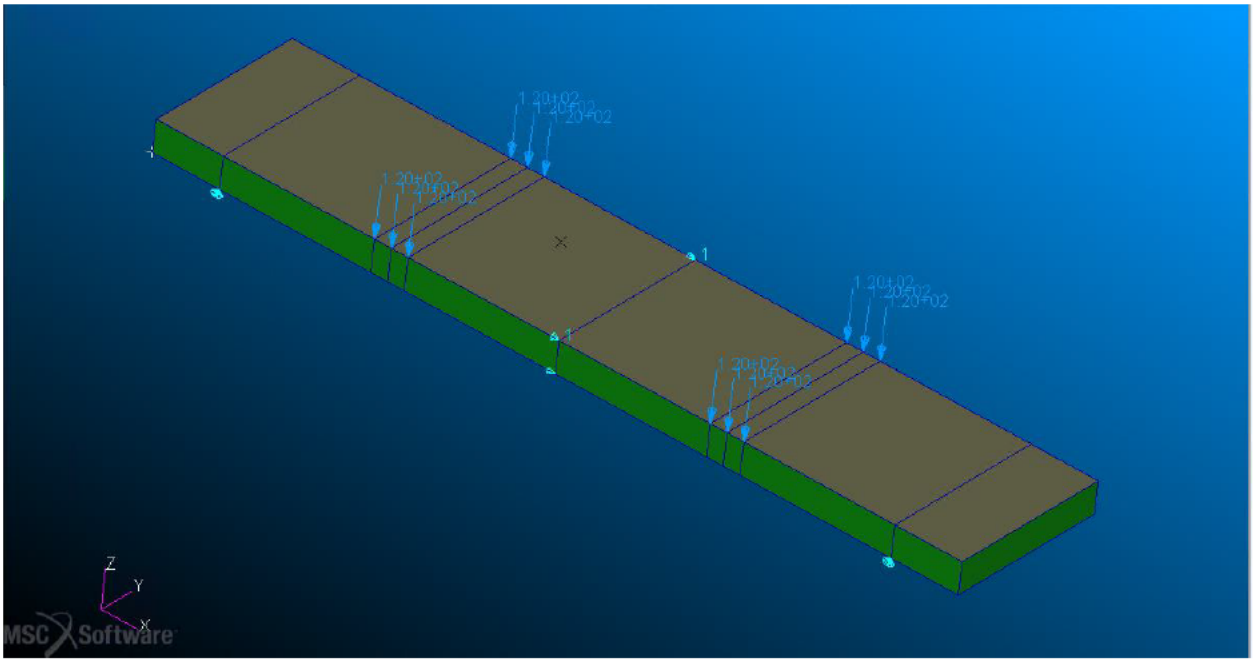


Figure 7-11: Boundary conditions of sandwich panel FE model under load case "Load"

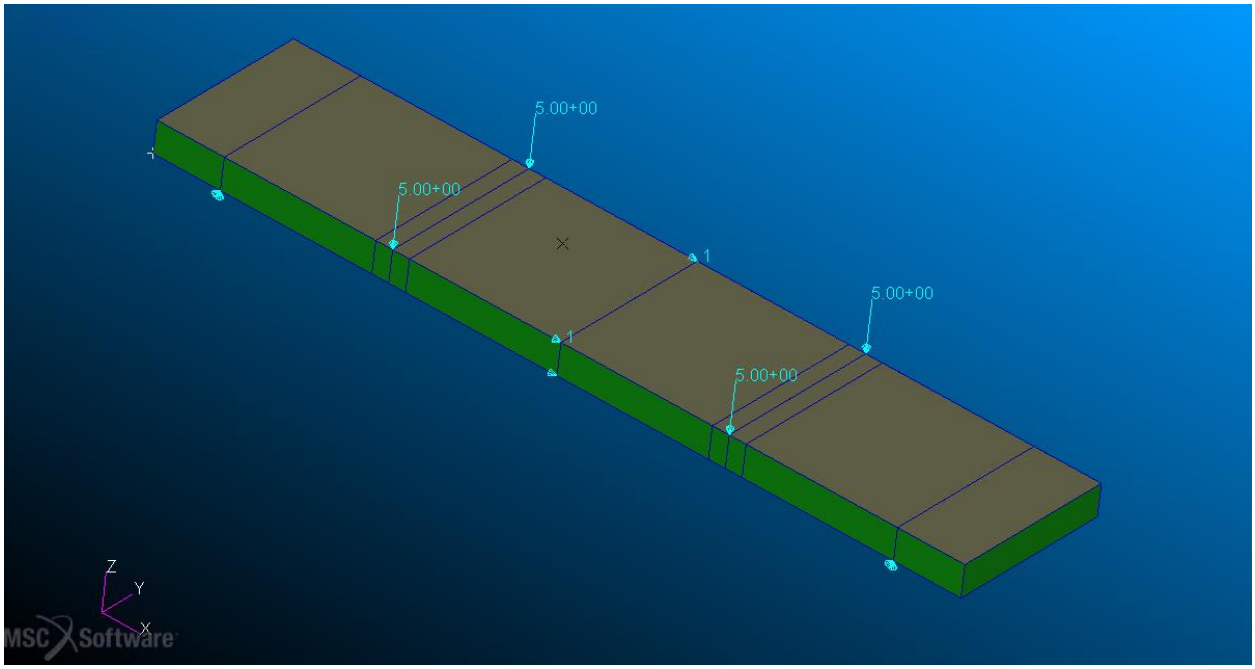


Figure 7-12: Boundary conditions of sandwich panel FE model under load case "Displacement A"

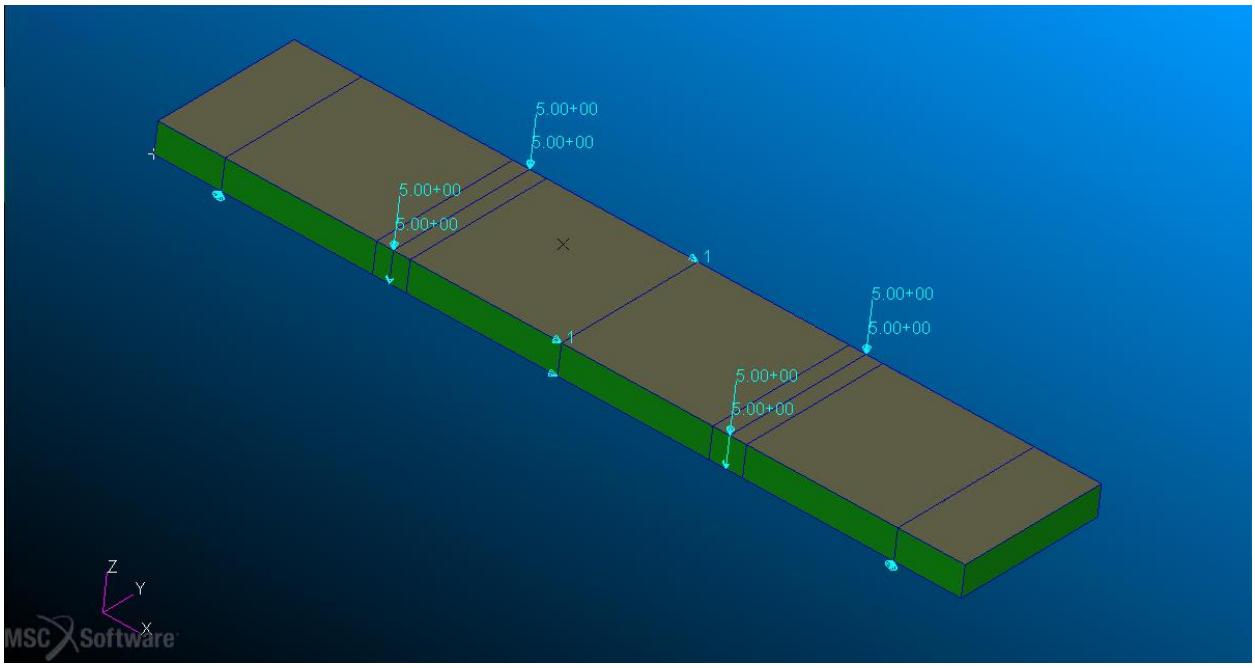


Figure 7-13: Boundary conditions of sandwich panel FE model under load case "Displacement B"

The following tables show the simulation results of these three load cases.

Table 7-4: FE simulated results for load, deflections, and load-deflection ratios of the sandwich panel with nylon face sheets

| FE Models | | $F$ $[N]$ | $f_m$ $[mm]$ | $\frac{F}{f_m}\left[\frac{N}{mm}\right]$ | $f_s$ $[mm]$ | $\frac{F}{f_s}\left[\frac{N}{mm}\right]$ | $\frac{F}{(f_m - f_s)}\left[\frac{N}{mm}\right]$ |
|---|---|---|---|---|---|---|---|
| with 2D property face sheets | Load | 120.000 | 4.448 | 26.976 | 3.106 | 38.632 | 89.402 |
| | Displacement A | 188.854 | 6.883 | 27.438 | 4.999 | 37.775 | 100.273 |
| | Displacement B | 189.554 | 6.889 | 27.516 | 5.000 | 37.911 | 100.350 |
| with 2D property face sheets | Load | 120.000 | 4.448 | 26.975 | 3.243 | 37.007 | 99.512 |
| | Displacement A | 188.829 | 6.883 | 27.435 | 4.999 | 37.773 | 100.248 |
| | Displacement B | 189.530 | 6.889 | 27.513 | 5.000 | 37.906 | 100.346 |

Table 7-5: FE simulated results for flexural stiffness and shear stiffness the sandwich panel with nylon face sheets

| FE Models | | $(EI)$ $[Nm^2]$ | $S$ $[N]$ |
|---|---|---|---|
| with 2D property face sheets | Load | 1.430 | -6983.041 |
| | Displacement A | 1.604 | 20379.907 |
| | Displacement B | 1.606 | 22149.010 |
| with 3D property face sheets | Load | 1.592 | 14814.509 |
| | Displacement A | 1.604 | 20483.898 |
| | Displacement B | 1.606 | 22088.028 |

## 7.4 Evaluation and Discussion

Besides FEA, the $(EI)$ and $S$ of the specimens were also calculated with:

- CLT, *equations 4.11 - 4.18* and *4.27* for flexural stiffness
- FSDT, equations *4.19 - 4.25* and *4.28* for shear stiffness
- Analytic hand calculation, equation 4.33 for flexural stiffness

For CLT and FSDT, the material data used are similar as in FEA; for analytic hand calculation, $E_f$ was obtained with CLT calculation based on the layup of face sheets, and $E_c$ was taken from *subchapter 7.3.1.* The experimental and theoretical results are compared in *Table 7-6* and *Table 7-7*.

Table 7-6: Comparison of the $\frac{F}{f_m}$ , $\frac{F}{f_m}$ ,and $\frac{F}{f_m}$ ratios obtained from test and FE simulation

| Description | | | $\frac{F}{f_m}$ | $\Delta\frac{F}{f_m}$ | $\frac{F}{f_s}$ | $\Delta\frac{F}{f_s}$ | $\frac{F}{(f_m - f_s)}$ | $\Delta\frac{F}{(f_m - f_s)}$ |
|---|---|---|---|---|---|---|---|---|
| Test | (As reference) | | 18.535 | - | 25.151 | - | 70.249 | - |
| FEA | QUAD4/HEX8 & face sheets with 2D properties | Load | 26.976 | 45.54% | 38.632 | 53.60% | 89.402 | 27.27% |
| | | Displacement A | 27.438 | 48.04% | 37.775 | 50.19% | 100.273 | 42.74% |
| | | Displacement B | 27.516 | 48.45% | 37.911 | 50.73% | 100.350 | 42.85% |
| | QUAD4/HEX8& face sheets with 3D properties | Load | 26.975 | 45.54% | 37.007 | 47.14% | 99.512 | 41.66% |
| | | Displacement A | 27.435 | 48.02% | 37.773 | 50.18% | 100.248 | 42.70% |
| | | Displacement B | 27.513 | 48.44% | 37.906 | 50.71% | 100.346 | 42.84% |

Table 7-7: Comparison of flexural stiffness and shear stiffness obtained from the test, FE simulation and theoretical hand calculation

| Description | | | $(EI)$ $[Nm^2]$ | $\Delta$ $(EI)$ | $S$ $[N]$ | $\Delta S$ |
|---|---|---|---|---|---|---|
| Test ( As reference) | | | 1.124 | - | 6037.620 | - |
| CLT / FSDT | | | 1.650 | 46.81% | 62145.000 | 929.30% |
| Analytic hand calculation | | | 1.441 | 28.21% | - | - |
| FEA | QUAD4/HEX8 & face sheets with 2D properties | Load | 1.430 | 27.26% | -6983.041 | -215.66% |
| | | Displacement A | 1.604 | 42.74% | 20379.907 | 237.55% |
| | | Displacement B | 1.606 | 42.85% | 22149.010 | 266.85% |
| | QUAD4/HEX8 & face sheets with 3D properties | Load | 1.592 | 41.65% | 14814.509 | 145.37% |
| | | Displacement A | 1.604 | 42.70% | 20483.898 | 239.27% |
| | | Displacement B | 1.606 | 42.84% | 22088.028 | 265.84% |

It was discovered that there is a vast difference between the experimental and theoretical results. A specimen was printed again to investigate this problem, and it was discovered that the roof layers were not printed correctly. The first till third roof layers were printed with holes due to the triangular infill structure in the specimens. This phenomenon was caused by either low fill density or under extrusion by the nozzle [55]. This issue might also initiate the enormous deviation in the $(EI)_{exp}$ and $S_{exp}$ observed in *subchapter 7.2*.

Due to the printing error, the stiffness properties of the sandwich core obtained from FE simulations in *subchapter 7.3.1* could not be verified. Nevertheless, because of the erroneous results obtained in the test, the stiffness properties values from FEA were used for further material investigation in the next test session.

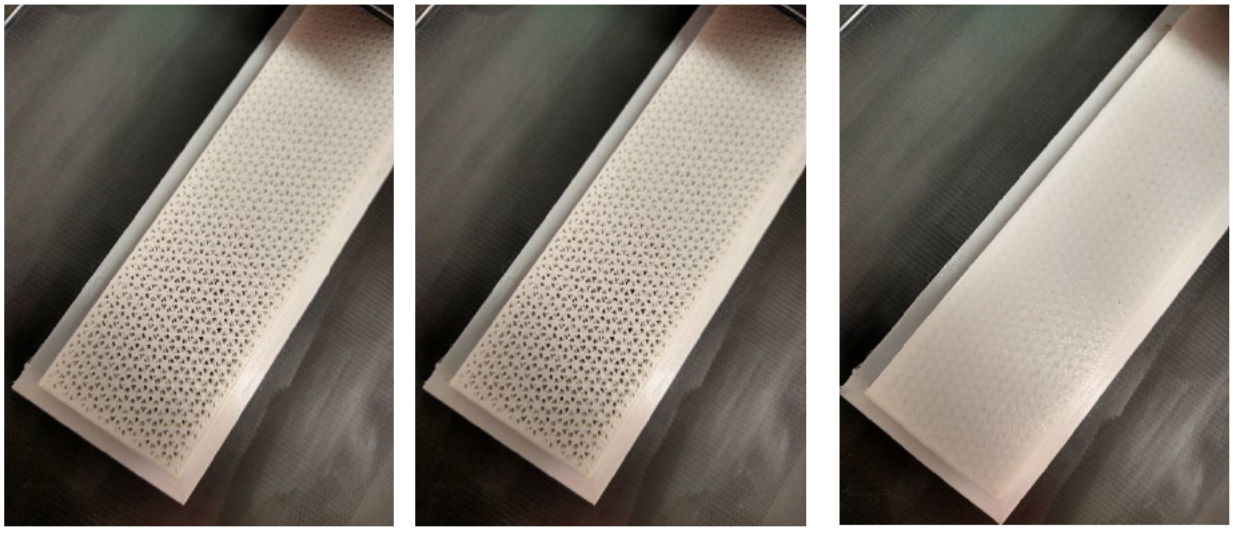

(a) (b) (c)

Figure 7-14: (a) First (b) Second (c) Third layer of roof printed after the triangular infill structure

Besides, shear modulus with a negative value was obtained from the FE model with face sheets assigned with 2D properties in PATRAN. The $f_s$ value obtained was lower than the one from FE models with face sheets assigned with 3D property. Thus, shear locking

was suspected to happen in this FE model. Therefore, the FE model with 2D properties in the face sheets will be closely observed in the next session.

## 7.5 Difficulties and Challenges

Only the simplified equation for shear stiffness was found for the analytic hand calculation. The dimensions of specimens were intentionally planned not to fulfil the conditions for simplification. Thus, analytical calculation of the shear stiffness was not done.

The core structure has anisotropic stiffness properties. Hence, the elastic modulus in the L and W direction of the core structure are different. However, due to the limitation of the dimension of the print bed, specimens to determine the flexural modulus in the W direction could not be printed. Thus, only the flexural modulus in the L direction was tested in this session.

Besides, a few specimens were printed with “black spots” during specimens’ fabrication, which is assumed to be the residual of Onyx material in the nozzle; because this thesis was parallel with another thesis that fabricates Onyx specimens with Mark Two. Even though multiple purge lines were being printed to remove Onyx from the nozzle after changing plastic types, the black spots still occur in the middle or top part of the specimens (no evidence of black spots in the floor layers or bottom part). These faulty pieces were disposed and were not used for testing.

# 8 Four-Point Flexural Test of Sandwich Panel

After the stiffness properties of the printed nylon layers, the printed CFRP layers and the cellular infill structure were determined, four-point flexural test specimens, which consist of all components mentioned above, were conducted to validate the finding of the previous tests.

## 8.1 Design and Production of Specimens

The sandwich panel specimens have the same dimensions as the specimens in *chapter 7*, $L \times W \times H = 192 \times 39 \times 8\,mm$. The details and cross section of the specimens are illustrated in *Figure 8-1.* The "isotropic fiber" was selected for the CFRP layers, and the infill was set to "triangular infill" with 50% fill density. The specimens were printed with two layers of walls. In total, three specimens were printed in this session. A new carbon filament spool was used to fabricate the specimens in this session.

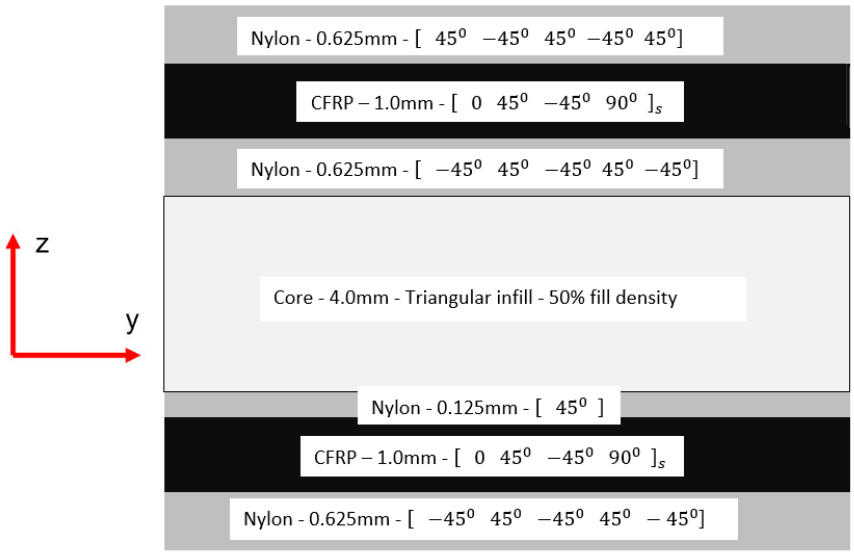


Figure 8-1: Cross section of the sandwich panel specimen

## 8.2 Test Setup, Procedures and Results

### 8.2.1 Test Setup and Procedures

The four-point flexural test in this session had the same setup as *chapter 7*, as the same sensors and fixtures were used; specimens were also printed in the same dimension, $L \times W \times H = 192 \times 39 \times 8\,mm$.

The same test procedures and settings as *chapter 7* were also applied in this test session, with a crosshead speed of $r = \frac{2mm}{min}$ along with crosshead displacement $s = 5mm$, and specimens subjected to a preload of $1N$. Each specimen was tested five times. The dimensions of the printed specimens are summarised in *Appendix D*.

### 8.2.2 Test results

The test results were processed with the same method mentioned in *subchapter 7.2.3.* The $F$ against $(f_m - f_s)$, $F$ against $f_m$ and $F$ against $f_s$ relations were plotted into graphs, and their gradients were used to calculate the $(EI)_{exp}$ and $S_{exp}$. *Figure 8-2 - Figure 8-4* display the relation of $F$ against $(f_m - f_s)$, $F$ against $f_m$ and $F$ against $f_s$ respectively.

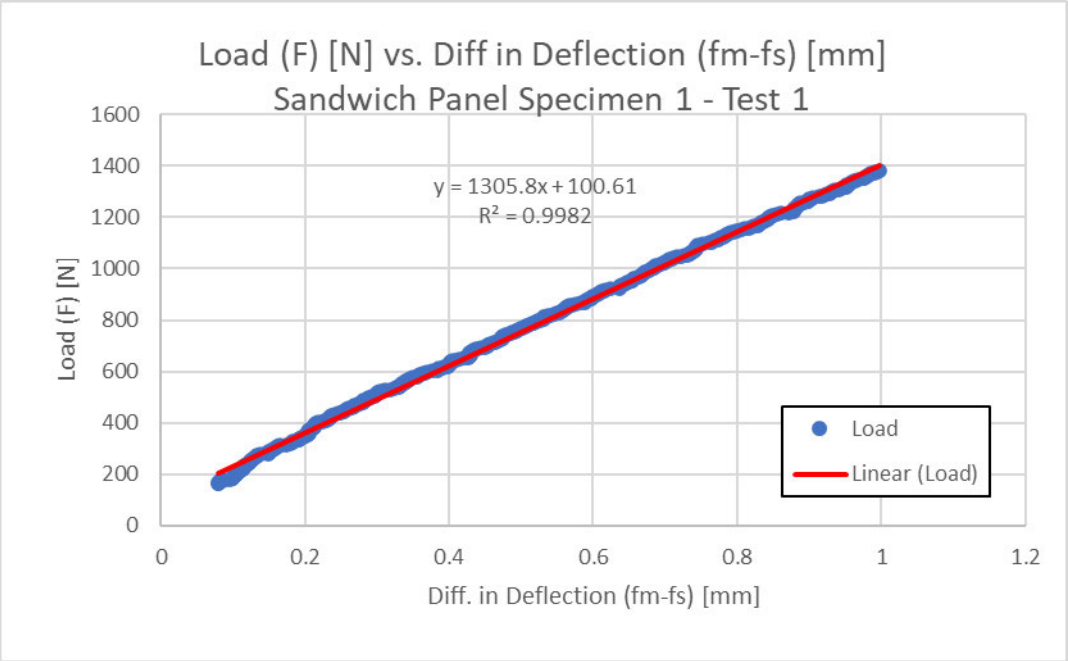


Figure 8-2: Graph of $F$ against $(f_m - f_s)$ (processed). [Sandwich panel specimen 1 - test 1]

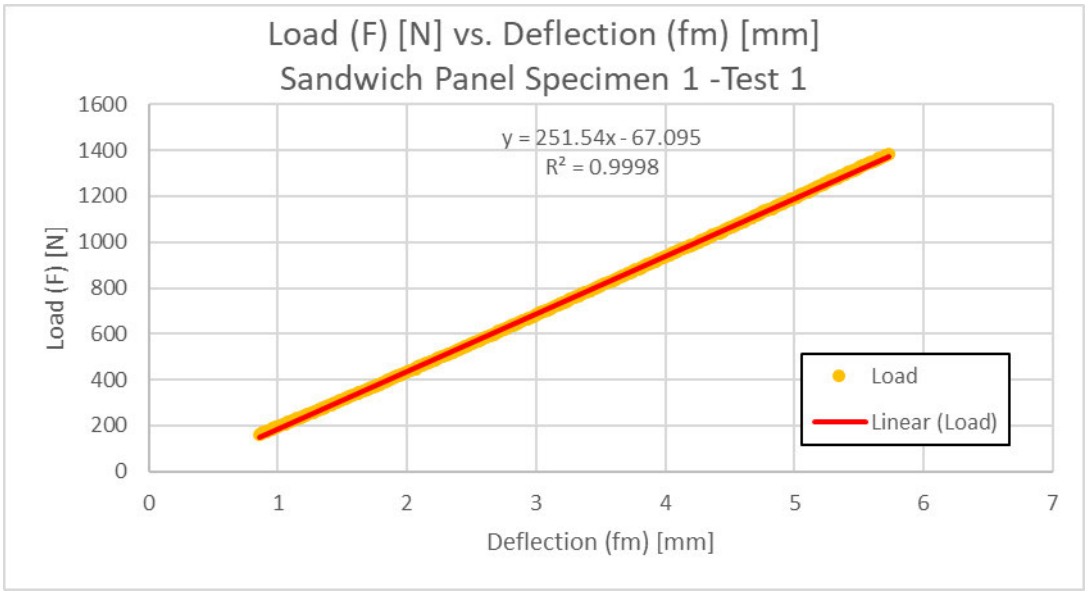


Figure 8-3: Graph of $F$ against $f_m$ (processed). [Sandwich panel specimen 1 - test 1]

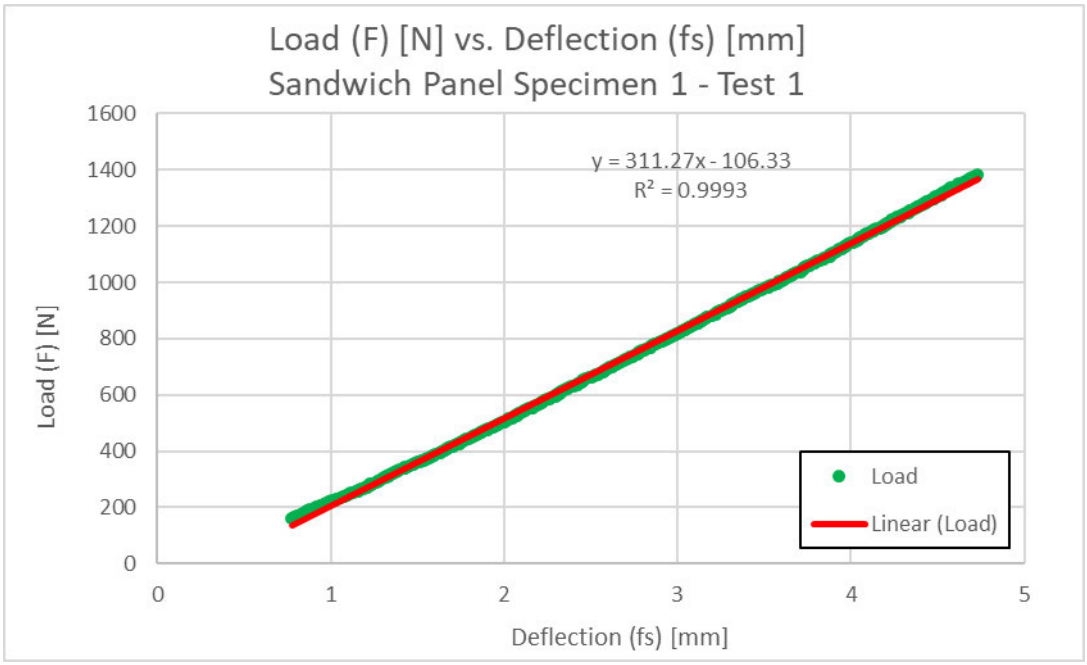


Figure 8-4: Graph of $F$ against. $f_s$ (processed). [Sandwich panel specimen 1 - test 1]

The results are shown in *Table 8-1*. The deviations of the results were also observed. It was reported that, the $(EI)_{exp}$ has a deviation of $7.87\%$ and the $S_{exp}$ has $10.09\%$.

Table 8-1: Experimental obtained results of a four-point flexural test for sandwich panel specimens

| *Specimen* | *Test no.* | $max\ F$ $[N]$ | $max\ f_m$ $[mm]$ | $\frac{max\ F}{max f_m}\left[\frac{N}{mm}\right]$ | $\frac{F}{(f_m - f_s)}\left[\frac{N}{mm}\right]$ | $(EI)_{exp}$ $[Nmm^2]$ | $(EI)_{exp}$ $[Nm^2]$ | $\frac{F}{f_m}\left[\frac{N}{mm}\right]$ | $\frac{F}{f_s}\left[\frac{N}{mm}\right]$ | $S_{exp}$ $[N]$ |
|---|---|---|---|---|---|---|---|---|---|---|
| *1* | 1 | 1382.600 | 5.728 | 241.371 | 1305.800 | 20892800.000 | 20.893 | 251.540 | 311.270 | 15241.624 |
| | 2 | 1394.500 | 5.665 | 246.169 | 1332.100 | 21313600.000 | 21.314 | 251.640 | 309.900 | 14608.390 |
| | 3 | 1394.200 | 5.759 | 242.099 | 1354.600 | 21673600.000 | 21.674 | 250.760 | 307.530 | 14043.900 |
| | 4 | 1382.400 | 5.757 | 240.142 | 1303.900 | 20862400.000 | 20.862 | 249.590 | 308.390 | 14918.378 |
| | 5 | 1393.900 | 5.776 | 241.347 | 1358.100 | 21729600.000 | 21.730 | 251.780 | 308.910 | 14151.094 |
| *2* | 1 | 1440.400 | 5.694 | 252.981 | 1422.300 | 22756800.000 | 22.757 | 261.560 | 320.220 | 14436.877 |
| | 2 | 1420.900 | 5.605 | 253.506 | 1393.900 | 22302400.000 | 22.302 | 258.990 | 317.830 | 14585.178 |
| | 3 | 1422.900 | 5.697 | 249.745 | 1416.000 | 22656000.000 | 22.656 | 258.990 | 316.530 | 14092.698 |
| | 4 | 1402.400 | 5.689 | 246.519 | 1370.700 | 21931200.000 | 21.931 | 254.910 | 312.840 | 14362.026 |
| | 5 | 1442.400 | 5.825 | 247.631 | 1390.200 | 22243200.000 | 22.243 | 257.050 | 315.130 | 14352.209 |
| *3* | 1 | 1436.700 | 5.703 | 251.916 | 1395.000 | 22320000.000 | 22.320 | 260.060 | 319.230 | 14679.439 |
| | 2 | 1433.600 | 5.616 | 255.262 | 1382.900 | 22126400.000 | 22.126 | 260.370 | 320.450 | 15032.702 |
| | 3 | 1425.500 | 5.666 | 251.588 | 1409.500 | 22552000.000 | 22.552 | 259.980 | 318.440 | 14408.046 |
| | 4 | 1427.600 | 5.747 | 248.429 | 1369.300 | 21908800.000 | 21.909 | 258.520 | 318.400 | 15018.979 |
| | 5 | 1401.100 | 5.574 | 251.359 | 1365.100 | 21841600.000 | 21.842 | 260.340 | 321.440 | 15460.595 |
| ***Average*** | | **1413.407** | **5.700** | **248.004** | **1371.293** | **21940693.333** | **21.941** | **256.405** | **315.101** | **14626.142** |

## 8.3 Finite Element Analysis of Sandwich Panel

FE modelling and simulation were also conducted in this test session to estimate the load exerted onto the specimens during the four-point flexural test, as well as to evaluate the flexural test results. The method described in *subchapter 7.3.2* and *Appendix* was used to model the sandwich specimens. Four models were created and simulated. *Table 8-2* shows the description of each FE model.

Table 8-2: Description of the FE models of sandwich panel with both nylon and CFRP in the face sheets

| FE Model | Element type and material properties dimension in face sheets | Source of material data of the face sheets | | Element type and material properties dimension in core | Source of material data of core |
|---|---|---|---|---|---|
| | | Nylon | CFRP | | |
| A | QUAD4; 2D properties | Tensile test results in *chapter 5* | Tensile test results in chapter 6 | HEX8; 3D properties | FEA in *subchapter 7.3.1* |
| B | QUAD4; 3D properties | Tensile test results in *chapter 5* | Tensile test results in chapter 6 | HEX8; 3D properties | FEA in *subchapter 7.3.1* |
| C | QUAD4; 2D properties | Tensile test results in *chapter 5* | *Suer 2018* [2] | HEX8; 3D properties | FEA in *subchapter 7.3.1* |
| D | QUAD4; 3D properties | Tensile test results in *chapter 5* | *Suer 2018* [2] | HEX8; 3D properties | FEA in *subchapter 7.3.1* |

The material properties of the core and the nylon in face sheets assigned to the FE model are described in *Table 7-3*; the material properties of CFRP obtained from tensile test and *Suer 2018* [2] are shown in *Table 8-3.*

Table 8-3: Material data of the CFRP in face sheets

| Material Data | CFRP (*Liew*) | | CFRP (*Suer 2018* [2]) | |
|---|---|---|---|---|
| | 2D | 3D | 2D | 3D |
| $E_{11}\ [MPa]$ | 56899.320 | 1660.617 | 60520 | 60520 |
| $E_{22}\ [MPa]$ | 5585.024 | 5585.024 * | 5150 | 5150 * |
| $E_{33}\ [MPa]$ | – | 5585.024 * | – | 5150 * |
| $G_{12}\ [MPa]$ | 1968.613 | 1968.613 ** | 2000 | 2000 ** |
| $G_{23}\ [MPa]$ | – | 1968.613 ** | – | 2000 ** |
| $G_{31}\ [MPa]$ | – | 1968.613 ** | – | 2000 ** |
| $\nu_{12}\ [-]$ | 0.36 | 0.36 | 0.27 | 0.27 |
| $\nu_{23}\ [-]$ | – | – | – | – |
| $\nu_{31}\ [-]$ | – | – | – | – |

* Assumption: $E_{22} = E_{33}$

** Assumption: $G_{12} = G_{31} = G_{23}$

Same as *subchapter 7.3.2*, three load cases were defined to each FE model: "Load", "Displacement A", and "Displacement B".

- "Load" : Total load of $1410N$ exerts to the sandwich panel model
- "Displacement A": Load path of $5mm$ at the point of load application on the sandwich panel
- "Displacement B": Load path of $5mm$ at the point of load application on the sandwich panel. No change in thickness occurs in the sandwich panel.

The FE models created were then simulated, and the simulation results are summarised in the following tables.

Table 8-4: FE simulated results for load, displacements and load-displacement ratio of the sandwich panel with both nylon and CFRP in face sheets

| FE Models | | $F$ $[N]$ | $f_m$ $[mm]$ | $\frac{F}{f_m}\left[\frac{N}{mm}\right]$ | $f_s$ $[mm]$ | $\frac{F}{f_s}\left[\frac{N}{mm}\right]$ | $\frac{F}{(f_m - f_s)}\left[\frac{N}{mm}\right]$ |
|---|---|---|---|---|---|---|---|
| A | Load | 1410.000 | 5.756 | 244.953 | 4.328 | 325.823 | 986.908 |
| | Displacement A | 1630.514 | 6.635 | 245.759 | 4.989 | 326.822 | 990.832 |
| | Displacement B | 1634.037 | 6.646 | 245.864 | 5.000 | 326.807 | 992.672 |
| B | Load | 1410.000 | 5.760 | 244.787 | 4.332 | 325.485 | 987.326 |
| | Displacement A | 1626.872 | 6.629 | 245.410 | 4.987 | 326.236 | 990.546 |
| | Displacement B | 1630.787 | 6.640 | 245.586 | 5.000 | 326.157 | 994.140 |
| C | Load | 1410.000 | 5.538 | 254.605 | 4.169 | 338.251 | 1029.573 |
| | Displacement A | 1691.412 | 6.627 | 255.246 | 4.989 | 339.056 | 1032.608 |
| | Displacement B | 1694.978 | 6.636 | 255.406 | 5.000 | 338.996 | 1035.797 |
| D | Load | 1410.000 | 5.549 | 254.095 | 4.173 | 337.878 | 1024.709 |
| | Displacement A | 1687.592 | 6.619 | 254.958 | 4.986 | 338.453 | 1033.494 |
| | Displacement B | 1691.575 | 6.631 | 255.120 | 5.000 | 338.315 | 1037.458 |

Table 8-5: FE simulated results for flexural stiffness and shear stiffness the sandwich panel with both nylon and CFRP in face sheets

| FE Models | | $(EI)$ $[Nm^2]$ | $S$ $[N]$ |
|---|---|---|---|
| A | Load | 15.791 | 40404.955 |
| | Displacement A | 15.853 | 40328.889 |
| | Displacement B | 15.883 | 39916.230 |
| B | Load | 15.797 | 40043.546 |
| | Displacement A | 15.849 | 39930.588 |
| | Displacement B | 15.906 | 39110.723 |
| C | Load | 16.473 | 40858.462 |
| | Displacement A | 16.522 | 40832.767 |
| | Displacement B | 16.573 | 40136.827 |
| D | Load | 16.395 | 41614.659 |
| | Displacement A | 16.536 | 40201.902 |
| | Displacement B | 16.599 | 39323.721 |

## 8.4 Evaluation and Discussion

The $(EI)$ of the sandwich panel specimens were also calculated with CLT, while $S$ were calculated with FSDT. The experimental results, the results of FE simulation as well as the results calculated with CLT and FSDT were put to a side-by-side comparison. *Table 8-6* and *Table 8-7* show the comparison of the results.

Table 8-6: Comparison of the $\frac{F}{f_m}$, $\frac{F}{f_m}$, and $\frac{F}{f_m}$ ratios obtained from test and FEA

| Description | | | $\frac{F}{f_m}$ | $\Delta\frac{F}{f_m}$ | $\frac{F}{f_s}$ | $\Delta\frac{F}{f_s}$ | $\frac{F}{(f_m - f_s)}$ | $\Delta\frac{F}{(f_m - f_s)}$ |
|---|---|---|---|---|---|---|---|---|
| Test (As reference) | | | 256.405 | - | 315.101 | - | 1371.293 | - |
| FEA | A | Load | 244.953 | -4.47% | 325.823 | 3.40% | 986.908 | -28.03% |
| | | Displacement A | 245.759 | -4.15% | 326.822 | 3.72% | 990.832 | -27.74% |
| | | Displacement B | 245.864 | -4.11% | 326.807 | 3.72% | 992.672 | -27.61% |
| | B | Load | 244.787 | -4.53% | 325.485 | 3.30% | 987.326 | -28.00% |
| | | Displacement A | 245.410 | -4.29% | 326.236 | 3.53% | 990.546 | -27.77% |
| | | Displacement B | 245.586 | -4.22% | 326.157 | 3.51% | 994.140 | -27.50% |
| | C | Load | 254.605 | -0.70% | 338.251 | 7.35% | 1029.573 | -24.92% |
| | | Displacement A | 255.246 | -0.45% | 339.056 | 7.60% | 1032.608 | -24.70% |
| | | Displacement B | 255.406 | -0.39% | 338.996 | 7.58% | 1035.797 | -24.47% |
| | D | Load | 254.095 | -0.90% | 337.878 | 7.23% | 1024.709 | -25.27% |
| | | Displacement A | 254.958 | -0.56% | 338.453 | 7.41% | 1033.494 | -24.63% |
| | | Displacement B | 255.120 | -0.50% | 338.315 | 7.37% | 1037.458 | -24.34% |

Table 8-7: Comparison of $(EI)$ and $S$ of the sandwich panel obtained from test, FEA and theoretical calculation

| | | | $(EI)$ $[Nm^2]$ | $\Delta$ $(EI)$ | $S$ $[N]$ | $\Delta S$ |
|---|---|---|---|---|---|---|
| Test (As reference) | | | 21.941 | - | 14626.142 | - |
| CLT / FSDT | CFRP material Properties by Liew | | 17.997 | -17.98% | 186008.095 | 1171.75% |
| | CFRP material Properties by Suer | | 18.593 | -15.26% | 188050.000 | 1185.71% |
| FEA | A | Load | 15.791 | -28.03% | 40404.955 | 176.25% |
| | | Displacement A | 15.853 | -27.75% | 40394.527 | 176.18% |
| | | Displacement B | 15.883 | -27.61% | 39700.582 | 171.44% |
| | B | Load | 15.797 | -28.00% | 40042.548 | 173.77% |
| | | Displacement A | 15.849 | -27.77% | 39771.224 | 171.92% |
| | | Displacement B | 15.906 | -27.50% | 38917.636 | 166.08% |
| | C | Load | 16.473 | -24.92% | 40858.462 | 179.35% |
| | | Displacement A | 16.522 | -24.70% | 40832.767 | 179.18% |
| | | Displacement B | 16.573 | -24.47% | 40136.827 | 174.42% |
| | D | Load | 16.395 | -25.28% | 41614.659 | 184.52% |
| | | Displacement A | 16.536 | -24.63% | 40201.902 | 174.86% |
| | | Displacement B | 16.599 | -24.35% | 39323.721 | 168.86% |

It is observed that the FE models C and D have better results than A and B due to the erroneous experimental obtained stiffness properties of the CFRP layers mentioned in *subchapters 6.3* and *6.4*. An improvement of $\frac{F}{f_m}$ were seen in in results of FE simulation, as compared to the results of *Wolf 2020* [3] with a deviation of $12\%$. FE model A and B have a deviation of around $5\%$, while C and D have an approximate $1\%$ deviation,

Besides, the $\frac{F}{f_s}$ and $\frac{F}{(f_m - f_s)}$ were also investigated. It is reported that the $\frac{F}{f_s}$ obtained from FE models have lower accuracy (deviation $\approx 5 - 8\%$). And the $\frac{F}{(f_m - f_s)}$ by FEA are around $25 - 28\%$ lower than the experimentally obtained values. The large deviation of $\frac{F}{(f_m - f_s)}$ also leads to the enormous deviation in $(EI)$. The most significant deviation is observed in $S$. The values obtained from FSDT are ten times the experimental results, and the FE simulated results are almost double of the experimental results.

The deviation of the results is caused by the selection of test processes and standards in the previous chapters. Because the sandwich panel specimens were tested with the four-point flexural test and the face sheets of the sandwich panel specimens are relatively thick; Therefore, the flexural test under standards of *DIN EN ISO 178* [32] and *DIN EN ISO 14125* [33] should be conducted to obtain the stiffness properties of the printed nylon and CFRP layers instead of the tensile tests done in *chapter 5* and *6*.

Besides, due to the critical printing error during the production of the sandwich core structure specimens (*subchapter 7.5*), the stiffness properties of the sandwich core used in this test session were estimated with FE simulation in *subchapter 7.3.1*. These values were not verified. Thus, the reliability of these values is also being questioned. Also, the models might also be overly constrained.

It is also noticed that the FE models with 2D properties assigned to elements for face sheets delivered slightly better results than those with face sheets elements assigned with 3D properties. Due to the lack of information on the stiffness properties of printed nylon and CFRP layers, two assumptions $G_{12} = G_{13} = G_{23}$ and $E_{22} = E_{33}$ were made. However, based on the comparison of results, it is concluded that $G_{12} \neq G_{13} \neq G_{23}$ and $E_{22} \neq E_{33}$. The enormous deviation in $S$ also support that $G_{13} \neq G_{23}$. Hence, the $E_{33}$, $G_{13}$ and $G_{23}$ should also be tested.

The problem with carbon filament loops at specimens' edges is mentioned in *subchapter 6.3* also contributed to the deviation of results values. The loops affect the stiffness properties of printed CFRP layers, and as a result, the printed CFRP layers are likely to have anisotropic material properties. This also supports the statement of $G_{12} \neq G_{13} \neq G_{23}$ and $E_{22} \neq E_{33}$ discussed in the previous paragraph.

## 8.5 Difficulties and Challenges

During the production of the specimens, the nozzle of nylon filament was clogged very often. It happened while the printer was printing the CFRP layers. The printing process was forced to stop and restart when the nozzle was clogged. There were six printing attempts, and only three specimens were produced.

Besides, the fibre stringing issue was also observed on the complete printed specimens, see *Figure 8-5*. This issue is likely caused by wet nylon [56]. However, when *Buhl*, a student assistant in charge of the printer, tried to print a part consisting of nylon and CFRP to investigate the printing issue, no issue occurred. Therefore, the root cause of this issue remains unknown. It was assumed that the clogging and fibre stringing issues were caused by the residual of Onyx in the nozzle (see also *subchapter 7.5*), as the 3D printer also printed specimens with Onyx in parallel to the specimens in this thesis.

These issues might result in the deviation of the stiffness properties of the sandwich panel specimens. For the solution suggestion, only one type of plastic should be used for printing with one nozzle. When another type of plastic is used for printing, the nozzle shall be changed as well. Moreover, there should be no fabrication of specimens with different types of plastics in parallel with the same nozzle.

Figure 8-5: Fibre stringing observed on the complete printed sandwich panel specimens

# 9 Conclusion and Outlook

The aim of this thesis is to determine the stiffness properties of the nylon sandwich core structure printed by the Markforged Mark Two 3D printer experimentally. Laboratory tests were conducted to achieve this aim: tensile test with printed nylon specimens to determine the orthotropic stiffness properties of printed nylon layers, tensile test with CFR specimens to determine the orthotropic stiffness properties of CFRP layers, and four-point flexural test to determine the stiffness properties of the cellular structured sandwich core printed with nylon. Finally, a four-point flexural test with sandwich panel specimens consisting of printed nylon layers, printed CFRP layers and printed nylon sandwich core structure was conducted for the validation test results.

In the tensile test with nylon specimens, three specimen sets were tested. The generalised elastic modulus of each set of specimens was obtained, and the orthotropic stiffness properties of the printed nylon layers were calculated based on the generalised elastic modulus with the aid of CLT.

Next, the tensile test with CFR specimens was conducted with three specimens sets. The generalised elastic modulus of the specimens was obtained. Through the rule of mixture equation, the elastic modulus of the CFRP proportion in each specimen was calculated. After that, the orthotropic stiffness properties of the printed CFRP layers were obtained with the CLT. Discrepancies of the stiffness properties were observed between the experimentally obtained values and the theoretical values calculated with micromechanics theory. This issue was caused by the loops printed at the edges of the specimens. Besides, the test results were erroneous because the fibre filament spool used to fabricate the specimens was already wet before fabricating the specimens.

Then, four-point flexural test was carried out to study the stiffness properties of the nylon sandwich core structure printed by Mark Two. The specimens were printed with roof and floor layers which act as the face sheets of sandwich structures due to the predefined printer settings by Markforged. Correction and improvements on finite element models built by *Wolf 2020* [3] were executed. FE models of the core structure as well as FE models that replicate the entire specimens were built in this test session for the estimation of the stiffness properties of the nylon sandwich core structure. However, this test session was failed due to the printing error in specimens. On the other hand, the estimated values of the sandwich core stiffness properties obtained from FE simulation were not verified due to this printing error.

Another four-point flexural test was carried out with sandwich panel specimens to validate the findings in previous test sessions. The stiffness properties of the printed nylon layers obtained through a tensile test and the FEA estimated stiffness properties of the nylon sandwich core were applied in this test session. As for the stiffness properties of printed CFRP layers, both experimentally obtained values in this thesis and the values obtained by *Suer 2018* [2] were used for the validation. FEA of the sandwich panel specimens were performed in parallel with the four-point flexural test. A minor improvement in the results obtained was observed. However, most experimentally obtained results significantly differ from the FE simulated results. The error lies in either the stiffness properties of the CFRP layers or the FE estimated stiffness properties of the nylon sandwich core or vice versa. Besides, the limitations of the printer also contributed to the differences in the results.

The stiffness properties of the nylon sandwich core structure were also not determined in both of the four-point flexural tests conducted in this thesis. Due to these limitations, a satisfactory result for this thesis cannot be achieved

Up to this point in time, the orthotropic stiffness properties of the printed CFRP layers are not determined. The values obtained by *Suer 2018* [2] were partially determined through calculation via micromechanics theory with a false estimation of the fibre volume ratio. The tensile test in this thesis failed due to the wet or damaged carbon filament. It is necessary to determine the stiffness properties (both tensile and flexural) of the printed CFRP in future research. The tensile test and flexural test mentioned in *subchapter 2.4.1* shall be conducted. The nylon which surrounding the printed CFRP layers should be removed before testing in order to ease the test process as well as improve the accuracy of the results.

A fatal printing error was also discovered: the layers above the infill structure cannot be printed correctly. For future research, a method of fabricating the core structure without the roof and floor layers or a method to remove the roof and floor layers without damaging the core structure should be investigated. Without the roof and floor layers, the test method mentioned in *subchapter 2.4.2* can be conducted if the fixtures are available in the future. Also, the test results obtained can be used to verify the simulation results of the FE models in *subchapter 7.3.1*.

During the test, it was also observed that the CFRP loops printed at the edges of the specimens affect its stiffness properties. Specimens without the loops should be fabricated and tested. Moreover, the influence of CFRP loops on the stiffness properties of the specimens can be studied by comparing the test results of specimens with and without the loops.

Besides the physical test, the FE model developed shall also be improved. For instance, the elements in the FE model of the sandwich core structure shall be assigned with orthotropic material properties. Some changes in the boundary conditions in this model should be done as well, as the model is suspected to be overly constrained.

All the tests conducted in this thesis were only focused on the elastic mechanical properties of the materials. The test to determine the plastic mechanical properties shall also be conducted in the future.

# 10 References

[1] D. Zenkert, *The handbook of sandwich construction*. Cradley Heath: EMAS Publishing, 1997.

[2] E. Suer, “Herstellung, Berechnung und Untersuchung der mechanischen Eigenschaften von verschiedenen ebenen Proben des MarkForged - Mark Two,” Projektarbeit, Department Fahrzeugtechnik und Flugzeugbau, Hochschule für Angewandte Wissenschaften Hamburg, Hamburg, 2018.

[3] T. Wolf, “Vorschläge für mechanische Validierungsversuche an mit einem Markforged Mark Two Drucker hergestellten Sandwichproben,” Projektarbeit, Department Fahrzeugtechnik und Flugzeugbau, Hochschule für Angewandte Wissenschaften Hamburg, Hamburg, 2020.

[4] H. Schürmann, *Konstruieren mit Faser-Kunststoff-Verbunden,* 2nd ed. Berlin, Heidelberg: Springer, 2007.

[5] H. Domininghaus, P. Elsner, P. Eyerer, and T. Hirth, Eds., *Kunststoffe: Eigenschaften und Anwendungen,* 8th ed. Berlin, Heidelberg: Springer, 2012.

[6] MatWeb, *Overview of materials for Nylon 6, Unreinforced.* [Online] Available: http://www.matweb.com/search/DataSheet.aspx?MatGUID=fb48404b7e04433bb3ee3d2a0af922ff. Accessed on: Aug. 07 2021.

[7] MatWeb, *Overview of materials for Nylon 66, Unreinforced.* [Online] Available: http://www.matweb.com/search/DataSheet.aspx?MatGUID=a2e79a3451984d58a8a442c37a226107. Accessed on: Aug. 07 2021.

[8] Markforged, Inc., “Material Datasheet: Composites,” Jan. 2021. [Online] Available: http://static.markforged.com/downloads/composites-data-sheet.pdf. Accessed on: Jul. 18 2021.

[9] Markforged, Inc., “Material Specifications: Composites,” 2018. Accessed on: Jul. 18 2021.

[10] M. Sauer, “Evaluation of the Mechanical Properties of 3D Printed Carbon Fiber Composites,” Master Thesis, Department Mechanical Engineering, South Dakota State University, Vermillion, 2018.

[11] L. Pyl, K.-A. Kalteremidou, and D. van Hemelrijck, “Exploration of specimen geometry and tab configuration for tensile testing exploiting the potential of 3D printing freeform shape continuous carbon fibre-reinforced nylon matrix composites,” *Polymer Testing*, vol. 71, pp. 318–328, 2018.

[12] G. Chabaud, M. Castro, C. Denoual, and A. Le Duigou, “Hygromechanical properties of 3D printed continuous carbon and glass fibre reinforced polyamide composite for outdoor structural applications,” *Additive Manufacturing*, vol. 26, pp. 94–105, 2019.

[13] T. Finke and A. Kreuziger, “Untersuchung einer Faserverstärkung von konstruktiven Kerbstellen an einem gedruckten Faser- Verbund- Probebauteil,” Schwerpunktarbeit,

Department Fahrzeugtechnik und Flugzeugbau, Hochschule für Angewandte Wissenschaften Hamburg, Hamburg, 2019.

[14] Markforged, Inc., *Carbon Fiber: The backbone of aluminum-strength composite parts.* [Online] Available: https://markforged.com/materials/continuous-fibers/continuous-carbon-fiber. Accessed on: Jul. 08 2021.

[15] L. G. Blok, M. L. Longana, H. Yu, and B. Woods, “An investigation into 3D printing of fibre reinforced thermoplastic composites,” *Additive Manufacturing*, vol. 22, pp. 176–186, 2018.

[16] G. D. Goh *et al.,* “Characterization of mechanical properties and fracture mode of additively manufactured carbon fiber and glass fiber reinforced thermoplastics,” *Materials & Design*, vol. 137, pp. 79–89, 2018.

[17] O. Frankfurt, “Vergleichsuntersuchungen zur Festigkeit von gedruckten und konventionell gefertigten Faser-Verbund-Bauteilen,” Schwerpunktarbeit, Department Fahrzeugtechnik und Flugzeugbau, Hochschule für Angewandte Wissenschaften Hamburg, Hamburg, 2018.

[18] W. Wu *et al.,* “Influence of Layer Thickness and Raster Angle on the Mechanical Properties of 3D-Printed PEEK and a Comparative Mechanical Study between PEEK and ABS,” (eng), *Materials (Basel, Switzerland)*, vol. 8, no. 9, pp. 5834–5846, 2015.

[19] X. Zhang, L. Chen, T. Mulholland, and T. A. Osswald, “Effects of raster angle on the mechanical properties of PLA and Al/PLA composite part produced by fused deposition modeling,” *Polym Adv Technol*, vol. 30, no. 8, pp. 2122–2135, 2019.

[20] Shilpesh R. Rajpurohit and Harshit K. Dave, “Impact Of Process Parameters On Tensile Strength Of Fused Deposition Modeling Printed Crisscross Poylactic Acid,” (en), 2018.

[21] J. T. Cantrell *et al.,* “Experimental characterization of the mechanical properties of 3D-printed ABS and polycarbonate parts,” *Rapid Prototyping Journal*, vol. 23, no. 4, pp. 811–824, 2017.

[22] I. Durgun and R. Ertan, “Experimental investigation of FDM process for improvement of mechanical properties and production cost,” *Rapid Prototyping Journal*, vol. 20, no. 3, pp. 228–235, 2014.

[23] K. Wang *et al.,* “Effects of infill characteristics and strain rate on the deformation and failure properties of additively manufactured polyamide-based composite structures,” *Results in Physics*, vol. 18, p. 103346, 2020.

[24] C. Chen, “Investigations on Hot-Formed Plastic Parts Made by Additive Manufacturing,” Master Thesis, Ruhr-University Bochum; German Aerospace Center; Hamburg University of Applied Sciences, Bochum, Hamburg, 2020.

[25] A. K. Sood, R. K. Ohdar, and S. S. Mahapatra, “Parametric appraisal of mechanical property of fused deposition modelling processed parts,” *Materials & Design*, vol. 31, no. 1, pp. 287–295, 2010.

[26] A. K. Sood, R. K. Ohdar, and S. S. Mahapatra, “Experimental investigation and empirical modelling of FDM process for compressive strength improvement,” *Journal of Advanced Research*, vol. 3, no. 1, pp. 81–90, 2012.

[27] B. M. Tymrak, M. Kreiger, and J. M. Pearce, “Mechanical properties of components fabricated with open-source 3-D printers under realistic environmental conditions,” *Materials & Design*, vol. 58, pp. 242–246, 2014.

[28] Markforged, Inc., *3D Printing Settings Impacting Part Strength.* [Online] Available: https://markforged.com/resources/learn/design-for-additive-manufacturing-plastics-composites/understanding-3d-printing-strength/3d-printing-settings-impacting-part-strength. Accessed on: Jun. 13 2021.

[29] *Kunststoffe – Bestimmung der Zugeigenschaften – Teil 2: Prüfbedingungen für Form- und Extrusionsmassen*, DIN EN ISO 527-2:2012-06, 2012.

[30] *Kunststoffe - Bestimmung der Zugeigenschaften -Teil 4: Prüfbedingungen für isotrop und anisotrop faserverstärkte Kunststoffverbundwerkstoffe*, EN ISO 527-4 : 1997, 1997.

[31] *Kunststoffe – Bestimmung der Zugeigenschaften – Teil 5: Prüfbedingungen für unidirektional faserverstärkte Kunststoffverbundwerkstoffe*, DIN EN ISO 527-5:2010-01, 2010.

[32] *Kunststoffe – Bestimmung der Biegeeigenschaften*, DIN EN ISO 178:2019-08, 2019.

[33] *Faserverstärkte Kunststoffe – Bestimmung der Biegeeigenschaften*, DIN EN ISO 14125:2011-05, 2011.

[34] *Test Method for Shear Properties of Composite Materials by the V-Notched Beam Method*, ASTM D5379/D5379M-12, 2012.

[35] *Prüfung von Kernverbunden - Schubversuch*, DIN 53 294, 1982.

[36] *Test Method for Shear Properties of Sandwich Core Materials*, ASTM C273/C273M-20, 2020.

[37] *Test Method for Flatwise Compressive Properties of Sandwich Cores*, ASTM C365/C365M-16, 2016.

[38] *Pruefung von Kernverbunden - Zugversuch*, DIN 53 292, 1982.

[39] A. Jędral, “Review of Testing Methods Dedicated for Sandwich Structures with Honeycomb Core,” *Transactions on Aerospace Research*, vol. 2019, no. 2, pp. 7–20, 2019.

[40] *Test Method for Node Tensile Strength of Honeycomb Core Materials*, ASTM C363/C363M-16, 2016.

[41] *Pruefung von Kernverbunden - Biegeversuch*, DIN 53 293, 1982.

[42] Markforged, Inc., *Carbon Fiber Composite 3D Printer: Markforged Mark Two.* [Online] Available: https://markforged.com/3d-printers/mark-two. Accessed on: Jul. 09 2021.

[43] Markforged, Inc., *Carbon Fiber Composite 3D Printer: Markforged Mark Two.* [Online] Available: https://markforged.com/3d-printers/mark-two. Accessed on: Jun. 19 2021.

[44] Markforged, Inc., *3D Printer Types & Technologies.* [Online] Available: https://markforged.com/resources/learn/3d-printing-basics/3d-printing-introduction/3d-printer-types-technologies. Accessed on: Jun. 16 2021.

[45] AMETEK, Inc., "EZ Series: EZ20 20 kN Universal Materials Testing Machine," Specification Sheet, Sep. 2009. [Online] Available: https://www.metesco.nl/media/product/534/files/LLOYD%20EZ20%20Metesco%20TwinColumnMachinespecs.pdf. Accessed on: Dec. 09 2021.

[46] MSC Software Corporation, *Patran - Complete FEA Modeling Solution.* [Online] Available: https://www.mscsoftware.com/product/patran. Accessed on: Jun. 15 2021.

[47] MSC Software Corporation, *MSC Nastran - Multidisciplinary Structural Analysis.* [Online] Available: https://www.mscsoftware.com/product/msc-nastran. Accessed on: Jun. 15 2021.

[48] R. M. Jones, *Mechanics of composite materials,* 2nd ed. Philadelphia: Taylor & Francis, 1999.

[49] L. P. Kollár and G. S. Springer, *Mechanics of Composite Structures*. Cambridge: Cambridge University Press, 2003.

[50] K. Rohwer, "Transverse Shear Stiffness in Layered Finite Elements," Deuteche Forchungs- und Versuchsanstalt für Luft- und Raumfahrt E.V. Institut für Strukturmechanik, Braunschweig, Nov. 1987.

[51] J. R. Vinson, *The behavior of sandwich structures of isotropic and composite materials*. Lancaster, Pa.: Technomic Publ, 1999.

[52] M. S. Agerer, *Schubmodul - Begriffserklärung.* [Online] Available: https://www.maschinenbau-wissen.de/skript3/werkstofftechnik/metall/27-schubmodul. Accessed on: Jul. 30 2021.

[53] N. TANIGUCHI, T. NISHIWAKI, N. HIRAYAMA, H. NISHIDA, and H. KAWADA, "Dynamic tensile properties of carbon fiber composite based on thermoplastic epoxy resin loaded in matrix-dominant directions," *Composites Science and Technology*, vol. 69, no. 2, pp. 207–213, 2009.

[54] Leichtbau Labor, "Vierpunktbiegung," Poster of 4-Point-Flexural Test in Lightweight Construction Laboratory, HAW Hamburg, Hamburg, 2021.

[55] Simplify3D, *Gaps in Top Layers.* [Online] Available: https://www.simplify3d.com/support/print-quality-troubleshooting/gaps-in-top-layers/. Accessed on: Feb. 02 2022.

[56] Markforged, Inc., *Troubleshooting Common Print Issues.* [Online] Available: https://support.markforged.com/portal/s/article/Troubleshooting-Common-Print-Issues#residue. Accessed on: Dec. 28 2021.

# Appendix A

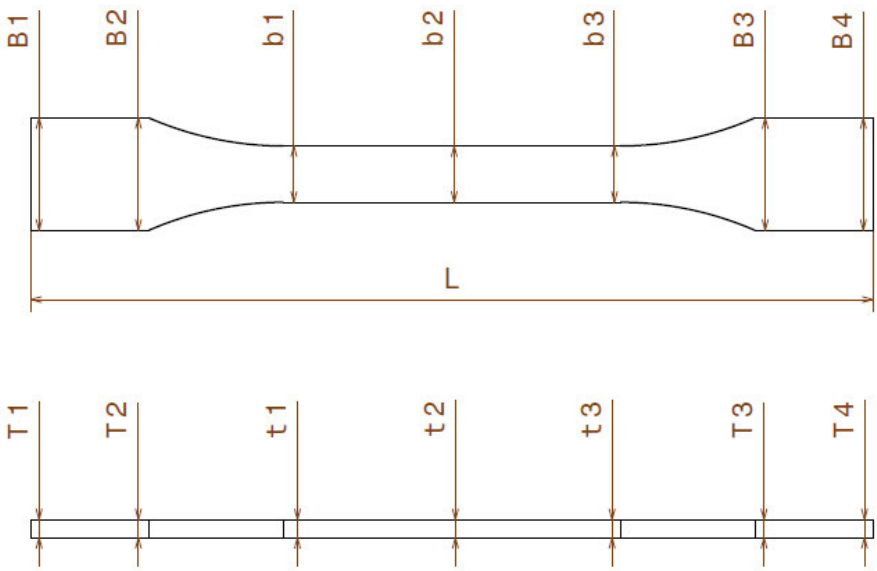


Figure A - 1: Variables in the geometry of nylon specimens

Table A - 1: Geometry of the "0°" nylon specimens

| Specimen | L [mm] | B1 [mm] | B2 [mm] | B3 [mm] | B4 [mm] | T1 [mm] | T2 [mm] | T3 [mm] | T4 [mm] |
|---|---|---|---|---|---|---|---|---|---|
| 1 | 149.80 | 19.93 | 19.98 | 20.02 | 19.97 | 3.24 | 3.26 | 3.36 | 3.34 |
| 2 | 149.75 | 19.98 | 19.99 | 20.01 | 19.96 | 2.22 | 3.19 | 3.35 | 3.32 |
| 3 | 149.90 | 19.96 | 19.99 | 19.99 | 19.91 | 3.19 | 3.23 | 3.36 | 3.31 |
| 4 | 149.90 | 19.97 | 19.98 | 19.95 | 19.90 | 3.23 | 3.22 | 3.38 | 3.34 |
| 5 | 149.75 | 19.96 | 19.96 | 19.92 | 19.90 | 3.20 | 3.21 | 3.34 | 3.31 |
| 6 | 149.80 | 19.90 | 19.94 | 19.88 | 19.88 | 3.20 | 3.24 | 3.36 | 3.39 |

| Specimen | b1 [mm] | b2 [mm] | b3 [mm] | t1 [mm] | t2 [mm] | t3 [mm] |
|---|---|---|---|---|---|---|
| 1 | 10.3 | 10.29 | 10.28 | 3.22 | 3.23 | 3.23 |
| 2 | 10.29 | 10.28 | 10.29 | 3.17 | 3.21 | 3.24 |
| 3 | 10.27 | 10.27 | 10.28 | 3.2 | 3.22 | 3.23 |
| 4 | 10.26 | 10.26 | 10.27 | 3.18 | 3.24 | 3.24 |
| 5 | 10.24 | 10.24 | 10.25 | 3.2 | 3.19 | 3.23 |
| 6 | 10.23 | 10.24 | 10.22 | 3.17 | 3.22 | 3.21 |

Table A - 2: Geometry of the "$0°/90°$" nylon specimens

| Specimen | L [mm] | B1 [mm] | B2 [mm] | B3 [mm] | B4 [mm] | T1 [mm] | T2 [mm] | T3 [mm] | T4 [mm] |
|---|---|---|---|---|---|---|---|---|---|
| 1 | 150.00 | 19.96 | 20.04 | 20.03 | 20.05 | 4.00 | 3.99 | 3.97 | 3.93 |
| 2 | 149.75 | 19.93 | 20.01 | 19.96 | 19.94 | 4.03 | 4.03 | 4.01 | 3.99 |
| 3 | 150.00 | 19.97 | 19.98 | 20.02 | 19.98 | 4.00 | 3.97 | 3.92 | 3.90 |
| 4 | 149.65 | 19.96 | 19.98 | 19.99 | 19.97 | 4.00 | 4.00 | 3.98 | 3.97 |
| 5 | 149.75 | 19.96 | 20.00 | 19.95 | 19.97 | 3.98 | 2.97 | 4.03 | 4.01 |
| 6 | 149.90 | 20.03 | 19.96 | 20.03 | 20.04 | 3.92 | 3.92 | 3.97 | 3.97 |

| Specimen | b1 [mm] | b2 [mm] | b3 [mm] | t1 [mm] | t2 [mm] | t3 [mm] |
|---|---|---|---|---|---|---|
| 1 | 9.99 | 9.98 | 9.99 | 3.99 | 3.97 | 3.95 |
| 2 | 9.99 | 9.96 | 9.97 | 4.04 | 4.05 | 4.03 |
| 3 | 10.00 | 9.96 | 9.99 | 3.97 | 3.96 | 3.94 |
| 4 | 10.02 | 9.97 | 9.98 | 4.02 | 4.03 | 4.01 |
| 5 | 9.97 | 9.99 | 9.99 | 4.00 | 4.03 | 4.02 |
| 6 | 10.00 | 10.00 | 9.97 | 3.93 | 3.95 | 3.98 |

Table A - 3: Geometry of the "$\pm 45°$" nylon specimens

| Specimen | L [mm] | B1 [mm] | B2 [mm] | B3 [mm] | B4 [mm] | T1 [mm] | T2 [mm] | T3 [mm] | T4 [mm] |
|---|---|---|---|---|---|---|---|---|---|
| 1 | 149.75 | 19.88 | 19.93 | 20.00 | 19.93 | 4.01 | 4.01 | 3.97 | 3.95 |
| 2 | 149.65 | 19.85 | 19.90 | 20.03 | 19.93 | 4.01 | 4.01 | 4.02 | 3.99 |
| 3 | 149.60 | 19.93 | 19.92 | 19.97 | 19.94 | 3.99 | 4.00 | 4.03 | 4.02 |
| 4 | 149.75 | 19.98 | 19.94 | 19.94 | 19.90 | 3.96 | 3.91 | 4.02 | 4.03 |
| 5 | 149.80 | 19.93 | 19.90 | 20.02 | 19.98 | 3.87 | 3.89 | 4.04 | 4.03 |
| 6 | 149.85 | 19.92 | 19.96 | 19.93 | 19.99 | 3.88 | 3.89 | 4.02 | 4.03 |

| Specimen | b1 [mm] | b2 [mm] | b3 [mm] | t1 [mm] | t2 [mm] | t3 [mm] |
|---|---|---|---|---|---|---|
| 1 | 10.06 | 10.08 | 10.06 | 4.03 | 4.02 | 4.01 |
| 2 | 10.05 | 10.05 | 10.09 | 4.06 | 4.06 | 4.05 |
| 3 | 10.04 | 10.04 | 10.08 | 4.05 | 4.06 | 4.06 |
| 4 | 10.06 | 10.04 | 10.05 | 3.97 | 4.01 | 4.02 |
| 5 | 10.04 | 10.06 | 10.05 | 3.96 | 4.00 | 4.02 |
| 6 | 10.06 | 10.08 | 10.07 | 3.94 | 3.96 | 4.00 |

# Appendix B

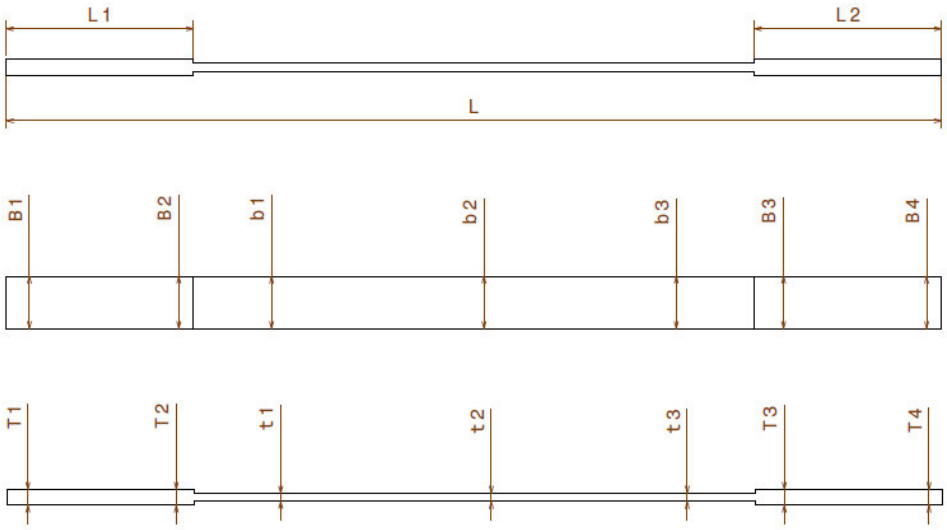


Figure B - 1: Variables in the geometry of CFR specimens

Table B - 1: Geometry of the "0°" CFR specimens

| Specimen | L [mm] | L1[mm] | L2[mm] |
|---|---|---|---|
| 1 | 250.40 | 50.45 | 50.40 |
| 2 | 250.35 | 50.35 | 50.40 |
| 3 | 250.40 | 50.35 | 50.35 |
| 4 | 250.40 | 50.25 | 40.40 |

| Specimen | B1 [mm] | B2 [mm] | B3 [mm] | B4 [mm] | b1 [mm] | b2 [mm] | b3 [mm] |
|---|---|---|---|---|---|---|---|
| 1 | 14.21 | 14.16 | 14.22 | 14.23 | 14.03 | 14.09 | 14.14 |
| 2 | 14.15 | 14.14 | 14.15 | 14.21 | 14.05 | 14.06 | 14.04 |
| 3 | 14.15 | 14.17 | 14.15 | 14.18 | 14.09 | 14.08 | 14.07 |
| 4 | 14.05 | 14.18 | 14.13 | 14.16 | 14.05 | 14.10 | 14.10 |

| Specimen | T1 [mm] | T2 [mm] | T3 [mm] | T4 [mm] | t1 [mm] | t2 [mm] | t3 [mm] |
|---|---|---|---|---|---|---|---|
| 1 | 4.58 | 4.64 | 4.67 | 4.68 | 2.72 | 2.77 | 2.74 |
| 2 | 4.61 | 4.67 | 4.61 | 4.56 | 2.75 | 2.72 | 2.71 |
| 3 | 4.61 | 4.62 | 4.61 | 4.56 | 2.72 | 2.67 | 2.61 |
| 4 | 4.51 | 4.59 | 4.56 | 4.53 | 2.71 | 2.69 | 2.67 |

Table B - 2: Geometry of the "$0°/90°$" CFR specimens

| Specimen | L [mm] | L1[mm] | L2[mm] |
|---|---|---|---|
| 1 | 250.35 | 50.25 | 50.25 |
| 2 | 250.30 | 50.30 | 50.25 |
| 3 | 250.35 | 50.25 | 50.30 |
| 4 | 250.25 | 50.25 | 50.25 |

| Specimen | B1 [mm] | B2 [mm] | B3 [mm] | B4 [mm] | b1 [mm] | b2 [mm] | b3 [mm] |
|---|---|---|---|---|---|---|---|
| 1 | 14.13 | 14.10 | 14.18 | 14.14 | 14.11 | 14.14 | 14.17 |
| 2 | 14.13 | 14.10 | 14.13 | 14.17 | 14.08 | 14.13 | 14.11 |
| 3 | 14.04 | 14.09 | 14.16 | 14.12 | 14.08 | 14.12 | 14.13 |
| 4 | 14.04 | 14.05 | 14.11 | 14.10 | 14.12 | 14.11 | 14.13 |

| Specimen | T1 [mm] | T2 [mm] | T3 [mm] | T4 [mm] | t1 [mm] | t2 [mm] | t3 [mm] |
|---|---|---|---|---|---|---|---|
| 1 | 4.62 | 4.66 | 4.64 | 4.57 | 2.72 | 2.68 | 2.61 |
| 2 | 4.56 | 4.64 | 4.55 | 4.53 | 2.66 | 2.71 | 2.65 |
| 3 | 4.57 | 4.61 | 4.61 | 4.62 | 2.63 | 2.67 | 2.64 |
| 4 | 4.49 | 4.61 | 4.57 | 4.47 | 2.63 | 2.66 | 2.59 |

Table B - 3: Geometry of the "$\pm 45°$" CFR specimens

| Specimen | L [mm] | L1[mm] | L2[mm] |
|---|---|---|---|
| 1 | 250.20 | 50.25 | 50.35 |
| 2 | 250.25 | 50.25 | 50.25 |
| 3 | 250.20 | 50.25 | 50.25 |
| 4 | 250.25 | 50.20 | 50.25 |

| Specimen | B1 [mm] | B2 [mm] | B3 [mm] | B4 [mm] | b1 [mm] | b2 [mm] | b3 [mm] |
|---|---|---|---|---|---|---|---|
| 1 | 14.11 | 14.12 | 14.19 | 14.19 | 14.05 | 14.11 | 14.08 |
| 2 | 14.01 | 14.15 | 14.13 | 14.11 | 14.07 | 14.15 | 14.08 |
| 3 | 14.10 | 14.06 | 14.12 | 14.09 | 14.08 | 14.12 | 14.08 |
| 4 | 14.09 | 14.08 | 14.17 | 14.14 | 14.04 | 14.09 | 14.14 |

| Specimen | T1 [mm] | T2 [mm] | T3 [mm] | T4 [mm] | t1 [mm] | t2 [mm] | t3 [mm] |
|---|---|---|---|---|---|---|---|
| 1 | 4.61 | 4.52 | 4.63 | 4.50 | 2.61 | 2.61 | 2.58 |
| 2 | 4.56 | 4.60 | 4.59 | 4.55 | 2.63 | 2.60 | 2.55 |
| 3 | 4.55 | 4.55 | 4.65 | 5.63 | 2.63 | 2.67 | 2.61 |
| 4 | 4.61 | 4.52 | 4.59 | 4.52 | 2.63 | 2.61 | 2.58 |

# Appendix C

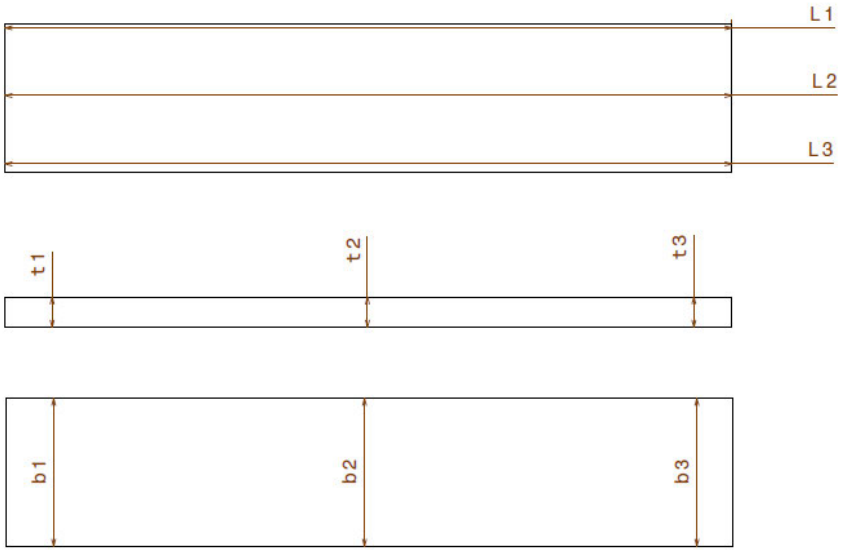


Figure C - 1: Variables in the geometry of nylon sandwich core specimens

Table C - 1: Geometry of the nylon sandwich core specimens

| Specimen | 1 | 2 | 3 | Average |
|---|---|---|---|---|
| L1 [mm] | 191.90 | 191.80 | 191.70 | 191.78 |
| L2 [mm] | 192.00 | 191.90 | 191.50 | |
| L3 [mm] | 191.90 | 191.70 | 191.60 | |
| b1 [mm] | 38.90 | 39.00 | 39.00 | 38.98 |
| b2 [mm] | 39.10 | 38.90 | 39.00 | |
| b3 [mm] | 38.90 | 39.00 | 39.00 | |
| t1 [mm] | 8.01 | 8.02 | 8.00 | 8.02 |
| t2 [mm] | 8.04 | 8.10 | 8.07 | |
| t3 [mm] | 7.94 | 8.02 | 7.98 | |

# Appendix D

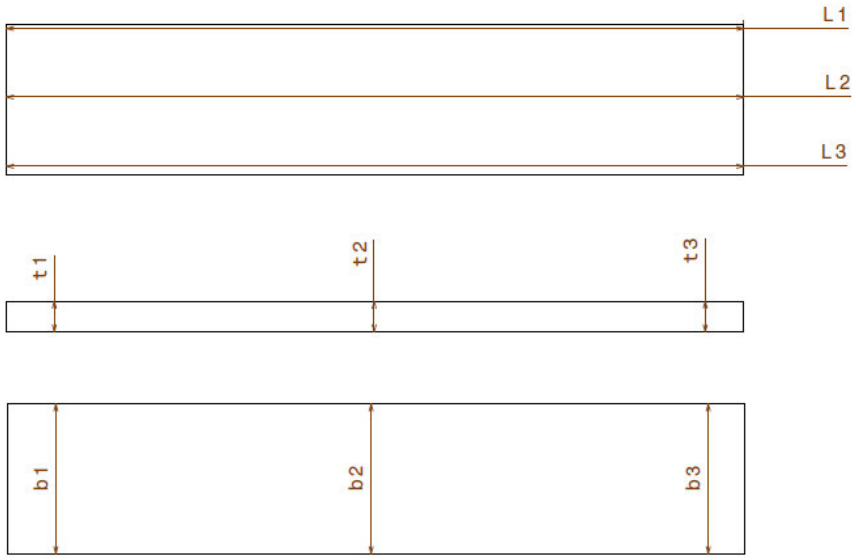


Figure D - 1: Variables in the geometry of sandwich panel specimens

Table D - 1: Geometry of the sandwich panel specimens

| Specimen | 1 | 2 | 3 | Average |
|---|---|---|---|---|
| L1 [mm] | 192.30 | 192.30 | 192.20 | 192.26 |
| L2 [mm] | 192.20 | 192.30 | 192.30 | |
| L3 [mm] | 192.30 | 192.20 | 192.20 | |
| b1 [mm] | 39.20 | 39.10 | 39.10 | 39.19 |
| b2 [mm] | 39.30 | 39.40 | 39.30 | |
| b3 [mm] | 39.10 | 39.10 | 39.10 | |
| t1 [mm] | 8.10 | 8.06 | 8.07 | 8.08 |
| t2 [mm] | 8.15 | 8.13 | 8.13 | |
| t3 [mm] | 8.04 | 8.01 | 8.01 | |

# Appendix E

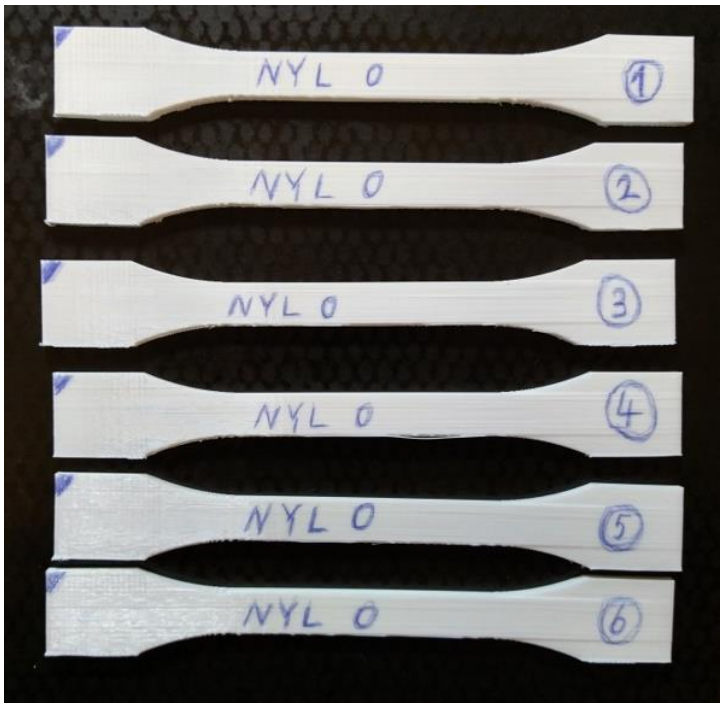


Figure E - 1: Printed "0°" nylon specimens


Figure E - 2: Printed "0°/90°" nylon specimens:


Figure E - 3: Printed "±45°" nylon specimens:

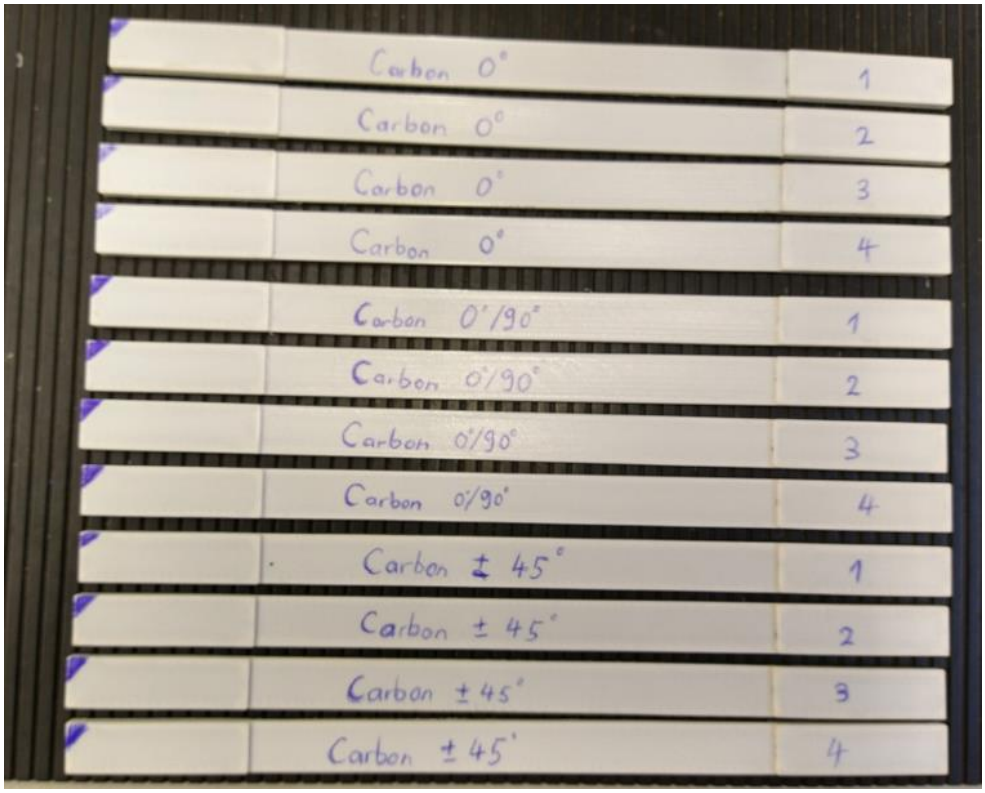


Figure E - 4: Printed CFR specimens

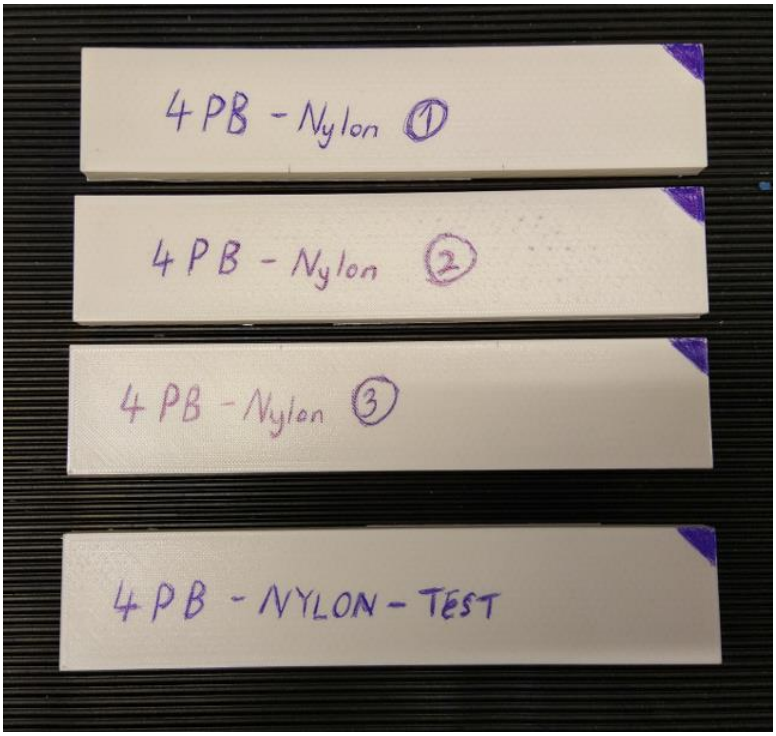


Figure E - 5: Printed nylon sandwich core specimens

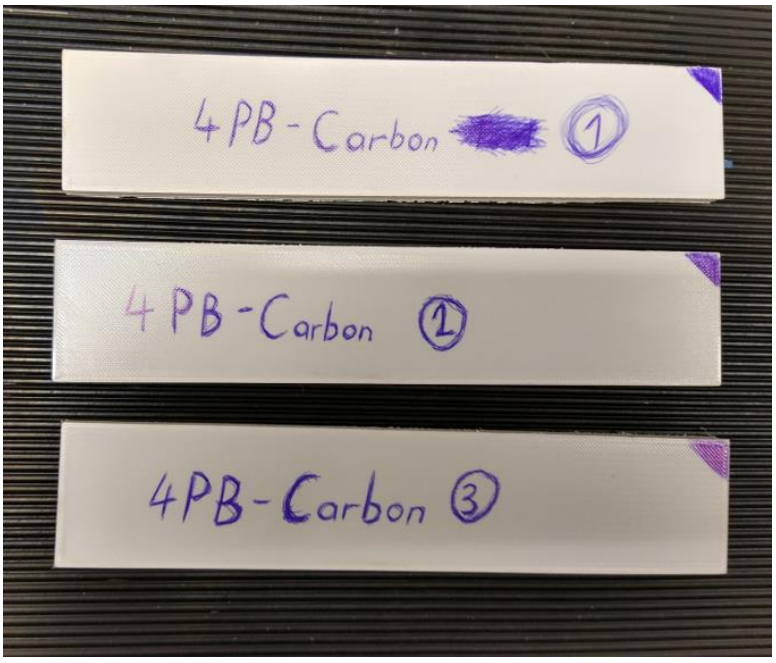


Figure E - 6: Printed sandwich panel specimens

# Appendix F

Table F - 1: Comparison of elastic modulus of "$0°$" nylon specimens between the first and fifth load cycle

| Specimen | Elastic modulus [MPa] | | Difference (%) |
|---|---|---|---|
| | 1st cycle | 5th cycle | |
| 1 | 1654.200 | 1736.100 | 4.95% |
| 2 | 1698.800 | 1794.100 | 5.61% |
| 3 | 1688.600 | 1570.100 | -7.02% |
| 4 | 1665.400 | 1750.900 | 5.13% |
| 5 | 1680.500 | 1685.400 | 0.29% |
| 6 | 1576.200 | 1800.900 | 14.26% |
| | | Average | 3.87% |

Table F - 2: Comparison of elastic modulus of "$0°/90°$" nylon specimens between the first and fifth load cycle

| Specimen | Elastic modulus [MPa] | | Difference (%) |
|---|---|---|---|
| | 1st cycle | 5th cycle | |
| 1 | 1502.600 | 1720.500 | 14.50% |
| 2 | 1376.100 | 1457.200 | 5.89% |
| 3 | 1581.600 | 1627.900 | 2.93% |
| 4 | 1461.800 | 1500.200 | 2.63% |
| 5 | 1562.200 | 1601.100 | 2.49% |
| 6 | 1581.400 | 1620.000 | 2.44% |
| | | Average | 5.15% |

Table F - 3: Comparison of elastic modulus of "$\pm 45°$" nylon specimens between the first and fifth load cycle

| Specimen. | Elastic modulus [MPa] | | Difference (%) |
|---|---|---|---|
| | 1st cycle | 5th cycle | |
| 1 | 1465.600 | 1561.900 | 6.57% |
| 2 | 1459.400 | 1692.100 | 15.94% |
| 3 | 1406.600 | 1449.400 | 3.04% |
| 4 | 1374.700 | 1549.500 | 12.72% |
| 5 | 1460.200 | 1647.600 | 12.83% |
| 6 | 1478.900 | 1613.400 | 9.09% |
| | | Average | 10.03% |

# Appendix G

Table G - 1: Comparison of elastic modulus of "0°" CFR specimens between the first and fifth load cycle

| Specimen | Elastic modulus [MPa] | | Difference (%) |
|---|---|---|---|
| | 1st cycle | 5th cycle | |
| 1 | 21580.000 | 17787.000 | -17.58% |
| 2 | 21753.000 | 23069.000 | 6.05% |
| 3 | 23600.000 | 24231.000 | 2.67% |
| 4 | 22244.000 | 21699.000 | -2.45% |
| | | Average | -2.83% |

Table G - 2: Comparison of elastic modulus of "0°/90°" CFR specimens between the first and fifth load cycle

| Specimen | Elastic modulus [MPa] | | Difference (%) |
|---|---|---|---|
| | 1st cycle | 5th cycle | |
| 1 | 12447.000 | 12545.000 | 0.79% |
| 2 | 12650.000 | 11350.000 | -10.28% |
| 3 | 12359.000 | 12475.000 | 0.94% |
| 4 | 12539.000 | 12666.000 | 1.01% |
| | | Average | -1.88% |

Table G - 3: Comparison of elastic modulus of "±45°" CFR specimens between the first and fifth load cycle

| Specimen | Elastic modulus [MPa] | | Difference (%) |
|---|---|---|---|
| | 1st cycle | 5th cycle | |
| 1 | 3467.600 | 3702.800 | 6.78% |
| 2 | 3540.100 | 3525.900 | -0.40% |
| 3 | 3298.000 | 3417.000 | 3.61% |
| 4 | 3462.300 | 3667.400 | 5.92% |
| | | Average | 3.98% |

# Appendix H

Table H - 1: Comparison of FE modelling method before and after improvement

| | | Wolf 2020 [3] | Liew |
|---|---|---|---|
| ***Material*** | Nylon | The printed stacked nylon layers (i.e. 5 layers printed above or below the CFRP layers) are considered as one in the "Composite Layup" function<br><br>Isotropic | Each printed nylon layer is considered as an individual layer in the "Composite Layup" function<br><br>2D and 3D orthotropic material property |
| | Carbon | 2D orthotropic | 2D and 3D orthotropic |
| | Core | 3D anisotropic | 3D orthotropic |
| ***Boundary conditions*** | Load | CID Distributed load | Total load |
| | Displacement | Nodal displacement | Nodal displacement |
| ***Element type*** | Face sheet | QUAD4 | QUAD4 |
| | Core | HEX8 | HEX8 |

Hochschule für Angewandte Wissenschaften Hamburg
*Hamburg University of Applied Sciences*

## Erklärung zur selbstständigen Bearbeitung einer Abschlussarbeit

Gemäß der Allgemeinen Prüfungs- und Studienordnung ist zusammen mit der Abschlussarbeit eine schriftliche Erklärung abzugeben, in der der Studierende bestätigt, dass die Abschlussarbeit „– bei einer Gruppenarbeit die entsprechend gekennzeichneten Teile der Arbeit [(§ 18 Abs. 1 APSO-TI-BM bzw. § 21 Abs. 1 APSO-INGI)] – ohne fremde Hilfe selbständig verfasst und nur die angegebenen Quellen und Hilfsmittel benutzt wurden. Wörtlich oder dem Sinn nach aus anderen Werken entnommene Stellen sind unter Angabe der Quellen kenntlich zu machen."

*Quelle: § 16 Abs. 5 APSO-TI-BM bzw. § 15 Abs. 6 APSO-INGI*

Dieses Blatt, mit der folgenden Erklärung, ist nach Fertigstellung der Abschlussarbeit durch den Studierenden auszufüllen und jeweils mit Originalunterschrift als letztes Blatt in das Prüfungsexemplar der Abschlussarbeit einzubinden.
Eine unrichtig abgegebene Erklärung kann -auch nachträglich- zur Ungültigkeit des Studienabschlusses führen.

**Erklärung zur selbstständigen Bearbeitung der Arbeit**

Hiermit versichere ich,

Name: Liew

Vorname: Xiang Shan

dass ich die vorliegende Masterarbeit bzw. bei einer Gruppenarbeit die entsprechend gekennzeichneten Teile der Arbeit – mit dem Thema:

Stiffness analysis of a nylon sandwich core structure produced by a Markforged Mark Two printer

ohne fremde Hilfe selbständig verfasst und nur die angegebenen Quellen und Hilfsmittel benutzt habe. Wörtlich oder dem Sinn nach aus anderen Werken entnommene Stellen sind unter Angabe der Quellen kenntlich gemacht.

*- die folgende Aussage ist bei Gruppenarbeiten auszufüllen und entfällt bei Einzelarbeiten -*

Die Kennzeichnung der von mir erstellten und verantworteten Teile der -bitte auswählen- ist erfolgt durch:

| Hamburg | 28.02.2022 | [redacted] |
|---|---|---|
| Ort | Datum | Unterschrift im Original |